The sensitivity of simulated temperatures in climate models to aerosols over southern Africa

TE Makgoale

orcid.org 0000-0002-5197-4353

Dissertation accepted in fulfilment of the requirements for the degree *Master of Science in Geography and Environmental Management* at the North-West University

Supervisor:	Prof RM Garland
Co-supervisor:	Prof RP Burger

Graduation December 2021

27020150

Abstract

The purpose of this study is to investigate the sensitivity of Southern African surface temperatures to aerosols using two general circulation models (GCMs), namely the Goddard Institute for Space Studies (GISS) – modelE and the Conformal-Cubic Atmospheric Model (CCAM). Southern Africa's seasonal surface temperatures have been simulated with and without the aerosol schemes for the period 2000 – 2014. The simulated surface temperatures obtained without the aerosol scheme were evaluated against gridded surface temperature observations from the Climate Research Unit (CRU). A temporal and spatial distribution of simulated aerosol optical depth at 550 nm (AOD_{550}) were compared against AEROsol Robotic NETwork (AERONET) and satellite observations. In general, the GCMs adequately represent the seasonal surface temperature over Southern Africa. However, there is a general pattern in both GCMs of localized positive bias that ranges between 1.0 – 2.5˚C, over the western part of the domain, and a slight negative bias at the eastern part. It was found that both GCMs were able to capture the temporal and spatial distribution of AOD_{550} but underestimate the magnitude of AOD_{550} over Southern Africa. The results indicate that AOD_{550} over Southern Africa varies with respect to space and time, during September – November (SON) AOD_{550} reaches a maximum value of 0.8 while relatively low AOD_{550} occurs in March - May (MAM) season. Sensitivity results have shown that aerosols induce a surface temperature change that is spatially dependent over Southern Africa. Generally, negative changes in surface temperature that range between 0.25 – 1.5 °C and 1.0 – 3.5°C are induced for GISS modelE and CCAM respectively. However, there are localized positive changes in surface temperature of about 0.5 – 1.0°C that were simulated by GISS modelE in some parts of Southern Africa especially during the MAM season.

Keywords: GCMs, surface temperature, aerosol optical depth, model simulations, AERONET, MODIS, and Southern Africa

Preface

Atmospheric aerosols from human activity can influence climate directly through scattering and absorption of solar radiation. The scattering and the absorbing ability of particles differ with respect to their properties. Aerosol particles such as sulphates and nitrates scatter incoming solar radiation, hence cause cooling at the surface of the Earth (Hatzianastassiou *et al*., 2007; Podgorny and Ramanathan *et al*., 2001; Rap *et al*., 2013). In contrast, absorbing aerosols, such as black carbon, absorb solar radiation, which consequently warms the layer of the atmosphere around these particles (Zhang and Wang, 2011; Bond *et al*., 2013). Aerosols can also impact the climate indirectly by modifying the radiative properties of clouds (Lohman and Feichter, 2005; Rap *et al*., 2013). Due to the relatively short atmospheric lifetimes of aerosols and heterogeneous distribution through space and time, the impact of aerosols on radiative balance and the surface temperature remains highly uncertain (Myhre *et al*., 2013). This uncertainty limits the knowledge about climate change. In this study, the sensitivity of simulated temperatures to aerosols over Southern Africa (10°N - 50°S and 0°W - 60°E) is Investigated. The study has been carried out using two GCMs forced with Coupled Model Inter-comparison Project Phase 5 (CMIP5) emissions to simulate aerosols' optical depth at 550nm (AOD_{550}) and surface temperature over Southern Africa.

This thesis has been developed into seven chapters to respond to the scientific objectives. Chapter one presents a general background of the study which includes the role of atmospheric aerosols in the Earth system and the importance of incorporating aerosols in GCMs that are used in simulation and projection of climate variability and change. The aim and objectives of this study are also outlined in this chapter. Chapter two provides a detailed literature review relevant to atmospheric aerosols and their interactions with climate. This includes aerosol particle characteristics, aerosol radiative properties, results from previous measurement campaigns, and aerosol's impact on regional climate. In chapter two, a review of the fundamental concepts around atmospheric aerosols was conducted. Chapter three provides a brief description of the study area, datasets used, analytical tools and the methods used to achieve the research objectives. In chapter four, the first sensitivity analysis results are presented. The results were achieved using the Goddard Institute for Space Studies (GISS) – modelE that participated in CMIP5. Chapter five presents the sensitivity analysis from the Conformal-Cubic Atmospheric Model (CCAM). Chapter six provides the climate model inter-comparison. In this chapter, the underlying differences between the GCMs in simulating the impact of aerosols on surface temperature is presented. Chapter seven provides a summary of the research findings and future research recommendations.

This study contributes to the understanding of the sensitivity of simulated regional surface temperature to aerosol particles. The findings from this work have been shared with the broader scientific community. Preliminary results of this research have been presented in the colloquium at the South African Weather Service (SAWS), 3rd National Conference on Global Change, held in Durban in 2016 and South African Society of Atmospheric Sciences (SASAS), held in Cape Town in 2016. Part of the results have been submitted for conference proceedings at SASAS 2018 and were presented during the conference, which was held in Durban.

There are certainly many great people to thank for the support, encouragement, and friendship throughout this study. However, first and foremost I would like to forward special gratitude to my thesis promoters or supervisors Prof Rebecca Garland (*Council for Scientific and Industrial Research, CSIR, Pretoria*) and Dr Roelof Burger (*Climatology Research Group, CRG, North West University, Potchefstroom*) for their valuable ideas, approachability, and guidance on achieving a Master's degree, the process starting from the registration to the final writing up of this dissertation. I am very grateful to stand at the shoulder of these giants. Special thanks are also owed to Dr Joel Botai (SAWS) for his advice and willingness to give technical support whenever needed. I would also like to thank my colleagues Mr. Gift Rambuwani for overwhelming friendship through this journey and Dr Abiodun Adeola and Dr Gabriel Lekalala for support and always being available to proofread any piece of writing.

Appreciation is due to National Aeronautics and Space Administration (NASA) GISS modelling group, especially Dr Susanne E. Bauer and Miss Keren Mezuman for GISS-modelE simulations and for always being ready to answer any technical question related to model output. Also, Dr Francois Engelbrecht and Mr Jacobus van der Merwe from the CSIR Climate Studies, Modelling and Environmental Health group are being thanked for CCAM simulations and technical advice.

This thesis would never have been possible without the financial support from the National Research Foundation (NRF) CSIR Grand number 9157. A special thanks also goes to the SAWS for logistical support on travelling arrangements to conferences, additional financial support (especially registrations and tuition fees for 2017, 2018 and 2019 academic years) and research facilities among others include computers, data storage, and data analysis software.

Table of Contents

Abbreviations

AERONET:	Aerosol Robotic Network
AOD:	Aerosol Optical Depth
AOD:	Aerosol Optical Thickness
CCAM:	Conformal-Cubic Atmospheric Model
CCN:	Cloud Condensation Nuclei
CDO:	Climate Data Operator
CMIP:	Coupled Model Inter-comparison Project Phase
CRG:	Climatology Research Group
CRU:	Climate Research Unit
CSIR:	Council for Scientific and Industrial Research
CSIRO:	Commonwealth Scientific and Industrial Research Organization
GCM:	General Circulation Models
GFDL:	Geophysical Fluid Dynamics Laboratory
GHG:	Greenhouse Gas Gases
GISS:	Goddard Institute for Space Studies
IPCC:	Intergovernmental Panel on Climate Change
MAE:	Mean Absolute Error
MATRIX:	Multiconfiguration Aerosol Tracker of Mixing
ME:	Mean Error
MODIS:	Moderate Resolution Imaging Spectroradiometer
NASA:	National Aeronautics and Space Administration
NRF:	National Research Foundation
OMA:	One Moment Aerosol
RMSE:	Root Mean Square Error
SADC:	Southern African Development Community
SASAS:	South African Society of Atmospheric Sciences

SAWS: South African Weather Service

SD: Standard Deviation

SMAPE: Symmetric Mean Absolute Percentage Error

SSA: Single Scattering Albedo

SST: Sea Surface Temperature

List of Figures

List of Tables

Chapter 1: Background

1.1. Introduction

Since the beginning of the 20th century, mean surface temperatures have increased drastically due to emission of greenhouse gases from human activities. Global temperature records show that the mean surface temperature has increased by approximately 0.8°C since the year 1880 through 2011 (Hansen *et al*., 2010). For the southern hemisphere, the mean surface temperature has increased by 1.12°C over the period 1901 - 2010 (Jones *et al*., 2012). A further increase of about 0.3 – 1.7°C under Representative Concentration Pathways (RCP) 2.6 scenario, 1.1 – 2.6 °C (RCP4.5 scenario), 1.4 – 3.1°C (RCP6.0 scenario) and 2.6 – 4.8°C (RCP8.5 scenario) relative to the 1985 - 2005 base period is projected by 2100 (Stocker *et al*, 2013b). Southern Africa's mean surface temperature could even be higher than the global average because projections point towards an increase with a rate that is 1.5 higher than the global rate (Engelbrecht *et al*., 2015). Associated with an increase in average temperatures is a change in shape and scale of the probability density functions of temperature and precipitation. This translates into an increased in magnitude, frequency and duration of weather and climate extremes (e.g. Trenberth, 2007; Solomon *et al*., 2007; Seneviratne *et al*., 2012). Weather and climate extremes can pose a threat to the health and well-being of human society, ecosystems, infrastructure, and wildlife, especially in vulnerable areas (Easterling *et al*., 2000; Meehl *et al*., 2000). An increase in occurrence and severity of weather and climate extremes under global warming place Southern Africa among one of the most vulnerable regions in the world (Foster *et al*., 2007), mainly because its economy strongly depends on climate-sensitive sectors and the region has low technological capacity for adaptation. To assist policy developers and government sectors to develop climate-smart plans and adapt to climate change and associated extremes, reliable information on climate variability and change is needed.

Climate variability and change information can be made possible using Global Climate Models (GCMs). The development and application of GCMs have played an important role in understanding the physical, chemical, and biological processes that drive climate variability and change. GCMs use physical laws, mathematical laws, and basic equations of motion and numerical analysis to predict climate variability and climate change (IPCC, 2007). This equation of motion together with physical and mathematical laws help in understanding how different components of the climate system interact with one another. Availability of Earth observations from *in situ* observing tools, satellite, radar, remote sensing, and lightning

detection sensors also play an important role in the model prediction of climate variability and change. They play an important part in climate model forcing and evaluation (Flato *et al*., 2013). It has been demonstrated in the most recent Intergovernmental Panel on Climate Change (IPCC) reports that climate models can reproduce observed features of the climate system when climate components, physical and chemical processes are well-represented (IPCC, 2013). Furthermore, data in the form of emission scenarios can also be used in GCMs to simulate possible future climate change. The skill in simulating climate variability and climate change has been increasing over the years because of the availability of supercomputers (e.g. Palmer, 2016; Stanley, 2017; Kalnay, 2018). Moreover, there has been a continuous improvement in GCMs over the past decades. The GCMs have improved horizontal and vertical resolution, improved dynamical core, improved representation of physical processes and improved incorporation of land and oceanic processes that are key drivers of climate which lead to an improvement in climate system simulation (e.g. Knutti *et al*., 2010b; Das *et al*., 2012; Seiki *et al*., 2015). The current generation of GCMs can incorporate aerosol modules and aerosol effects on the climate system. The detail within aerosol modules across GCMs vary. The features include the ability to treat complex chemical and physical processes that control the aerosols' lifecycles such as emission, transport, scavenging through interaction with clouds, and gas and aqueous chemical reactions and deposition.

While global warming has been agreed to be caused by the emission of greenhouse gases (GHGs) such as carbon dioxide (CO_2) (e.g. Solomon *et al*., 2010; Seinfeld and Pandis, 2006; Hartmann *et al*., 2013; Anderson *et al*., 2016), the role of aerosols in the climate system has been widely recognized since the beginning of the 1990s (e.g. Langner and Rodhe, 1991; Kiehl and Rodhe, 1995; Mitchell *et al*., 1995; Hansen *et al*., 1997; Kaufman *et al*., 2002a). After several decades of studies and breakthrough findings, aerosols' forcing on climate remains the largest source of uncertainties in predicting climate and projecting future climate outlook (e.g. Forster *et al*., 2007; Stevens and Feingold, 2009; Northrop and Chandler, 2014; Tinker *et al*., 2016).

Aerosols impact climate through scattering and absorbing shortwave radiation (i.e. aerosols' direct radiative effect). The scattering and absorption abilities of aerosols vary with aerosol species. Aerosols' particles such as sulphates and nitrates scatter incoming solar radiation, hence causing cooling at the earth's surface (Podgorny and Ramanathan, 2001; Hatzianastassiou *et al*., 2007; Ahn *et al*., 2007; Ayash *et al*., 2008; Levy *et al*., 2013; Rap *et al*., 2013). On the other hand, aerosol particles such as black carbon, tend to absorb solar radiation, consequently warming the atmosphere layer around the particles which are found (Ramanathan and Carmichael, 2008; Zhang and Wang, 2011; Bond *et al*., 2013; Myhre *et al*.,

2013; Heald *et al*., 2014). This could decrease the amount of solar radiation that reaches the Earth's surface, possibly leading to surface cooling (Krishnan and Ramanathan, 2002; Kinne *et al*., 2003). Aerosols play an important role in the formation of clouds, they act as cloud condensation nuclei (CCN) and can modify cloud properties, hence impact the climate. Aerosols' effect on cloud properties is complex and can lead to warming or cooling (Lohmann and Feichter, 2005; Rap *et al*., 2013).

Direct and indirect radiative effects of aerosols are identified as important and are poorly understood in climate science studies (IPCC, 2013). At the global scale, the direct and indirect radiative forcing due to aerosols are estimated to be -0.4 ($\pm$0.3) and -1.0 (+0.5/-1.0) watt per square meter (W m^{-2}), respectively (Hansen *et al.*, 1998). The existing uncertainty is associated with inadequate knowledge of the magnitude of radiative forcing because of aerosols' relatively short atmospheric lifetime that leads to inhomogeneity in space and time. Moreover, there is large uncertainty regarding their optical properties and processes in the climate system, which in turn contributes to uncertainty in quantifying their climate impact (e.g. Matsui and Pielke, 2006; Strawa *et al*., 2003; Solomon *et al*., 2007; Curci *et al*., 2015). At the regional scale, the uncertainty regarding the radiative effect is anticipated to be larger as compared to global effect (e.g. Kinne *et al*., 2003; Regayre *et al*., 2015). These uncertainties impact regional climate predictions (Lee *et al*., 2016). The seasonal changes in radiative forcing due to aerosols have a direct impact on regional surface temperature. Therefore, a better understanding of the sensitivity of GCMs to aerosols is key to improve regional climate projections that will help to better understand and prepare for future climate change.

1.2. Motivation

The motivation of this study arose from the fact that internationally there is growing recognition of the potential impacts of aerosols on regional climate. Southern Africa is one of the regions in the world that experiences high loading of aerosols of different types. The aerosol burden in Southern Africa is mostly affected by mineral dust (e.g. Piketh *et al*., 1999a; Bhattachan *et al*., 2012; Tesfaye *et al*., 2015), biomass burning aerosols emitted during the fire seasons (e.g. Liu *et al*., 2000; Abel *et al*., 2003; Swap *et al*., 2003; Lu *et al*., 2018), marine aerosols (e.g. Mélin *et al*., 2013) and anthropogenic aerosols (e.g. Kuik *et al*., 2015). Volcanic aerosols from the remote site are also transported to Southern Africa through large scale circulation of winds (e.g. Bègue *et al*., 2017; Shikwambana and Venkataraman, 2018) contributing to the aerosols loading over the region. This aerosol burden tends to accumulate and recirculate over the region due to the quasi-stationary anticyclone circulation systems over the region; this increases the potential effect of these aerosols on regional climate. Most coal-fired power stations over the region do not have emissions controls (e.g. Pretorius *et al*., 2015; 2016). This

has the potential to add more to the current aerosol burden in Southern Africa now and into the future.

Great effort has been made to study the physical and optical properties of Southern African aerosols' characteristics from ground-based measurements (e.g. Eck *et al*., 2003; Formenti *et al*., 2003; Haywood *et al*., 2003; Laakso *et al*., 2012), remote sensing satellite (e.g. Tesfaye *et al*., 2011; Kanika *et al*., 2013; Kumar *et al*., 2014; Adesina *et al*., 2016) and model simulations (e.g. Matichuk *et al*., 2007; Tesfaye *et al*., 2011). Over Southern Africa, there is a strong seasonal variation of aerosol optical depth (AOD) with high values occurring during austral winter (June to September). This seasonal variability of AOD can have a significant impact on regional climate (e.g. Tummon *et al*., 2010). The current study investigates how the seasonal variation of AOD impacts Southern African simulated surface temperature in two different GCMs.

1.3. Aim and Objectives

The primary aim of this study is to investigate the sensitivity of simulated temperatures in two different climate models to aerosols over Southern Africa. For this purpose, the study uses two different GCMs to simulate Southern Africa's surface air temperature and AOD. Surface temperature simulations were performed with and without the aerosol schemes, and the difference in these simulations was investigated to give an idea of how aerosols affect surface temperature. This study concentrated on the seasonal distribution of AOD because there is relatively strong seasonal variability of aerosols that could affect seasonal surface temperatures over Southern Africa. Simulations were achieved using two GCMs namely the Goddard Institute for Space Studies (GISS) modelE and Conformal Cubic Atmospheric Model (CCAM). With GISS modelE, two aerosol schemes were tested i.e. the Multiconfiguration Aerosol Tracker of mIXing state (MATRIX) and the One-Moment Aerosol (OMA) schemes. Different GCMs were used with different aerosols schemes to investigate the difference in the sensitivity of surface temperature to aerosols.

The objectives of this study are summarized as follows:

GISS-modelE GCM

Objective 1: Evaluate the skill of GISS-modelE in simulating Southern African surface temperature.

Objective 2: Evaluate the skill of GISS-modelE in simulating Southern African AOD.

Objective 3: Investigate the sensitivity of simulated temperature in GISS-modelE climate model to aerosols over Southern Africa.

CCAM GCM

Objective 4: Evaluate the skill of CCAM in simulating Southern African surface temperature.

Objective 5: Investigate the sensitivity of simulated temperature in CCAM climate model to aerosols over Southern Africa.

Climate Model Inter-comparison

Objective 6: Investigate the difference between GCMs simulations of surface temperature with the implementation of different aerosols' schemes.

Chapter 2: Fundamental Concepts

2.1. Atmospheric Aerosols

The atmosphere consists of small particles that range from nanometres to tens of micrometres in size, depending upon the source, and are known as atmospheric aerosols. Atmospheric aerosols are tiny solid and liquid particles that are suspended in the air. They are often visible as smoke, dust or haze and they form part of air pollution in many areas (Wang *et al*., 2001; Seinfeld and Pandis, 2006). Aerosols can have an adverse effect on the environment, human health, and climate (Jacobson, 2001, 2002; Andreae *et al*., 2005; Zhang *et al*., 2012). However, knowledge of how they affect climate is still limited, due in part to their complex chemical and physical properties. Aerosols vary in terms of physical and chemical properties because they are derived from different emission sources. At a global scale, a great number of aerosols' particles are emitted from natural sources and they occur in the atmosphere in the absence of human activities, this includes soil dust, sea salt, forest fires, and volcanic dust. On the other hand, there are aerosol particles that originate from anthropogenic activities; these are then referred to as anthropogenic aerosols. The anthropogenic aerosols make up to 10 percent of the total amount of particles in the atmosphere (Wolf and Hidy, 1997). The major chemical components include nitrates (NO_3), sulphates (SO_4), organic, and inorganic carbonaceous mixtures (Budhavant *et al*., 2018). Aerosols can be categorized as primary or secondary, whereby primary aerosols are particles that are emitted directly into the atmosphere (e.g. dust, sea salt), while secondary aerosols are produced in the atmosphere through gas-to-particle conversion. A predominant source of anthropogenic aerosols is fossil fuel combustion, especially coal and biomass burning (e.g. Wolf and Hidy, 1997; Solomon *et al*., 2007). They are relatively short-lived (days to weeks). The impacts of anthropogenic aerosols at a local and regional scale are significant (e.g. Andreae *et al*., 2005), and they are often linked to regional surface cooling (e.g. Krishnan and Ramanathan, 2002; Leibensperger *et al*., 2012; Persad and Caldeira, 2018), reduction in visibility (e.g. Emetere and Akinyemi, 2017) and degradation of air quality (e.g. Nakata *et al*., 2016; Bauer *et al*., 2016).

2.1.1. Aerosols Particle Size Distribution

Aerosol particle size distribution plays an important role in determining the lifetime of the aerosol in the atmosphere. The size distribution is related to the coagulation; condensation; and composition (Reid and Hobbs, 1998). The change in size distribution during transportation influences the Mie scattering calculations of radiative parameters (single scattering albedo,

extinction efficiency, asymmetry parameter), which plays a vital role in determining aerosol's impacts on climate (e.g. Tegen and Lacis, 1996).

Atmospheric aerosols' size ranges from about 0.001µm to 10µm in diameter, however aerosol particles can also be grouped in different size modes depending on their source of origin and age. The size modes of particles are differentiated by particle diameter (Seinfeld and Pandis, 1998; Alexandrov *et al*., 2005). Generally, the modes are categorized into (i) Nucleation/Aitken mode (0.001 – 0.1 µm), (ii) Accumulation mode (0.1 – 1.0 µm) and (iii) Coarse mode (> 1.0 µm) (see Figure 1). Nucleation /Aitken mode particles are formed from nucleation of gases to particles, they can cluster together and grow to the accumulation mode. Coarse mode particles are derived from mechanical processes such as breaking of sea waves and wind-blown dust and are globally significant.

The aerosol size distribution can be described using a lognormal distribution as follows:

$$N_a = n(D_p)dD_p = \frac{N_a}{\sqrt{2\pi}D_p\, In\,(\sigma_g)}\, exp\left[-\frac{(InD_p - InD_g)^2}{2In^2\sigma_g}\right] dD_p \quad (2.1)$$

where N_a is the total aerosols number concentration ($particles/cm^3$); D_g is the geometric mean diameter (µm); σ_g is the geometric standard deviation (unit less); $n(D_p)dD_p$ is the particle number concentration ($particles/cm^3$); and D_p to $D_p + dD_p$ is the diameter range.

The values of the mean diameter (D_g) and the geometric standard deviation can be calculated using equation (2.2) and (2.3) respectively:

$$logD_g = \frac{\int_0^\infty n(D_p) logD_p dD_p}{\int_0^\infty n(D_p) dD_p} \quad (2.2)$$

$$log\sigma_g = \sqrt{\frac{\int_0^\infty (logD_g - logD_p)^2 dD_p}{\int_0^\infty n(D_p) dD_p - 1}} \quad (2.3)$$

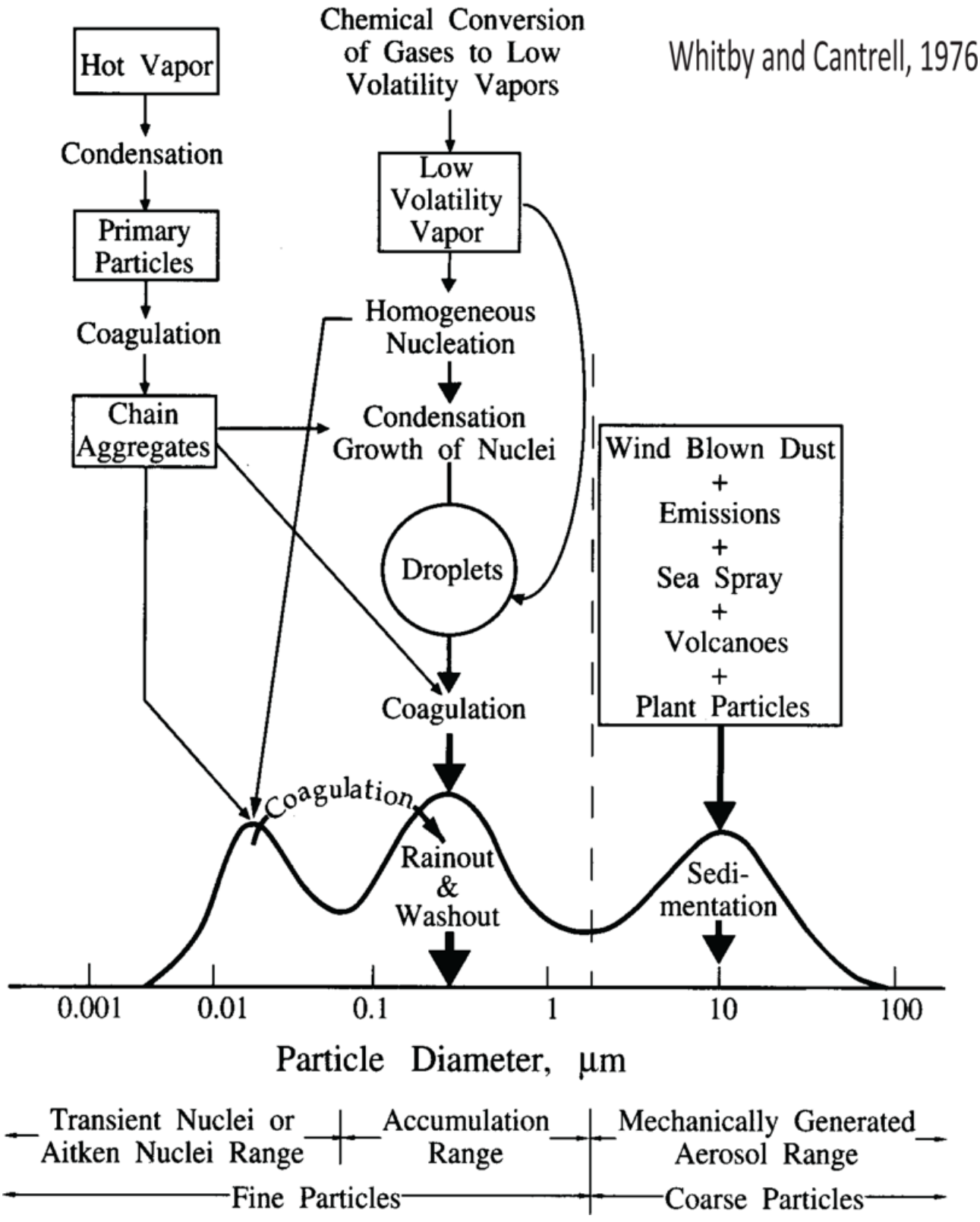

Figure 1: A schematic display of aerosol particle size distribution with their associated sources, sinks and modes (taken from Whitby and Cantrell, 1976).

2.2. Types of aerosols

There are various types of aerosols in the atmosphere that are formed by different processes. The nature of production and sources lead to particles of different chemical and optical properties. The following section explains the characteristics of different types of aerosols.

2.2.1. Mineral Dust Aerosols

Mineral dust is one of the most abundant aerosols emitted into the atmosphere with a global estimate of emissions of 1 000 - 5 000 million of tons per year (Huneeus *et al*., 2011) and makes up to one-third of the total global aerosol mass concentration (Penner *et al*., 2001; Tegen *et al*., 2002, 2004). Mineral dust aerosol has both natural and anthropogenic sources. Naturally, dust is dispersed into the atmosphere by the action of strong surface winds prevailing over semi-arid and arid areas. On the other hand, human activities, like agricultural practices (e.g. exposed land from overgrazing) and industrial practices (e.g. transportation of goods on a gravel road, construction and deforestation) contribute to the atmospheric burden of mineral dust aerosols. Mostly the mineral dust aerosols constitute of oxides (e.g. aluminium oxide (Al_2O_3), calcium oxide (CaO), iron oxide (FeO), silicon dioxide (SiO_2)) (Formenti *et al*., 2003; Perlwitz *et al*., 2015).

Africa is the largest source of dust in the atmosphere with the Sahara Desert being a major global contributor (e.g. Washington *et al*., 2003; Tanaka and Chiba, 2006). Even though dust is very common in desert areas, dust particles have atmospheric lifetime ranging from days to weeks and can be transported to the remote areas by the action of convection and large-scale circulation systems (e.g. Prospero, 1999; Knippertz and Todd, 2012). This makes mineral dust aerosols an important constituent of aerosol loading even at remote locations. For example, Aeolian dust from Sahara and Sahel regions can be transported across the Atlantic Ocean (e.g. d'Almeida, 1987; Prospero and Mayol-Bracero, 2013) and provides nutrients to the Amazon rainforest (Yu *et al*., 2015). Similarly, Asian dust can be carried out across the Pacific Ocean from the Gobi Desert to North America (Haung *et al*., 2015). It has been found that mineral dust from the Sahara region has contributed to North Atlantic sea surface cooling during the years 2005 and 2006 (e.g. Lau and Kim, 2007; Martinex Avellaneda *et al*., 2010); this shows that mineral dust is important even in areas where there are no sources of emission.

2.2.2. Sea Salt Aerosols

Sea salt aerosols are natural aerosols that are produced by physical processes over the sea surface (Kaufman *et al*., 2002). The particles occur through the bursting of air bubbles and tearing of drops from ocean waves (Blanchard and Woodcock, 1980). The production rate from wave tops depends on wind speed; wind speed of 10 $m\text{-}s^{-1}$ and higher have a potential to increase the production of a mass of small bubbles formed and hence increases the number concentration of sea salt aerosols. At moderate winds (i.e. less than 10 $m\text{-}s^{-1}$) the number concentration of sea salt aerosols is typically about 10 cm^{-3} and can increase up to 50 cm^{-3} under strong wind regimes (Andreas *et al*., 2001). Sea salt aerosols tend to absorb moisture (hygroscopic) from the air and are characterized by coarse particle size (Guo *et al*., 2019). The size of sea salt aerosols depends on the amount of humidity in the atmosphere. Their particle size is approximately 0.5 – 10 µm in diameter; due to their differences in particle size, sea salt aerosols have a great variety of atmospheric lifetimes (Murphy *et al*., 1998).

2.2.3. Sulphate Aerosols

Sulphate aerosols are a mixture of solid and liquid particles with a size range of 0.1 to 1.0 micrometre (µm) and are produced through either aqueous or gaseous phase reactions (Penner *et al*., 2001). Sources of tropospheric sulphate aerosols include industries, fossil and biomass burning that emit sulphur gases that consequently leads to the formation of sulphate aerosols in the atmosphere through chemical reactions. The sulphur gases that are produced by biological processes comprise of hydrogen sulphide (H_2S); dimethyl sulphide (DMS); sulphur dioxide (SO_2); and carbonyl sulphide (OCS). These biogenic gases can be oxidized via the gaseous phase to produce the gas SO_2, which eventually results in sulphate aerosols (e.g. Penner *et al*., 2001). The sulphur reactions that occur in both gaseous and aqueous phase have the potential to produce sulphate aerosols in the atmosphere (Gershenzon *et al*., 2001). Fossil burning contributes about 72 % of global sulphate aerosol concentrations while about 2% is produced by biomass burning sources (Haywood and Boucher, 2000, Qi and Wang, 2019). The other source of sulphate aerosols includes oceanic phytoplankton, which produces DMS that can be converted to sulphate aerosols. Sulphate aerosols derived from oceanic DMS contribute 19 % of the total sulphate aerosols in the atmosphere (Haywood and Boucher, 2000; Forster *et al*., 2007). Lastly, volcanic eruptions can also produce H_2S and SO_2 gases that are oxidized and form sulphate aerosols. Sulphate aerosols that are derived from volcanic activities make up to 7 % of the total sulphate aerosols in the atmosphere (stratosphere) (Forster *et al*., 2007).

2.2.4. Carbonaceous Aerosols

Carbonaceous aerosols contribute significantly to the total atmospheric particulate matter in the atmosphere. Generally carbonaceous aerosols make up about 20 - 50% of the total aerosol mass in the atmosphere (Putaud *et al*., 2010; Kanakidou *et* al., 2005). Carbonaceous aerosols are made up of organic matter derived from anthropogenic combustion sources and natural sources (Seinfeld and Pandis, 2006). Carbonaceous aerosols are relatively small (sub-micron) and mainly fall in the nucleation and Aitken modes. On average their atmospheric lifetime ranges from several days to weeks. Carbonaceous aerosols comprise of black carbon (BC) and organic carbon (OC). The former originates from anthropogenic combustion sources that include industrial emissions, domestic heating, and road transport and can also come from natural sources like biomass burning. BC particles are spherical in shape and can aggregate to form clusters or chains of soot. BC particles absorb sunlight and heat up the atmosphere where the particles are found. The absorption of light in the column of atmosphere results in positive radiative forcing, hence cooling of the surface temperature. The BC, coated with organic compounds, can act as CCN and hence change cloud albedo through indirect effects (Dusek *et al*., 2006; Koch *et al*., 2011; Cherian *et al*., 2017; Dalirian *et al*., 2018). BC often forms an internal mixture with other aerosol constituents; this mixed state is important in determining its climate effect (e.g. Chung and Seinfeld, 2005). For example, a coated BC absorbs more radiation than an uncoated one (Adachi *et al*., 2010).

The fraction of carbonaceous aerosols that are constituting of condensed organic compounds are called organic carbon (OC). These consist of small bright coloured aerosols that are mainly formed from the combustion of biogenic material and fossil fuels (Schultz *et al*., 2008; Zhang *et al*., 2013; Liu *et al*., 2016). OC aerosols can be emitted into the atmosphere primarily through combustion and secondarily through condensation of low vapor pressure compounds (Robinson *et al*., 2007; Gentner *et al*., 2012). OC can scatter solar radiation and may lead to the direct radiative effects (Boucher *et al*., 2013).

2.3. Aerosols Sink

After being emitted into the atmosphere, aerosol particles are transported through the air, where they can undergo several physical and chemical processes. These processes can alter their properties (i.e. composition, size, etc.). In the end, the particles will be removed from the atmosphere through deposition. This process plays an important role in regulating the concentration of particles in the atmosphere. Aerosol deposition can harm the environment through acting as a source of nutrients and pollution to marine and terrestrial ecosystems (e.g. Jickells *et al*., 2005; Duce *et al*., 2008; Mahowald *et al*., 2017). Deposition processes commonly occur through two mechanisms, namely dry and wet deposition (e.g. Knote *et al.*, 2015; Castillo *et al*., 2017; Wu *et al*., 2018). These mechanisms are influenced by aerosols'

properties (e.g. particle size, density, and composition) as well as prevailing atmospheric conditions (Seinfeld and Pandis, 2006). In the following two sub-sections, the detailed description of the aerosols' deposition mechanisms is provided.

2.3.1. Dry Deposition

Dry deposition is a process in which aerosol particles are removed from the atmosphere to settle upon the Earth's surface. Generally, aerosols' dry deposition occurs in the absence of rain (e.g. Petroff *et al*., 2008). After the particles have been ejected into the atmosphere from their emission sources, they are transported by actions of prevailing winds. At a later stage, dry deposition occurs through either impaction or gravitational sedimentation or interception. These processes depend on various factors such as particle properties, meteorological conditions and land surface (e.g. Wu *et al*., 2018). Dry deposition globally accounts for 10 – 20 % of particle removal from the atmosphere. Dry deposition can be estimated using deposition velocity, V_d defined by equation (2.4),

$$V_d = \frac{F_d}{C_a} \quad (2.4)$$

where V_d is the dry deposition velocity (ms^{-1}), F_d is the dry deposition flux ($g \cdot m^{-2}s^{-1}$) and C_a is the concentration of the substance on aerosol particles in the atmosphere (gm^{-3}).

2.3.2. Wet Deposition

Wet deposition is the process by which aerosol particles are removed from the atmosphere by the action of interacting with water in the atmosphere (either by rain droplets, hail, fog or snow). This process depends on the amount and intensity of precipitation and on particle properties. Wet deposition becomes the main form of sinking of aerosol particles especially in areas that receive high precipitation. This process can take several forms that include wash- and rain-out. Wash-out occurs through the process of below cloud scavenging, whereby aerosols are being incorporated into rain droplets and fall to the Earth's surface as rainwater. Rain-out occurs when aerosols act as cloud condensation nuclei (CCN) to grow to cloud droplets that eventually fall to the surface of the Earth as rain.

2.4. Aerosols' Properties

Aerosols vary greatly in their properties; in this section an overview is given of important properties that are related to refractive ability of aerosols.

2.4.1. Aerosols' Refractive Index

The aerosols' refractive index is a key parameter to measure their ability to scatter and absorb light, and of particles to obtain radiative effects. The different aerosol species constitute of different chemical compositions, which determine their complex refractive index. The complex refractive index (m) of an individual particle contains real and imaginary parts and can be expressed through the following equation (2.5):

$$m = n + ik \ (2.5),$$

where *n* is the real part of the refractive index which also indicates the phase velocity and *k* is the imaginary part of the refractive index. The real part, *n,* is responsible for scattering properties of a homogeneous particle (e.g. Jurányi *et al*., 2015) while the imaginary part, *k,* is responsible for absorption (Müller *et al*., 2009). Both the real and imaginary parts of the refractive index depend on the wavelength thereof. For example, whenever an imaginary part, *k* is equal to 0 at a given wavelength, this indicates that the particles do not absorb radiation at that wavelength. In general, the real part*, n* is found between 1.3 – 1.6 while the imaginary *k* varies from 5×10^{-9} to 5×10^{-1} at visible or IR wavelengths. **Table 1** shows a general example of real and imaginary parts of the refractive indices of different aerosol species at a visible wavelength (Lee and Adams, 2010).

Table 1: The real and imaginary parts of the aerosols' refractive index at visible wavelength (Lee and Adams, 2010).

Aerosol Component	Real Part	Imaginary Part	References
Sulphate,	1.43	1.0e-8	Hess *et al*. (1998)
Elemental Carbon	1.95	0.79	Bond and Bergstrom (2006)
Organic Carbon	1.53	0.006	Shettle and Fenn (1979)
Dust	1.56	0.006	Torres *et al*. (2002)
Sea-salt	1.50	1.0 e-8	Shettle and Fenn (1979)
Water	1.33	1.96e-9	Hale and Querry (1973)

2.4.2. Aerosol Optical Depth

Aerosol Optical Depth (AOD) is a parameter used to measure the attenuation of light by aerosol particles in the atmosphere. The AOD can be defined by equation (2.6):

$$AOD = \int_0^\infty \delta \exp(z) dz \ \ (2.6),$$

where dz is the vertical optical path, z is elevation and $\delta \exp\ (z)$ is the aerosol extinction coefficient (Stone *et al*., 2014). AOD is a unit-less parameter that measures the degree of light extinction by aerosol particles. The light extinction is proportional to AOD, i.e. light extinction increases as AOD increases. For example, more particles in the atmosphere (hazy condition)

will cause a high rate of extinction of light that results in high values of AOD (≥1) and the opposite is true about the clear sky.

2.4.3. Aerosol Extinction Coefficient

The extinction coefficient is a measure of the ability of a particle to absorb and scatter light at the given wavelength. It is given by Bouguer's law, also known as Lambert-Beer law (equation 2.7):

$$\frac{I}{I_0} = exp\,(-\sigma_e L) \quad (2.7),$$

where I is light intensity; I_0 is incident light intensity; σ_e is the extinction coefficient of the aerosol and L is a path length of the light through the aerosol. The extinction coefficient contains information about the aerosol particles' size distribution and concentration.

2.4.4. Aerosol Single Scattering Albedo

Single Scattering Albedo (SSA), ω_0 is the ratio of the scattering to the total extinction of light (sum of scattering and absorption) by aerosol particles (Hess *et al.,* 2010) and can be defined as:

$$\omega_0 = \frac{\sigma_s}{\sigma_a + \sigma_s} \quad (2.8),$$

where ω_0 is fraction of light extinction (lost light) σ_s and σ_a are scattering and absorption coefficients, respectively. The values of SSA, designated by ω_0, vary from 1 to below 0.5. ω_0 = 1 for extinction that results entirely from scattering particles and less than 0.5 for absorbing particles. ω_0 = 0 represent an unrealistic situation that the particle is fully absorbing, and all light extinction is due to absorbing (Wallace and Hobbs, 2006). The SSA is an important parameter to determine the direct effect of aerosols on climate and is proportional to radiative forcing sign (Seinfeld and Pandis, 2006; Leahy *et al*., 2007; Montilla *et al*., 2011)

2.5. Aerosol's Perturbation on Climate

The climate system is said to be at radiative balance when there is an energy balance between incoming solar radiation and outgoing terrestrial radiation. Any factor that can disturb climate system energy balance, can consequently cause climate perturbation and this is referred to as radiative forcing (Wm^{-2}). The radiative forcing is defined as the measure of the change in the net radiative fluxes because of some climate variables (IPCC, 2013). The major forcing mechanisms are results of a change in the composition of the atmosphere, for example, a change in aerosols in the atmosphere can result in the changes in radiative fluxes at the top

of the atmosphere, within an atmospheric column as well as at the surface. After climate system has reached a radiative balance, the relationship between the change in radiative forcing ΔF and the change in Earth's mean temperature ΔT_s can be expressed through the following equation:

$$\Delta T_s = \lambda \Delta F \quad (2.9),$$

where T_S is mean surface temperature (K), λ is the climate sensitivity parameter with units K/(Wm^{-2}) and ΔF is the change radiative forcing (Wm^{-2}).

Although aerosols make up a small fraction of the mass in the atmosphere, they pose a significant impact on Earth's radiative balance. At a global scale, radiative forcing due to aerosols and their climatic impact is apparent and it is thought to offset some of the global warming caused by the increased emissions of greenhouse gases (IPCC, 2013). However, due to aerosols' characteristics and heterogeneity in space and time, the estimation of their radiative forcing remains uncertain. Figure 2 summarizes the global radiative estimates from 1980 - 2011 of various radiative forcing agents. On the diagram, the length of the horizontal rectangular bar denotes a central or best estimate of the forcing, while each solid error line is an estimate of the uncertainty ranges associated with the forcing (Myhre *et al*., 2013). According to figure 2, the total aerosols effect, including direct effect and aerosol – cloud interactions is a negative radiative forcing on climate. However, there is large uncertainty (large error bar) regarding estimation of the magnitude of radiative forcing. Uncertainty arises from limited knowledge of their emission sources, optical properties, and complex distribution with respect to space and time (Myhre *et al*., 2013).

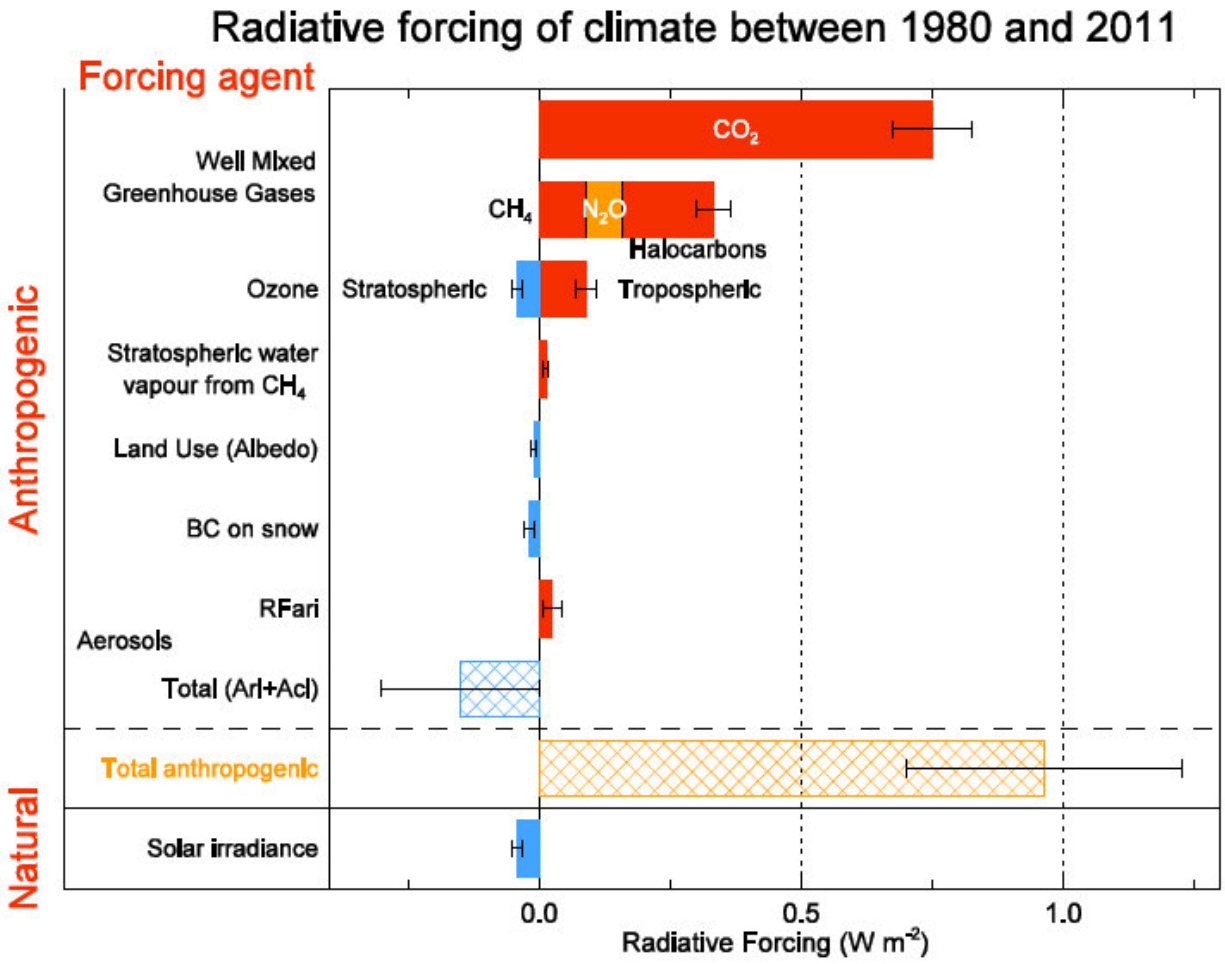

Figure 2: The radiative estimates since 1980 - 2011 of various radiative forcing agents. On the diagram, the length of horizontal rectangular bar denotes a central or best estimate of the forcing, while each solid error line is an estimate of the uncertainty ranges associated with the forcing (Myhre *et al*., 2013).

2.6. Aerosol Observation Techniques

This section describes the types of aerosol observations that were used in this study.

2.6.1. Ground based Observations

One of the widely distributed aerosol surface networks is the AErosol RObotic NETwork (AERONET) established by NASA and PHOtométrie pour le Traitement Opérationnel de Normalisation Satellitaire (PHOTONS) (Holben *et al.,* 1998). AERONET is a worldwide-established ground-based aerosol monitoring network and it provides long-term measurements of AOD and aerosol properties at high accuracy (e.g. Dubovik *et al*., 2000). There are now more than 700 AERONET stations distributed over the globe; figure 3 shows the geographical location of some of AERONET stations. The AERONET stations consist of

a robotical network of Cimel sun photometers. The sun photometer measurements are taken at an interval of 15 minutes at standard wavelengths of 340, 380, 440, 500, 675, 870, 936 and 1020 nm (Holben *et al*., 1998). Aerosol optical properties are retrieved at all wavelengths except for 940 nm, which is reserved for column water vapour. AERONET provides direct measurements of aerosol optical properties with a high temporal resolution, however, are limited in terms of global coverage (Dubovik *et al*., 2002; Lee *et al*., 2010). AERONET measurements are often linked with satellite measurements to account for limited global coverage (e.g. Xue *et al*., 2012; Mishra *et al*., 2016; Fu *et al*., 2018).

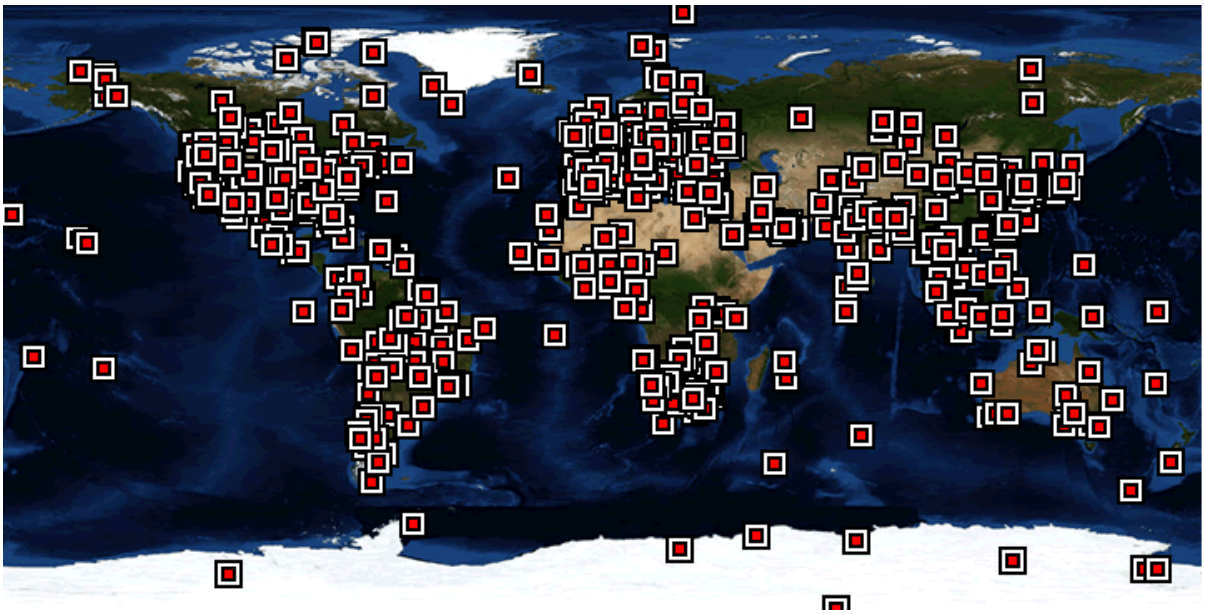

Figure 3: Global location AERONET stations (https://aeronet.gsfc.nasa.gov/ -13/04/2019).

2.6.2. Space based Observations

Aerosols' microphysical and optical properties can be retrieved from space borne sensors, the most popular of this being the Moderate Resolution Imaging Spectro-radiometer (MODIS). MODIS can produce global coverage in 1 or 2 days and the aerosol measurements they produce is AOD. During clear skies (maximum visibility) the reflectance and absorption of light by the atmosphere is low and this results in AOD value of less than 0.1, whereas during hazy conditions, the atmosphere's ability to reflect and absorb visible light is high which results in higher values of AOD (~1.0 or higher). Satellites can retrieve and provide long-term spatial coverage of AOD values at coarse resolution (e.g. 1° × 1°), aerosol types and size of distribution over land and ocean. However, these measurements are limited in terms of accuracy (Kaufman *et al*., 2002a; Myhre *et al*., 2005).

2.7. Aerosols over Southern Africa

Southern Africa is situated at the southernmost part of the African continent; the terrain ranges from forests, grasslands to deserts. Due to its unique geographical location, economical activities, atmospheric circulation and climate, Southern Africa is influenced by various kinds of aerosols. Various studies have attempted to characterize aerosol particles over the region; these studies have found that total loading in the atmosphere is composed of aerosols derived from biomass burning (e.g. Liu *et al*., 2000; Abel *et al*., 2003; Swap *et al*., 2003; Lu *et al*., 2018), mineral dust (e.g. Piketh *et al*., 1999a; Bhattachan *et al*., 2012; Tesfaye *et al*., 2015), and marine and anthropogenic activities (e.g. Mélin *et al*., 2013; Kuik *et al*., 2015).

Biomass burning arises from both natural and anthropogenic activities. Burning of vegetation can occur naturally through igniting of dry vegetation by lightning activities. On the other hand, anthropogenic biomass burning occurs through burning of dry vegetation on agricultural practice or domestic cooking and heating (Roden *et al*., 2005). Generally, most biomass burning results from anthropogenic activities (Bond *et al*., 2004). Over Southern Africa biomass burning occurs over savannah regions during the dry season (May to October) of every year. An effort to investigate the role of vegetation fires was conducted during the dry season of 1992 by the Southern Africa Research Initiative (SAFARI) experiment over Kruger National Park, South Africa (Lindesay *et al*., 1996; Swap *et al*., 2003). The fires contribute about 30% of global biomass burning aerosols (Scholes *et al*., 1996; Van der Werf, *et al*., 2010). These contribute a substantial amount of emissions of radiative and chemically important trace gases; this includes methane (CH_4), carbon monoxide (CO), ammonia (NH_3), nitrous oxide (N_2O), nitric oxide + nitrogen dioxide (NO_x) and many other species volatile organic compounds (VOC_s) that are released as a primary product during burning processes. Formation of ozone occurs as a secondary product of biomass burning (Helas *et al*., 1995). Biomass burning is also a major source of climatic important aerosol particles that include black carbon. Biomass burning emissions have various impacts on the environment such as changes in biogeochemical cycles, reduction in flora and fauna biodiversity, soil depletion and changes in radiative balance.

Aerosol loading over Southern Africa changes from one season to the next and from one region to another. The variability in seasonal emissions and meteorological transportation, the AOD exhibits a strong seasonal cycle. The seasonality of AOD climatology over Southern Africa has been widely studied using various tools including measurements and satellite techniques (e.g. Kirchstetter and Novakov, 2003; Haywood *et al*., 2003; Posfai *et al*., 2003; Laakso *et al*., 2008; Tiitta *et al*., 2013; Vakkari *et al*., 2013). Queface *et al*. (2011) studied climatology from long term observation sites of Mongu and Skukuza in Zambia and South

Africa respectively and found that AOD is described by seasonal means of (0.11 to 0.17), (0.20 to 0.27), and (0.30 to 0.27) from December to May, June to August and September to November, respectively. A similar magnitude of AOD with lows that range between 0.064 – 0.21, a median of 0.06 – 0.14 and peak of 0.095 – 0.50 has been found using AERONET data that are found over Southern African sites (Horowitz *et al*., 2017). The distribution of AOD also shows the latitudinal variation with a northern part towards the equator exhibiting high AOD, and low over the southern part. Satellite analysis shows that the high AOD over the region corresponds to the biomass-burning period (Tesfaye *et al*., 2011; Hersey *et al*., 2015).

Many studies have examined the relationship between seasonal varying AOD and radiative forcing ranging from the top of the atmosphere (TOA) and the surface over Southern Africa (e.g. Tummon *et al*., 2010; Tesfaye *et al*., 2011; Queface *et al*., 2011; Adesina *et al*.,2017; Lu *et al*., 2018; Adesina *et al*., 2019) Few studies have focused on the surface temperature response of the Southern African region to aerosol forcing. Tummon *et al*., (2010) has focused on the direct and semi direct aerosol effects on the Southern African regional climate and found that aerosols result in decreased simulated surface temperatures. This is argued to be the direct effect of aerosol scattering and absorption which reduces shortwave radiation that reaches the earth's surface. Using two earth system models, namely Community Earth System Model (CESM) and National Aeronautics and Space Administration (NASA) Goddard Institute for Space Studies (GISS) ModelE2, Gettelman *et al*. (2015) studied the impact of aerosol radiative effects on surface temperature. The experiment in both models when performed with aerosol emissions from different years (2000 – 1850, 2000 – 1980, 2010 – 2000), results in both model's aerosols induced changes of surface temperatures. CESM's experiment over Southern Africa shows significant cooling of surface temperature (0.9 – 1.5 °C) for the period 1850 to 2000, less cooling (0 – 0.6°C) for 1980 to 2000 and for the period 2000 to 2010, the southern and northern parts of Southern Africa show warming (0.3 – 0.5 °C) while the central part shows a slight cooling (0 – 0.3 °C). Regarding the experiment achieved with GISS ModelE2, the results show cooling (0.2 – 0.4 °C) over the southern and northern part and warming (0 – 0.3 °C) over the central part of Southern Africa for the period 1850 to 2000, cooling (0 – 0.4 °C) for period 1980 to 2000 and cooling (0 – 0.25 °C) over the central part of Southern Africa with slight warming (0 – 0.15 °C) elsewhere (Gettelman *et al*., 2015).

Chapter 3: Data and Methods

3.1. Study Area

The area considered in this study lies in the subtropics and extends from 10 °N to 35 °S and 0 °W to 60 °E (Figure 4). The study area is placed between the southern Atlantic Ocean in the west and Indian Ocean in the east. The climate of the study region is subtropical, and it varies from arid to humid subtropical conditions (Christensen *et al*., 2007). Most of the region receives rainfall in summer except the south-western part of South Africa, which receives winter rainfall from mid-latitude cyclones. Rainfall distribution is varying across latitude with northernmost countries like Congo, Tanzania, Cameroon, Gabon, Democratic Republic of the Congo and Equatorial Guinea receiving higher annual rainfall and lower variability, and southern countries like Angola, Botswana, Mozambique, Zambia, Namibia and Zimbabwe receive low annual rainfall and higher variability (e.g. Richard *et al*., 2001; Fauchereau *et al*., 2003; Hulme *et al*., 2005; UNEP and ICRAF, 2006). The main drivers of climate are large scale atmospheric patterns which include the South-easterly Wind System which transfers moisture from the Indian Ocean (e.g. Nicholson and Grist, 2003), sub-tropical eastern continental moist maritime system which experiences cyclones and the Inter-Tropical Convergence Zone (ITCZ) which results in wet and dry seasons over the tropics (Preston-Whyte and Tyson, 1988). Other weather systems such as ridging high-pressure systems play important role in moisture advection that triggers convective systems, convective systems are responsible for rainfall over the region (Taljaard, 1996). Most of the mean annual rainfall over southern Africa is associated with ridging high systems (Weldon and Reason, 2014). The El Niño-Southern Oscillation (ENSO) and Indian Ocean Dipole (IOD) also plays an important role in fluctuations in summer seasonal rainfall of the study area (e.g., Saji et al., 1999; Nicholson and Selato, 2000; Reason et al., 2000; Behera & Yamagata, 2001; Giannini et al., 2003; Christensen et al., 2007). The former is associated with the difference in temperature in the opposite parts of the Pacific Ocean, while the latter refers to its Indian Ocean equivalent. El Niño often results in drier than normal conditions while La Niña is associated with above-normal wet conditions over southern Africa (Cook, 2000; Reason and Jagadheesha, 2005; Rouault and Richard, 2005; Hoell et al., 2017; Pomposi et al., 2018). On the other hand, IOD oscillates between positive, neutral, and negative phases. A positive Indian Ocean Dipole means warmer sea temperatures in the western part of the Indian Ocean with the opposite in

the east. This results in wetter conditions in the west while drier in the east (Clark et al., 2003; Black et al., 2003). Both ENSO and IOD are linked through Walker Circulation (easterlies). Several studies have focused on the interaction between the two oceanic phenomena and found that El Niño is associated with positive IOD and La Niña with negative IOD (Reason et al., 2000; Hoell et al., 2017). Apart from ENSO and IOD, southern Africa receives enormous rainfall from subtropical lows such as Cut-off Lows (COLs). During the summer season, COLs cause a significant amount of rainfall over a short period of time can results in flooding over southern and eastern coastal areas of the region (Jury and Levey, 1993b; Singleton and Reason, 2007b).

The temperatures over the study area show a highly decadal and inter-annual variability over a longer timescale (Tyson *et al*., 2002). The multi-decadal (50 to 100 years) analysis of near-surface temperature over many parts of the study area points towards increasing warming signal (Kruger and Shongwe, 2004; Nicholson *et al*., 2013; Niang *et al*., 2014). There is strong evidence of significantly higher temperatures in recent years (last 2 decades) with minimum temperature warming at a faster rate relative to maximum temperatures (New *et al*., 2006; Collins, 2011; Kruger and Sekele, 2012; Funk *et al*., 2012).

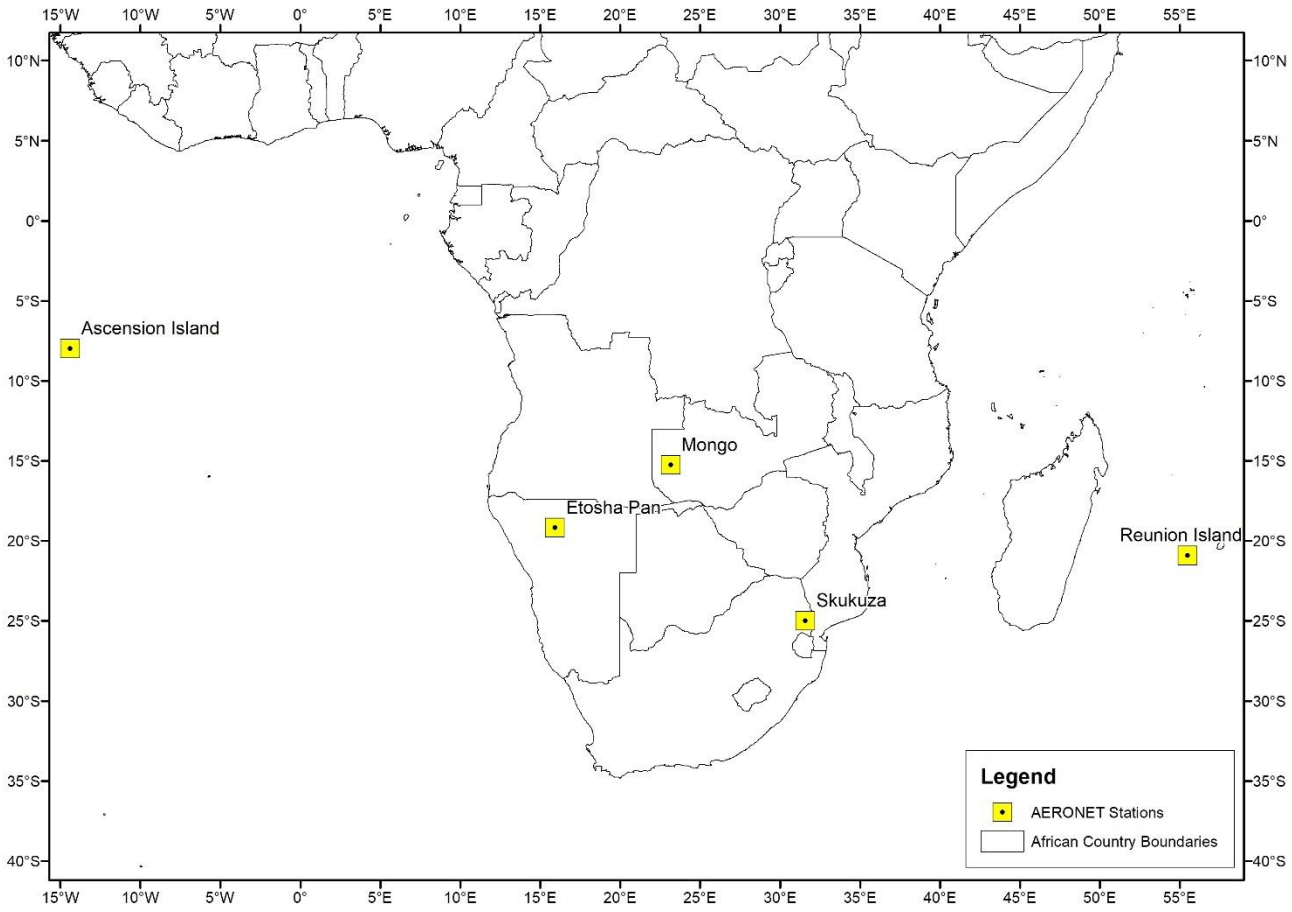

Figure 4:The map showing study domain 10 °N to 35 °S and 0 °W to 60 °E with AERONET Sun photometer stations used in this study shown in yellow boxes.

3.2. GCM Simulations

The simulations were achieved using two GCMs, namely the GISS modelE (Hansen *et al*., 2005; Schmidt *et al*., 2005) and the CCAM (McGregor, 2005). Two different GCMs were used to conduct climate model inter-comparison of surface temperature sensitivity to aerosols. Simulations have been done under the Atmospheric Model Inter-comparison Project (AMIP) experiment. In this experiment, both GCMs are constrained by sea ice and sea surface temperatures from 1979 to present climate (Gates *et al*., 1998). Surface air temperature and Aerosol Optical Depth (AOD) at 550nm (AOD_{550}) has been simulated at a coarse resolution of 2° × 2.5° (approximately 222 by 277 km) for period 2000 – 2014, using CMIP5 emissions in both models. The CMIP5 is a standard coordinated project aimed at providing infrastructure support for model simulations, validation, inter-comparison, data access and documentation. The GISS modelE (Hansen *et al*., 2005; Schmidt *et al*., 2005) and CCAM (McGregor, 2005) simulation utilized in this study is obtained from NASA-GISS climate model group and Council for Scientific and Industrial Research (CSIR), respectively. Both models consider sulphate,

dust, sea salt and carbonaceous aerosols. They are both AMIP style and have been run over Southern Africa region before.

Simulations with and without aerosol schemes were run globally with both models. However, this study analysis were carried out only over the region shown in Figure 4.

3.2.1. GISS-modelE Description

The GISS-modelE (Schmidt *et al*., 2005, 2006) is a coupled atmosphere - ocean model developed to participate in the CMIP5 by the NASA GISS. The GISS-modelE development process started three decades ago (e.g. Hansen *et al*., 1983; Hansen *et al*., 2000; Schmidt *el at*., 2006) and the current version can simulate different configurations of the climate system including the ocean, sea ice, land surface components, atmosphere, chemistry, aerosols and carbon cycle (Kim *et al*., 2011; Shindell *et al*., 2013; Miller *et al*., 2014; Schmidt *et al*., 2014).

Model Dynamics

The atmospheric model has a Cartesian grid and horizontal resolution of 2° × 2.5° (approximately 222 by 277 km). The model has forty (40) vertical hybrid sigma layers and a model top at 0.1 mb. The model employs physics from GISS model II improved representation of physical processes (Hansen *et al*., 1983) that enhance the ability to reproduce various components of the Earth's climate system. The atmosphere is coupled with two dynamic ocean components namely Russel and Hybrid Coordinate Ocean Model (HYCOM) (Russell *et al.,* 1995; Sun and Bleck, 2006). The model uses monthly varying sea surface temperatures (SST) and sea ice fields (Rayner *et al*., 2003).

Aerosol Scheme

The atmospheric composition and the aerosols' impact on the clouds are calculated using the MATRIX aerosols scheme (Bauer *et al*., 2008) The model forcing arise from ozone (O_3), well-mixed greenhouse gases (GHGs), stratospheric water vapour and tropospheric aerosols including black carbon (BC), nitrates, organic carbon (OC) and sulphates. Sulphates, BC, nitrates and OC are time variable; sea salt and soil dust are not (Hansen *et al*., 2007). The present-day nitrate emissions used are based on findings by Liao *et al*. (2004). Volcanic and mineral dust aerosols emissions used are described in Hansen *et al*. (2002). The representation of the mineral dust cycle is improved by a dust model embedded within the recent version of the GISS GCM. The dust model reflects the new measurements and the full descriptions are obtained in section 2 of Miller *et al*. (2006). For radiative calculations, aerosols

are approximated as externally mixed. The effect of humidity on nitrates, sulphates and OC aerosol sizes, is included and it is found that the humidity effect increases optical thickness and radiative forcing.

The one-moment aerosol (OMA) scheme is a mass-based scheme and has no microphysics. Aerosols are externally mixed, and the scheme transports 34 tracers (Bauer *et al*., 2007; Bauer and Koch, 2005; Koch *et al*., 2006; Tsigaridis *et al*., 2013). The aerosols modules in OMA scheme include carbonaceous aerosols (Koch *et al*., 2007), sulphates (Koch *et al*., 2007, 2011), sea salt (Koch *et al*., 2006; Tsigaridis *et al*., 2013), secondary organic aerosols (Tsigaridis and Kanakidou, 2007), nitrates (Bauer *et al*., 2007) and dust (Miller *et al*., 2006). The scheme also predicts dimethyl sulfide (DMS), methanesulonate (MSA), and sulphur dioxide (Koch *et al*., 2006). Aerosols' hydration is calculated in radiation code (Tang and Munakelwitz, 1994).

3.2.2. CCAM Description

CCAM is a global atmospheric circulation model developed by the Commonwealth Scientific and Industrial Research Organisation (CSIRO) (McGregor, 1996; 2005a; 2005b; MacGregor and Dix, 2001). The model has been run in a non-stretched mode to provide quasi-uniform horizontal resolution of 2° × 2.5°. The model has 27 sigma layers and a model top at 0.1 mb. CCAM employs semi-implicit semi-Lagrangian and wide range of physical parameterizations (McGregor, 1996).

Model Dynamics

The CCAM model employed the 2-time level semi-Lagrangian, semi-implicit method to derive the solution of hydrostatic equations. The horizontal advection is employed with total-variation-diminishing (TVD scheme) vertical advection (McGregor, 1996). The semi-Lagrangian horizontal advection, together with TVD scheme, handles the tropopause temperature gradient better. The model uses a reversibly staggered grid that pivots between the Arakawa A and C grids. This gives better dispersive behaviour for both the atmosphere and ocean models. The model incorporates a wide range of physical parameterisations. It employs the Geophysical Fluid Dynamics Laboratory (GFDL) long-wave and short-wave radiation parameterisation (Lacis and Hansen, 1974; McGregor and Dix, 2001); liquid and ice water schemes are employed to parameterize microphysical processes (e.g. precipitation formation in warm, strati-form, and mixed-phase clouds). It has employed a CSIRO mass-flux cumulus convection scheme that includes downdrafts and detrainment and gravity wave drag scheme. The stability dependent boundary layer scheme employed is based on Monin-Obukhov similarity theory (McGregor *et al*., 1993). The boundary layer scheme, together with the non-

local vertical mixing, enhances the mixing of cloudy boundary layered air. A canopy scheme of six layers for soil moisture, six layers for soil temperature and three layers for snow is included.

Aerosol Scheme

The interactive aerosol treatment is from the Mk3 CSIRO Atmospheric Global Climate Model (Gordon *et al*., 2002). The aerosol scheme employed treats the effect of carbonaceous aerosol (OC and BC), sulphate, sea salt and mineral dust (Rotstayn *et al*., 2012). The direct effect of aerosol species on shortwave radiation and dust impact on longwave radiation is handled by the radiation scheme (Chou and Lee, 2005; Rotstayn *et al*., 2007). The transportation of aerosols and other atmospheric spatial variables such as atmospheric water vapour occurs by vertical advection within convective clouds, horizontal advection and vertical turbulence mixing (Rotstayn and Lohmann, 2002b). The flux-corrected transport scheme is responsible to drive vertical advection (Van Leer, 1977). The semi-lagrangian scheme (McGregor, 1993) is used to handle the horizontal advection and vertical turbulence mixing treatment is based on stability depended on K-theory (Louis, 1979). Convective processes e.g. shallow; midlevel and deep convection are represented by the convective scheme (Gregory and Rowntree, 1990).

The sulphur cycle is handled by a single moment prognostic scheme with prognostic variables being sulphur dioxide (SO_2) and dimethyl sulphide (DMS). The sulphur emission, its chemistry and its wet and dry deposition, is calculated online with meteorology in the GCM. The sulphate chemistry and radiative forcing treatment are like that in ECHAM4 (Feichter *et al*., 1996). The oxidation product considered is only SO_2 and thus ignoring the other small yield, like methane sulfonic acid (MSA) (Rotstayn, and Lohmann, 2002). Cooke *et al*. (1996) used the BC module to model carbonaceous aerosol. The carbonaceous aerosol and sulphates' lifetime in the atmosphere are modulated by both dry and wet deposition. The sea-salt aerosol is diagnosed at each time step as a function of wind speed and is assumed to be well mixed in the marine boundary layer (O'Dowd *et al*., 1997). The framework obtained from Lu and Shao (1999), also includes emissions of windblown dust. The shortwave and longwave effects of different types of aerosol species are treated by the radiation scheme. The aerosol species include BC, tropospheric SO_4, sea salt, stratospheric aerosol, particulate organic matter (POM) and dust particles (Rotstayn *et al*., 2007). In the radiation scheme, the carbonaceous aerosol is assumed to be an internal mixture while other aerosol species are treated as an external mixture (Rotstayn *et al*., 2007; Rotstayn *et al*., 2013). The treatment of aerosol first and second indirect effects on liquid water clouds, is also included (Rotstayn *et al*., 2013). The calculation

of the first indirect effect follows Rotstayn and Liu (2009) and the calculation of aerosol second indirect effect follows Rotstayn and Liu (2005).

3.3. Observation Data

Observation data are commonly used in climate research to evaluate climate model performance. In this study, spatial data of near-surface temperature is used and that was compared against simulated near-surface temperature to investigate how well the GCMs simulate the climate of Southern Africa. For AOD_{550}, both station data and satellite data are used. Station data is used to evaluate the model 's ability to simulate temporal distribution, while the satellite data is used to evaluate the models' ability to simulate the spatial distribution of AOD_{550} over Southern Africa.

The surface temperature used is CRU TS3.22 obtained from the Climate Research Unit (CRU) of the University of East Anglia (New *et al*., 1999 and 2000). The CRU TS3.22 covers land areas and has been constructed from monthly observations from meteorological stations across the world using thin spline interpolation to get the grid at a resolution of 0.5 degrees in latitude and longitude (Harris *et al*., 2014). The raw CRU TS station records come with missing values and is not specifically homogenous. However, the data have undergone extensive quality control measures (e.g. Harris *et al*., 2014). The available time-series data is for the period 1901 – 2014; for this study however, data from 2000 - 2014 were used. The monthly values were averaged for seasons, i.e. December-January-February (DJF), March-April-May (MAM), June-July-August (JJA) and September-October-November (SON).

Long-term time series of AOD measured at 440nm and Angstrom exponent of extinction for 440nm to 870 nm were obtained from the AERONET website. As explained in section 3.5.1 below, the Angstrom exponent is used to convert AOD_{440} to AOD_{550} to compare to simulated AOD. AERONET database is provided in three different levels namely Level 1.0, Level 1.5, and Level 2.0 for data quality. Level 1.0 was defined as pre-screened data in Version 2, while Level 1.5 was defined as the near-real-time cloud cleared data and Level 2.0 as automatically cloud cleared manually quality-controlled data. For Version 3 which is used in this study, Level 1.5 and Level 2.0 definition have been modified, Level 1.5 represents near real-time automatic cloud screening and instrument anomaly quality controls while Level 2.0 applies pre-field and post-field calibrations (e.g. Smirnov *et al*., 2000; Giles *et al*., 2019). The AOD measurements used here, have been sampled on Ascension Island; Etosha Pan, Namibia; Mongu, Zambia; Reunion Island; and Skukuza, South Africa. These stations were found within the Southern African domain (see figure 4) and they provide an opportunity for investigating the temporal variability of aerosol optical properties within the study domain.

The gridded data of AOD at 550nm for period 2000 – 2014 are obtained from satellite-based instrument MODIS – Terra MOD08_M3 v6 (Levy *et al*., 2007; Platnick, *et al*., 2015). MODIS-Terra passes over study domain between 09:00 and 11:00 LT each day (Hersey *et al*., 2015). The instrument produces samples of AOD_{550} at global coverage every 1 – 2 days in 36 spectral bands. MODIS data have been quality controlled, the details about Quality Assurance or Quality Assessment (QA) can be found in the MODIS Atmosphere website (modis-atmos.gsfc.nasa.gov/reference_atbd.php; www.mcst.ssai.biz/L1B/L1B_docs). QA weighted average has been applied to data following Hubanks *et al.*, (2008). The QA process includes various flags like (i) confidence, (ii) retrieval status, (iii) retrieval processing path, (iv) retrieval method and (v) data or scene characteristics. For this study, the monthly mean AOD (MOD08_M3_v6) at a resolution of 1° × 1° is used. The seasonal averages of MODIS aerosol optical depth are retrieved from the Giovanni website (https://giovanni.gsfc.nasa.gov/giovanni/).

3.4. R- Programming

This study uses R-programming software to compute statistical analyses and plotting of statistical maps and spatial temperature anomalies maps. R is a free software environment within which a variety of statistical techniques can be implemented and visualized. It facilitates advanced data handling, analysis and graphical display. R provides a wide variety of statistical functions (e.g. classical statistical tests, linear modelling, nonlinear modelling, clustering, time series analysis etc.). The software can be easily extended through use or installation of more advanced modern statistical packages that are available through CRAN internet sites. Beside algorithm development, calculations and visualization, R can also be used for document writing through its LaTeX environment.

3.5. Methods

3.5.1. Climate Model Evaluation

To investigate if the model performs well in simulating the current climate, model evaluation against observations (detailed description in 3.3 above) was done. For this purpose, bias maps produced using R, were used to investigate any anomalies between observed and simulated data on a seasonal scale.

Before calculating the statistics used to evaluate each climate model's performance, the simulated fields were interpolated to a common grid using bilinear interpolation method. This was necessary due to the mismatch between the model grid resolution and observed CRU data grid resolution. The model output was interpolated to the CRU TS3.33 grid resolution.

The CRU TS3.22 is available for land cell only, whereas model simulations cover the ocean. Therefore, to ease the statistical quantitative comparison, the ocean values have been masked out using climate data operator (CDO).

The temporal variability of simulated AOD_{550} was compared against AERONET data observed at λ = 440nm for the year 2000 – 2014. Only years with 80% of data records were used. To ease the comparison with simulated AOD_{550}, the sun photometer AOD at λ = 440nm from AERONET was converted to AOD at λ = 550nm using the angstrom exponent (α) of extinction The angstrom exponent (α) of extinction from the AERONET data was calculated for 440 nm to 870 nm using equation (3.2) and was then used to adjust the monthly measured AOD at λ = 440 nm to AOD at λ = 550 nm using equation (3.3).

In the practical application, particle wavelengths (λ_1 ,λ_2) have corresponding AOD (τ_1 , τ_2), then angstrom exponent (α) is related to lambda (λ_1 , λ_2) and tau (τ_1 , τ_2) by equation (3.1):

$$\frac{\tau_1}{\tau_2} = \left(\frac{\lambda_1}{\lambda_2}\right)^{-\alpha} \quad (3.1)$$

In the logarithmic form,

$$\alpha = -\left(\frac{ln\frac{\tau_1}{\tau_2}}{ln\frac{\lambda_1}{\lambda_2}}\right) \quad (3.2)$$

$$\tau_1 = \tau_2\left(\frac{\lambda_1}{\lambda_2}\right)^{-\alpha} \quad (3.3)$$

$$\tau_\lambda = \tau_{\lambda_0}\left(\frac{\lambda}{\lambda_0}\right)^{-\alpha}$$

3.5.2. Aerosol Induced Surface Temperature Change

To investigate the sensitivity of simulated surface temperature to aerosols, two sets of simulation experiments, namely a ***control*** and a ***standard*** simulation, were used. Under the ***control***, a simulation was carried out without the aerosol scheme (i.e. prognostic aerosols set to 0). The output for 2000 - 2014 was analysed. The model output from this experiment is compared against CRU TS3.22 surface temperature to establish how well the model simulates the present climate of Southern Africa with no aerosols.

For the sensitivity analysis, it was firstly investigated if there has been any difference between the surface temperature simulated with and without the aerosol scheme. This was done using quantitative statistics, namely, the symmetric mean absolute percentage error (*SMAPE*); mean absolute error (*MAE*); root mean square error (*RMSE*); and mean error (*ME*) (see

equations 3.4, 3.5, 3.6 and 3.7, respectively). These statistics are commonly used to evaluate model performance against measured values whereby *SMAPE*, *MAE*, *RMSE* and *ME* of 0 indicate perfect fit (e.g. Moriasi *et al*., 2007). In our study, the *SMAPE*, *MAE*, *RMSE* and *ME* of 0 indicate that there are no differences between surface temperatures simulated with and without the aerosol scheme, and the value of greater or less than 0 indicates that aerosols induce surface temperature change over Southern Africa. To investigate whether the presence of aerosols in the model induces cooling or warming at the surface and the magnitude of change, seasonal anomalies for DJF, MAM, JJA and SON were calculated between surface temperatures simulated with and without aerosols scheme.

$$SMAPE = \frac{100\%}{n}\sum_{t=1}^{n}\frac{|F_t - A_t|}{(|A_t| + |F_t|)/2} \quad (3.4)$$

In equation 3.4, A_t is the simulated surface temperature without the aerosol scheme, F_t is the simulated surface temperature with the aerosol scheme, *t* represents time series and *n* is the number of years, fourteen (14) in this case. Here *n* and *t* remain the same for all the dataset and calculations.

$$MAE = \frac{\sum_{i=1}^{n}|y_i - x_i|}{n} = \frac{\sum_{i=1}^{n} e_i}{n} \quad (3.5)$$

In equation 3.5, y_i is the simulated surface temperature without the aerosol scheme and x_i is the simulated surface temperature with the aerosol scheme.

$$RMSE = \sqrt{\frac{\sum_{t=1}^{T}(\hat{y}_t - y_t)^{-2}}{T}} \quad (3.6.)$$

In equation 3.6, y_t is the simulated surface temperature without the aerosol scheme and $\hat{y}_t$ is the simulated surface temperature with the aerosol scheme at time *t.*

$$ME = \frac{\sum_{i=1}^{n} y_i - x_i}{n} \quad (3.7)$$

In equation 3.7, y_i is the simulated surface temperature without the aerosol scheme and x_i is the simulated surface temperature with the aerosol scheme.

Chapter 4: The sensitivity of simulated temperatures in GISS-modelE climate model to aerosols over Southern Africa

4.1. Introduction

Aerosol particles are highly variable in space and time. For that reason, a possible localized change exists in aerosols' radiative forcing that could consequently affect regional surface temperature (e.g. Tummon *et al*., 2010). In this chapter, the results of the sensitivity of simulated surface temperature to atmospheric aerosol loading over Southern Africa are presented using the GISS-ModelE climate model (Schmidt *et al*., 2006) that uses the MATRIX aerosol microphysical module and the OMA (Simple) aerosols scheme. The two aerosol schemes provide the detailed characterization of aerosol particles, processes, and their interaction with the climate (Bauer *et al*., 2008).

In previous studies, the GISS-ModelE climate model has been proved efficient for global scale atmospheric research application (e.g. Hansen *et al*., 2005; Schmidt *et al*., 2006; Bauer *et al*., 2008, 2013). The GISS-ModelE (climate model) has been widely used in the simulation of global surface temperature change and these results display a high spatial and temporal variability. The signal of temperature change is stronger at regional level (Hansen *et al*., 1999; 2010). One driver of regional surface temperature change involves radiative forcing due to aerosol particles. An assessment of aerosols' forcing, and its related impact on surface temperature, has been studied using climate models in other regions of the world (e.g. Liu and Liao, 2017). However, GISS-modelE has never been tested for the Southern African region.

In this chapter, the sensitivity results from GISS modelE with the implementation of two different aerosol schemes, namely the MATRIX and the OMA (simple) aerosol schemes, are discussed. Firstly, the simulated surface temperature achieved under control experiment is compared against CRU TS3.22 data (New *et al*., 1999; 2000); this would help to better understand the model's ability to simulate the present-day climate over Southern Africa (10°N to 35°S, 0°W to 60°E). Model simulated AOD_{550} is compared against AERONET and MODIS AOD_{550}. The sensitivity of simulated surface temperature to aerosols is quantified using the statistics outlined in chapter 3. Lastly, the aerosols' impact on surface temperature is discussed.

4.2. Results and Discussion

4.2.1. Surface Temperature Evaluation

The ability of the GISS modelE in simulating Southern African seasonal surface temperature is shown in figure 5. For the purpose of model evaluation, control simulations have been used. In general, the model appears to simulate the seasonal spatial patterns of Southern Africa's surface temperature relatively well. However, there is a bias that ranges between -2 and +2.5˚C. The model tends to overestimate surface temperature by approximately 1.0 – 2.5˚C over the western part (from 10° to 25°E) as well as the northern part of Southern Africa across all four seasons namely DJF, MAM, JJA and SON. This positive bias is more pronounced during JJA and SON seasons. The highest positive bias was approximately 3.5˚C over the western coast of Namibia and Angola over the region of Kaokoveld deserts found between 13°- 21°S. A negative bias that ranges between 1.0 – 2.0°C were simulated over the eastern part of Southern Africa. However, the maximum of this negative bias is less than the maximum of simulated positive bias in the west. Similar results were obtained by the Tummon *et al*. (2010) study when evaluating the RegCM3 RCM against CRU observation data. The study has found that the RegCM3 has a tendency of overestimating surface temperature over the western part of Southern Africa whilst underestimating temperature over the eastern part of Southern Africa. Many factors could contribute to uncertainty in model simulations of surface temperatures over Southern Africa (e.g. Crétat *et al*., 2012); these include poor model configuration and the inability of the model to reproduce regional circulation. The other source of uncertainty could be model resolution, the latitude and longitude resolution used in this study (2.0˚ × 2.5˚) is too coarse to capture some sub-grid scale features that play an important role in modulating the regional climate (e.g. Roeckner *et al*., 2006a). Other contributing factors include radiation, surface properties, cloud cover, advection and energy fluxes (e.g. Christensen *et al*., 1997; Tadross *et al*., 2006). This finding highlights that climate model development, especially for the African region, is needed.

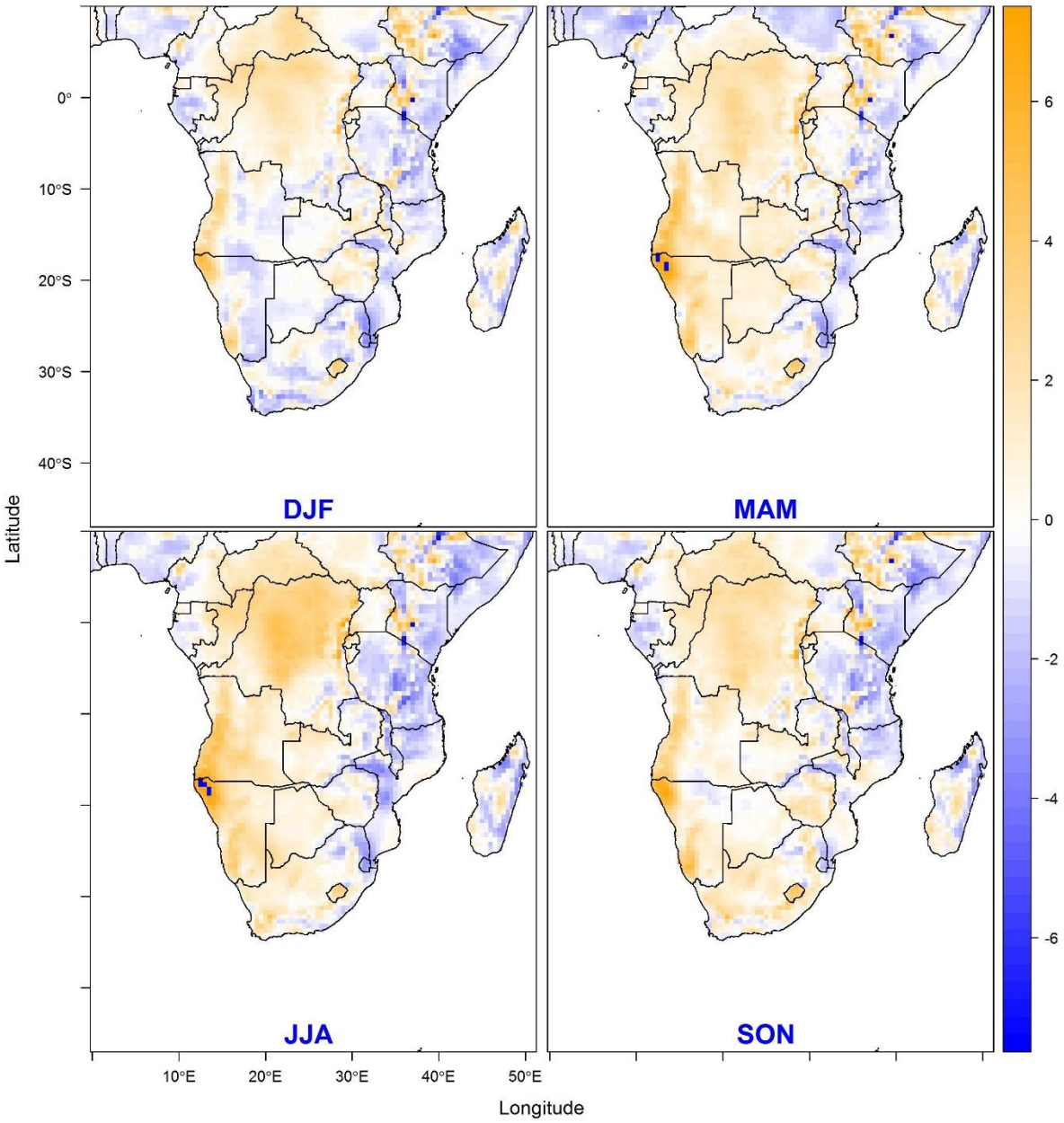

Figure 5:Southern African seasonal surface temperature bias (˚C), GISS-ModelE simulated surface temperature compared to reference data (CRU TS3.22).

4.2.2. Aerosols Optical Depth Evaluation

The other important parameter that has an impact on surface temperature is AOD; it is important that GCMs simulate AOD accurately, in order to simulate temperatures well. Here the model simulated AOD_{550} from GISS modelE with the implementation of MATRIX and OMA (simple) aerosol schemes are compared with measurements from five Southern African AERONET sites for the period 2000 – 2014 (namely Ascension Island, Etosha Pan, Mongu, Reunion Island and Skukuza). The AOD that was measured at the wavelength, λ = 440nm

has been converted to AOD at wavelength, λ = 550nm (see equation 3.1 to 3.3 in Chapter 3) to ease comparison with the model simulated AOD at wavelength, λ = 550nm.

The results of the comparison of observed and model simulated AOD_{550} are presented in figure 6 and figure 7. The empirical cumulative distribution functions (ECDFs) of simulated AOD_{550} is similar in its pattern to the distribution of AOD_{550} from the AERONET sites (figure 6 and figure 7). Simulations from both MATRIX (figure 6) and OMA (figure 7) aerosol schemes underestimate AOD_{550} at the Reunion Island; it must be noted that there were a few observations at this site and that could affect the distribution functions. The model can relatively reproduce the temporal distribution of AOD_{550} at the Ascension Island, Etosha Pan, Mongu and Skukuza. The magnitude of AOD_{550} are underestimated at the Ascension and Reunion Islands and slightly overestimated at the Etosha Pan, Mongu and Skukuza by the MATRIX aerosol scheme (figure 6). It must also be noted that the Etosha Pan site had relatively little observation data that resulted in less a smooth ECDF. About OMA (simple) aerosols scheme: the magnitude of AOD_{550} is to be underestimated at all sites except for Mongu site (figure 7). Mongu site is situated in biomass burning region over central Zambia, the AOD_{550} for Mongu site reached the highest during the peak of biomass burning activity (Swap *et al*., 2003; Tesfaye *et al*., 2011; Queface *et al*., 2011; Horowitz *et al*., 2017).

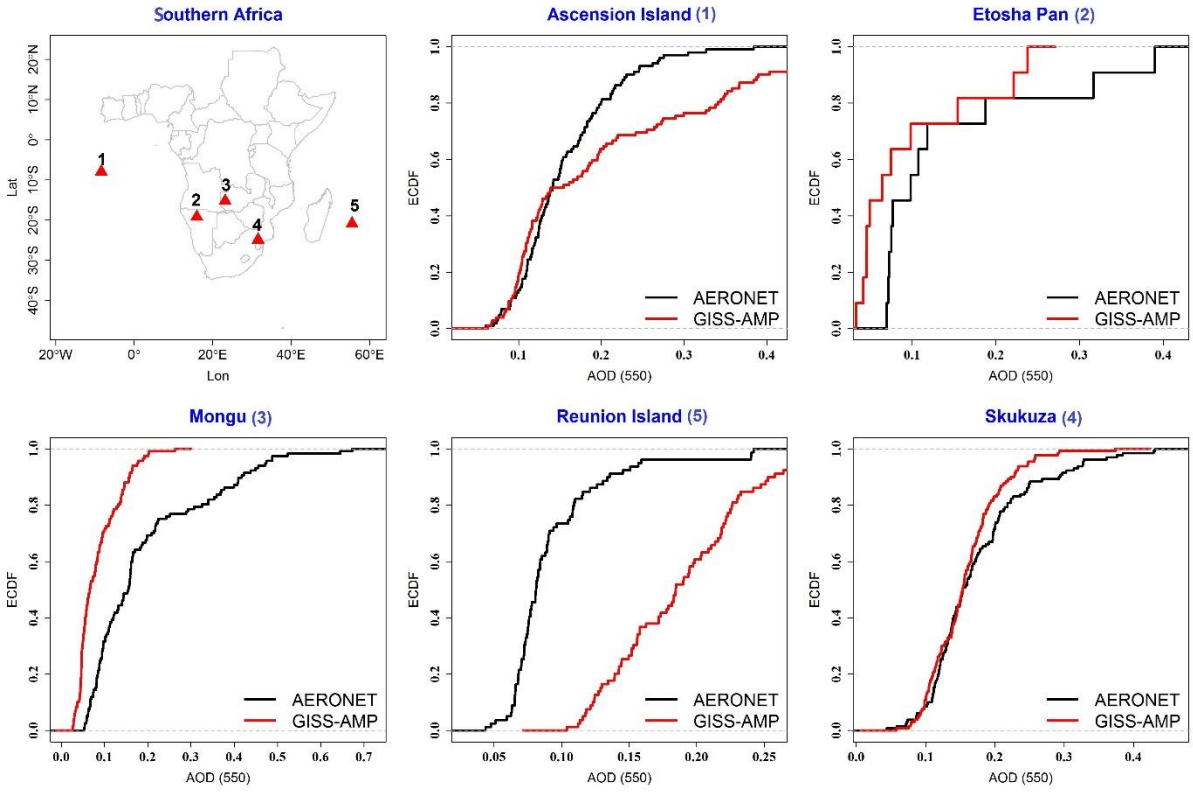

Figure 6: Empirical Cumulative Distribution Functions (ECDF) of AERONET measured AOD (black) and model GISS-modelE (MATRIX) simulated AOD_{550}, top right map shows Southern

African domain with numbered AERONET stations where the AOD measurements were retrieved.

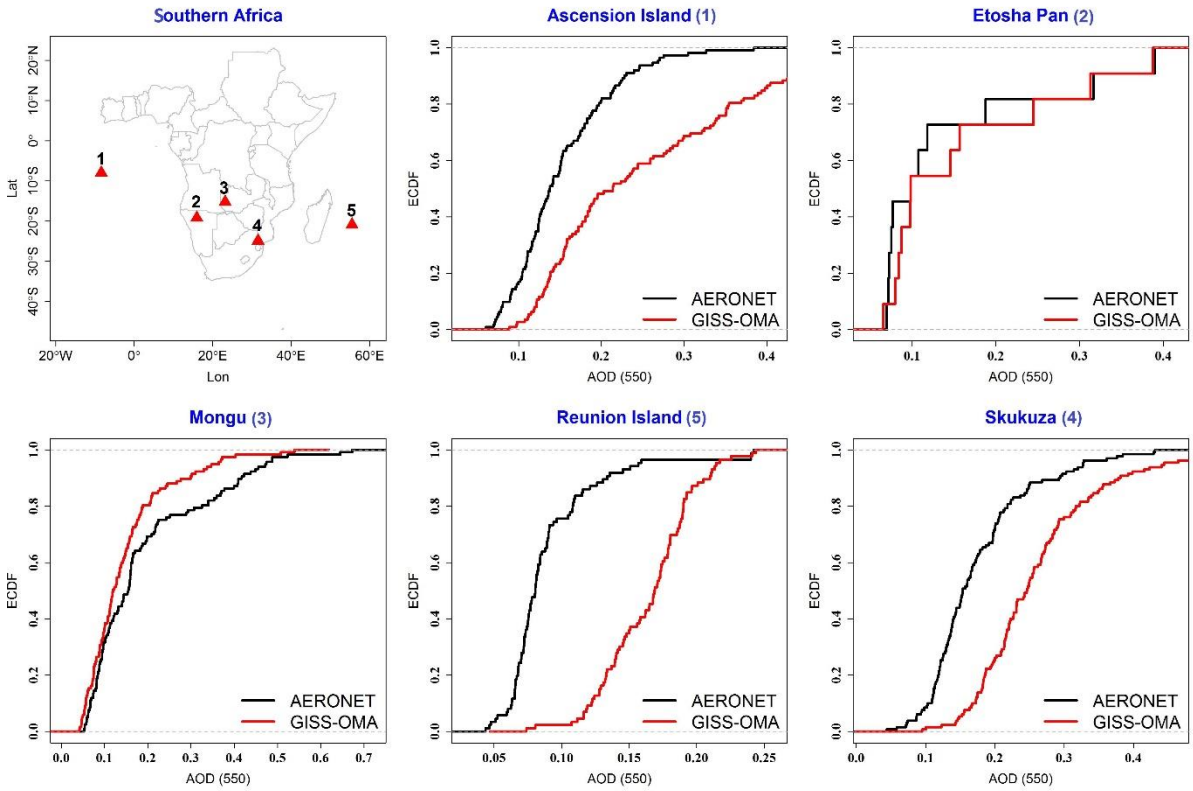

Figure 7: Empirical Cumulative Distribution Functions (ECDF) of AERONET measured AOD (black) and model GISS – modelE (OMA) simulated AOD_{550}, top right map shows Southern African domain with numbered AERONET stations where the AOD measurements were retrieved.

Figures 8 and 9 show that the spatial distribution of the seasonal mean of AOD_{550} over Southern Africa averaged from the year 2000 to 2014. In figure 8, the GISS-modelE simulation of AOD_{550} is compared with the implementation of the MATRIX aerosol scheme against the MODIS observations averaged from 2000 to 2014. The top row shows MODIS $AOD_{550,}$ while the bottom row shows GISS-modelE simulations and the name of seasons are depicted at the bottom of each map. Areas with white shading (e.g. the region around Cape Town and Madagascar) on MODIS spatial maps of AOD_{550} indicate areas without satellite retrievals and this could be the result of failed sensors or continuous cloud cover. It must be noted that MODIS instruments sample once a day (MODIS-Terra pass over 09:00 and 11:00 LT) and the model simulates all day long observations. This indicates that satellite data records per season are less than model simulations. For this study the average AOD_{550} per season is compared.

Figure 8 shows that the model can reproduce the spatial pattern of AOD_{550} over Southern Africa. However, the magnitude is significantly underestimated in all four seasons. In general, high loading of aerosols in the atmosphere occurs over the north-western part of Southern

Africa at 10 °S to 10°N of the equator where the magnitude of AOD_{550} ranging 0.4 to 0.8 is seen. Over the ocean, AOD_{550} magnitude ranges from 0.1 to 0.3. The peak in the eastern and central part is mainly affected by the biomass burning aerosols, especially during JJA and SON season. The model was unable to replicate the high AOD_{550} that ranges from 0.6 to 0.8 in JJA season over the western part of Southern Africa about 10° south of the equator.

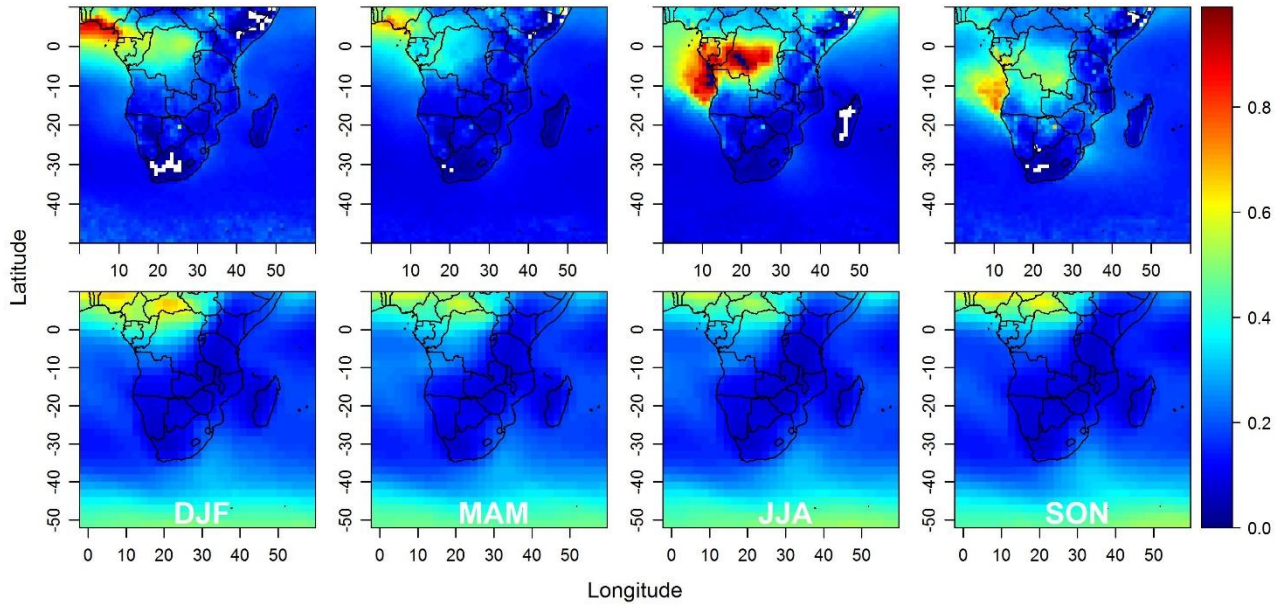

Figure 8:Seasonal mean of AOD_{550} over Southern Africa averaged over 2000 - 2014, top row shows MODIS observations and bottom row shows GISS-modelE simulated AOD_{550} with the implementation of MATRIX aerosol scheme. Seasons (i.e. DJF, MAM, JJA and SON) are depicted on the bottom row.

In figure 9, the GISS-modelE simulated AOD_{550} with the implementation of OMA (Simple) aerosol scheme is compared to the MODIS observations averaged from 2000 to 2014. In general, the GISS-modelE simulation with the implementation of OMA (simple) aerosol scheme can simulate the spatial distribution of AOD_{550}. Higher AOD_{550} that range between 0.6 – 1.0 were simulated over central and western Africa. However, the model has underestimated the AOD_{550} that ranges between 0.6 - 0.8 seen over central and western parts of the Democratic Republic of Congo (DRC). During DJF, the model slightly overestimated the magnitude of $AOD_{550,}$ in the MODIS high AOD_{550} of approximately 0.8 is seen off the coast of Nigeria while 0.8 simulated AOD_{550} occurred around the DRC region. It must be noted that the elevated AOD_{550} values seen over the southernmost part of the region on the plot are not established as real.

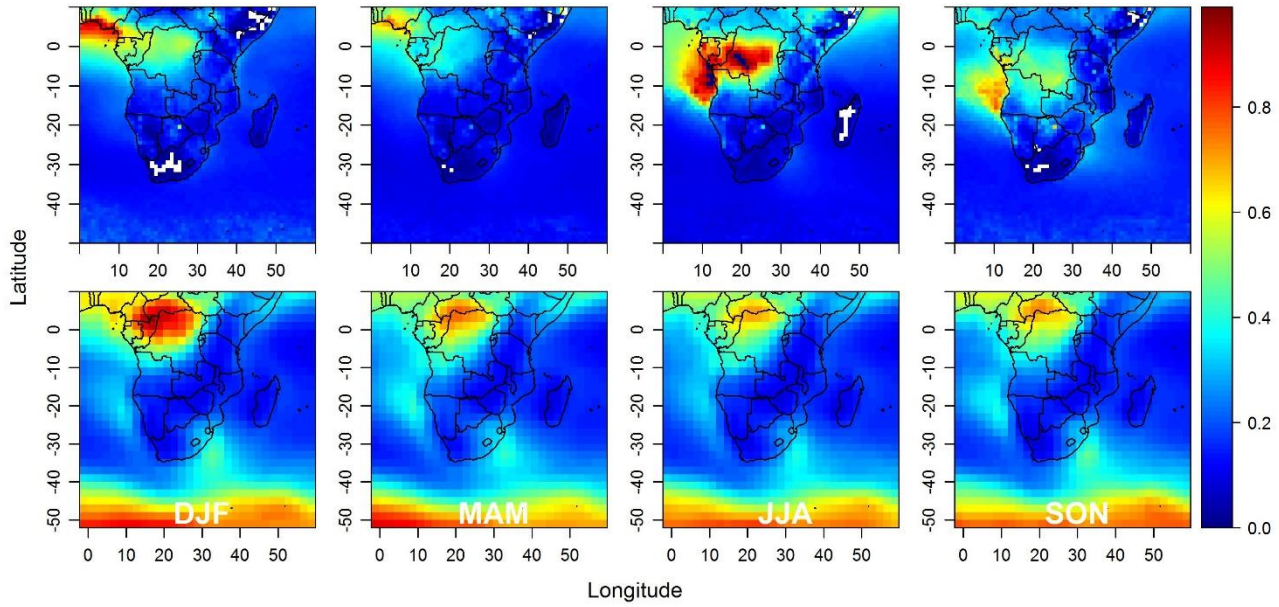

Figure 9:Seasonal mean of AOD_{550} over Southern Africa averaged over 2000 - 2014, top row shows MODIS observations and bottom row shows GISS-modelE simulated AOD_{550} with the implementation of OMA (Simple) aerosol scheme. Seasons (i.e. DJF, MAM, JJA and SON) are depicted the bottom row.

4.2.3. Statistical Quantification of Aerosols' Impacts

The sensitivity of Southern African surface temperature to aerosols has been quantified using quantitative statistics. Figure 10 and 11 show quantitative statistics of surface temperature simulated with the implementation of MATRIX and OMA (Simple) aerosol schemes, respectively. The investigation conducted was to establish if there is any difference in spatial pattern and magnitude of surface temperature simulated with and without the effect of aerosols using the symmetric mean absolute percentage error (*SMAPE*); mean absolute error (*MAE*); root mean square error (*RMSE*); and mean error (*ME*) (see equation 3 to 6 in Chapter 3). In this study a *SMAPE*, *MAE*, *RMSE* or *ME* value of 0 (perfect score) indicates that there is no difference between the surface temperatures simulated with and without aerosol effect, and the value of greater or less than 0 indicates that there is a difference (e.g. surface temperatures are sensitive to the presence of aerosols in the model).

For simulation with the implementation of MATRIX (figure 10)**,** *SMAPE* ranges between 0.1 – 0.2 over the Southern African Development Community (SADC) region and slightly above 0.05 in the northern part of Southern Africa. Relatively higher values that range from 0.4 – 2.0 are seen for *MAE* and *RMSE* over Southern Africa. The maximum values occur over the SADC region. The *ME* that range between 0.2 – 1.0 are seen over SADC and in the west and east coast of Southern Africa. The negative *ME* that range between 0.2 – 0.4 are seen over the

northern part of Southern Africa from 10 °S to 10°N of the equator. A similar spatial pattern is seen regarding the simulation with the implementation of OMA (Simple) (figure 11).

All the quantitative statistics show values that are greater or less than zero over land. This implies that the simulated Southern African surface temperature over land is sensitive to the aerosols' effect. Over the ocean, all quantitative statistics are close to zero because there is no change in temperature due to prescribed sea surface temperature in AMIP experiment (Gates *et al*., 1998).

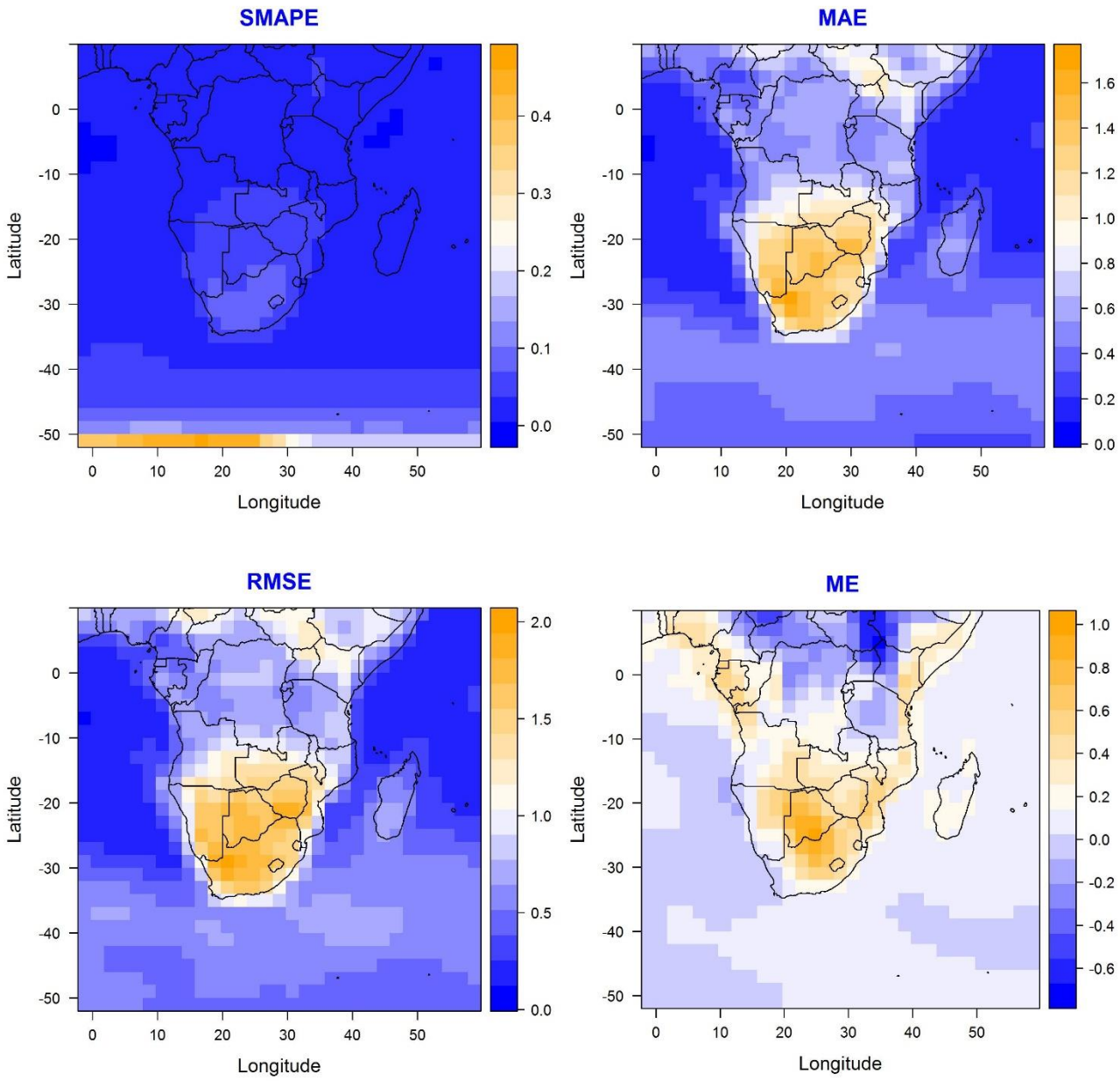

Figure 10:Statistical analysis of simulated mean aerosol induced changes in surface air temperature according to GISS-modelE (MATRIX), the statistics include SMAPE, MAE, RMSE and ME.

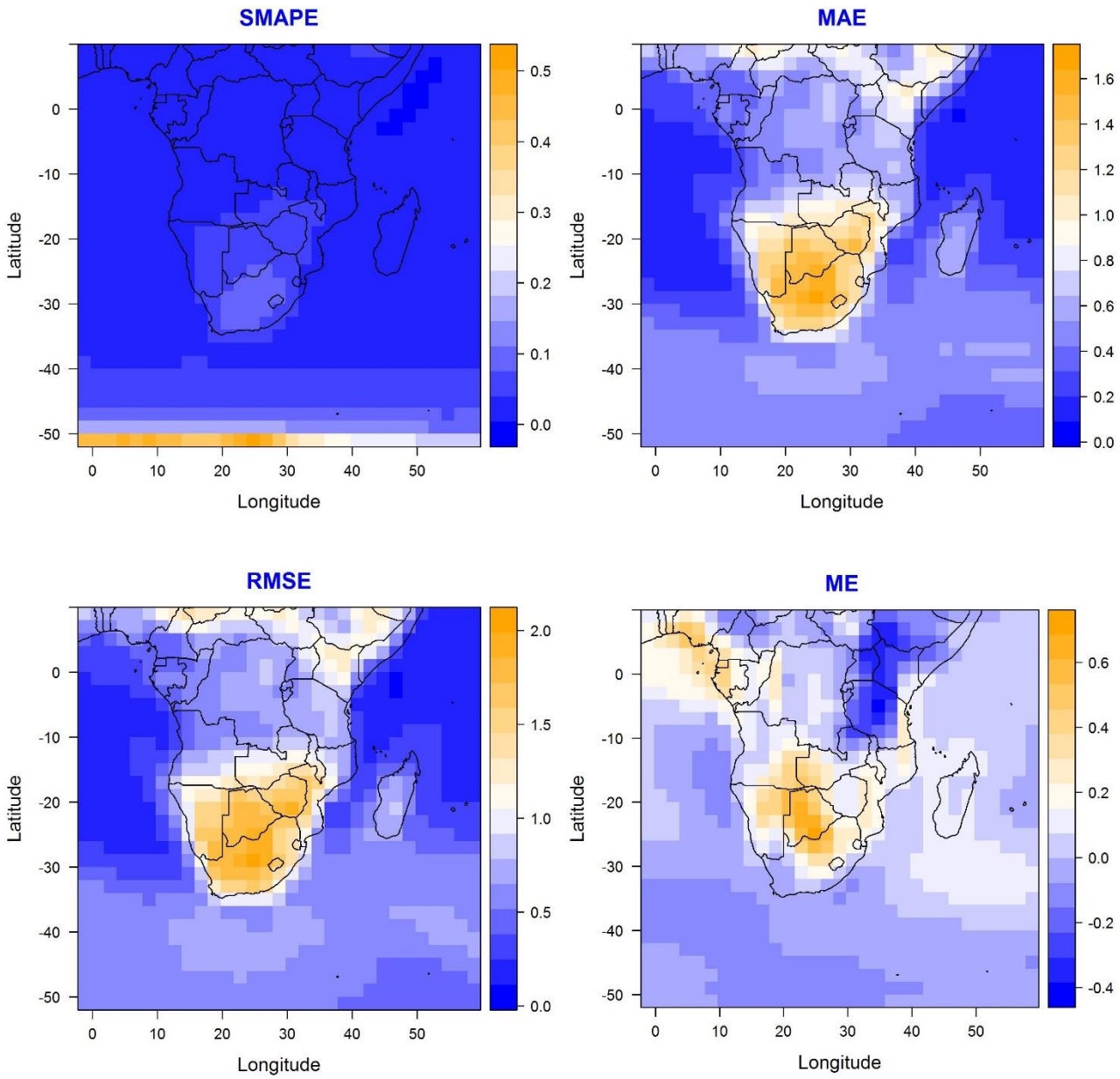

Figure 11:Statistical analysis of simulated mean aerosol induced changes in surface air temperature according to GISS-modelE OMA (Simple), the statistics include SMAPE, MAE, RMSE and ME (This figure is comparable to GISS modelE (MATRIX) analysis in figure 10).

4.2.4. Aerosol Induced Change in Surface Temperature

In section 4.2.3, it was established that aerosols affect the simulated Southern African surface temperature. Figure 12 and 13 looks at the seasonal spatial anomalies of simulated surface temperature induced by the presence of aerosols from MATRIX and OMA (Simple), respectively. These two figures help to better understand whether aerosols induce cooling or warming, and the magnitude of change thereof over the study area. To calculate the anomalies, the seasonal surface temperature simulated without aerosols was subtracted from

surface temperature simulated with the implementation of aerosol schemes. The negative values show that surface temperature simulated with the effect of aerosols is less than that simulated without aerosols; this implies that aerosols induce cooling of the surface temperature. The reverse is true for the warming of surface temperature.

Figure 12 shows the simulated seasonal mean aerosol induced changes in surface air temperature (°C) according to the GISS-modelE (MATRIX), which has been averaged over the years 2000 - 2014. There is a seasonal difference in surface temperature that is spatial dependent. During DJF, JJA and SON a relative cooling (blue in figure 12) of surface temperature that ranges between 0.25 – 1.5˚C is simulated over a large part of Southern Africa, except for the Botswana, Namibia, South Africa, Zimbabwe, Mozambique and Zambia regions that show slight warming (orange in figure 12) of approximately 0.5˚C. The MAM season exhibits surface warming that ranges from 0.25 – 0.75˚C. Not much change is simulated over the ocean.

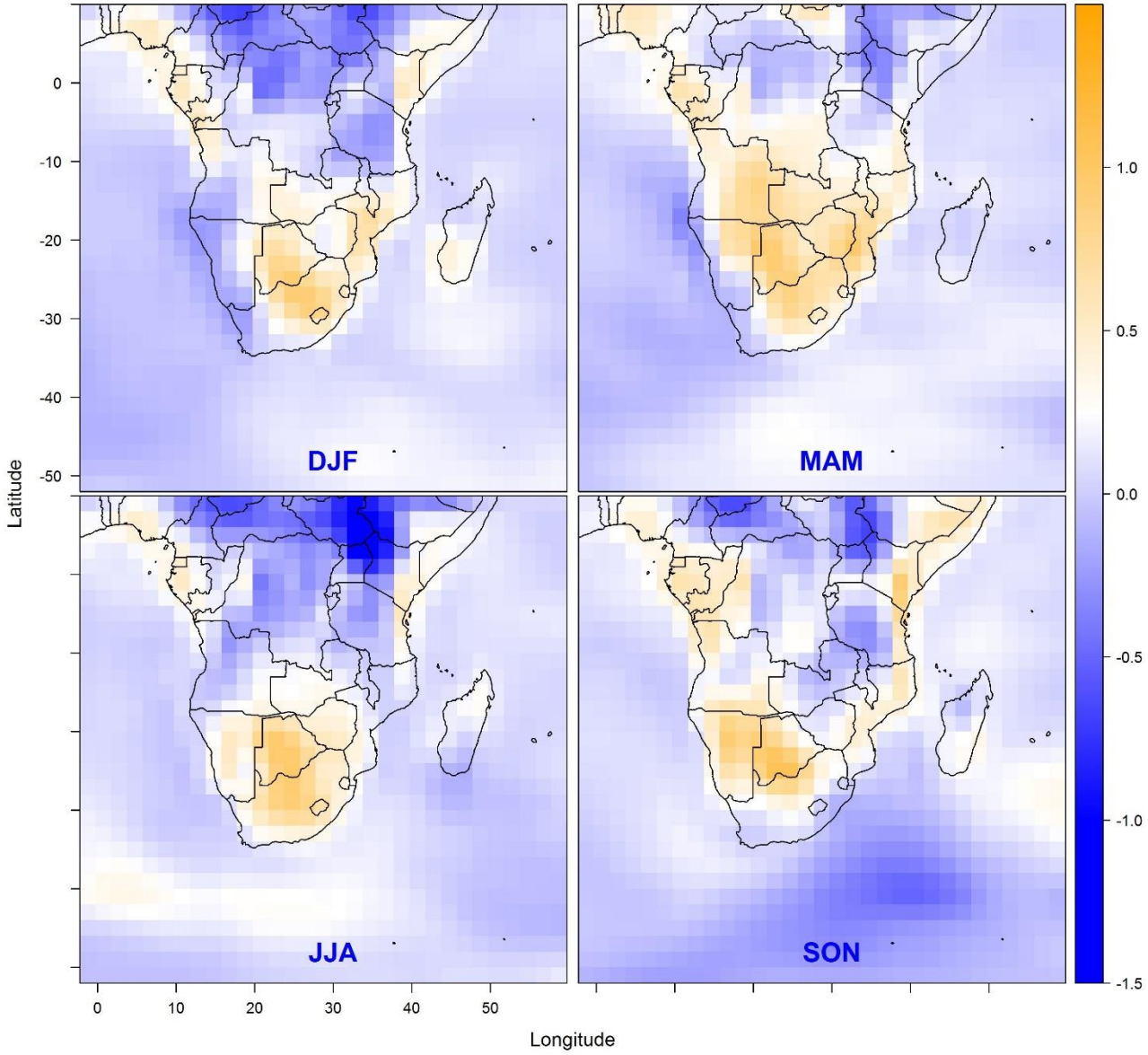

Figure 12: Simulated seasonal mean aerosols induced changes in surface air temperature (°C) according to the GISS-modelE (MATRIX), which has been averaged over the years 2000 – 2014.

Figure 13 shows the simulated seasonal mean aerosol induced changes in surface air temperature (°C) according to the GISS-modelE OMA (Simple), which has been averaged over the years 2000 - 2014. Surface temperature cooling of 0.5°C is simulated over the eastern part of Southern Africa during all seasons. A relatively higher cooling that ranges between 0.25 – 1.0°C is simulated over South Africa during the DJF, MAM and SON season. A slight warming of approximately 0.5 °C is simulated over South Africa and the west coast during JJA. A central and western part of Southern Africa shows a slight warming of approximately 0.25°C during all the seasons.

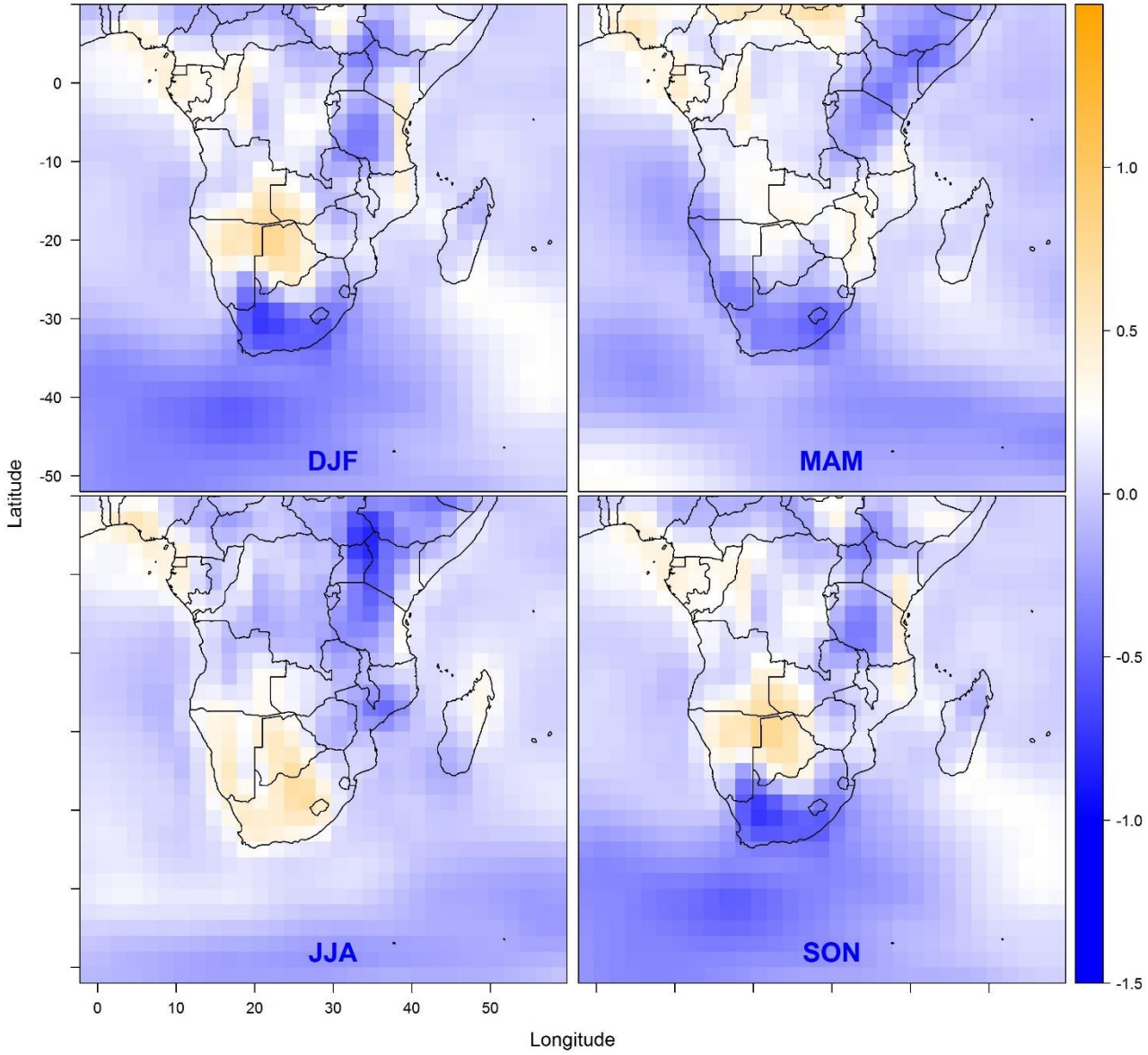

Figure 13: Simulated seasonal mean aerosol induced changes in surface air temperature (°C) according to the GISS-modelE (OMA), which has been averaged over the years 2000 – 2014 (This figure is comparable to GISS modelE (MATRIX) analysis in figure 12).

The experiment in this chapter has shown that aerosols have impacts on simulated surface temperatures; figures 12 and 13 above show surface temperature anomalies because of MATRIX and OMA aerosol schemes, respectively. It is quite clear from both figures that some areas over Southern Africa are simulated to experience cooling while others experience warming of surface temperature due to aerosols. Now the remaining aspect is to compare whether the two aerosol schemes (i.e. MATRIX and OMA) produce similar magnitude and

spatial distribution of warming or cooling signals. As discussed in 4.2.4 the MATRIX aerosol scheme results in warming of about 0.5°C over some regions that include Botswana, Namibia, South Africa, and Mozambique, while cooling is simulated over the other regions. On the other hand, the OMA aerosol scheme (figure 13) results in a cooling of about 0.25 – 1.0°C over a large part of Southern Africa during DJF, MAM and SO season. There is slight warming that was simulated over South Africa during JJA season.

However, by looking at the spatial distribution of surface temperature anomalies in figure 12, it is quite clear that the warming signal is more pronounced, especially in the southern part of Southern Africa. On the other hand, the OMA aerosol scheme results in more cooling over the southern part, especially over South Africa. By comparing figure 12 and 13 it is quite apparent that the OMA aerosol scheme has more cooling of surface temperature than the MATRIX aerosol scheme. This indicates that surface temperature responds differently to different aerosol schemes, the differences in how the aerosols are described in these schemes (i.e. characterization of aerosols and their processes) lead to differences in the sensitivity of simulated surface temperature to aerosols.

4.2.5. Relationship between warming/cooling and AOD

In figures 14 and 15, the magnitude and spatial distribution of seasonal AOD are compared to simulated surface temperature anomalies, the comparison is necessary to better understand the relationship between warning/cooling of surface temperature and AOD distribution.

In Figure 14, the four maps on the left show simulated seasonal mean AOD_{550} according to MATRIX aerosol scheme averaged from 2000 – 2014. Places where higher AOD_{550} were simulated are light green to dark red and places where low AOD_{550} were simulated are dark blue. The maps on the right show seasonal mean surface temperature anomalies; places experienced warming of surface temperature due to the presence of aerosols are light orange to dark orange whilst places that experienced cooling of surface temperature are light blue to dark blue. According to simulations achieved with the effect of the MATRIX aerosol scheme (Figure 14), the regions that experienced higher AOD_{550} are situated in the northwest part of the domain between 10°N and 10°S, the AOD_{550} ranges between 0.4 – 0.8 were simulated over these regions. Over these same regions, there are simulated negative and positive temperature anomalies that range between 0.4 – 0.8°C and 0.5 to1.0°C respectively. A relatively low AOD_{550} that range between 0.1 – 0.3 was simulated over the south and eastern part of Southern Africa where positive temperature anomalies of 0.5 – 1.5°C were simulated. Similarly, according to the OMA aerosol scheme (Figure 15), high loading of AOD_{550} has been simulated over the northwestern part of Southern Africa between 10°N and 10°S of the equator

where AOD_{550} reaches a maximum of 0.8. Elsewhere AOD ranges between 0 – 0.4. The corresponding seasonal temperature anomalies show the cooling of about 0.5 to 1.5°C over South Africa and the eastern part of Southern Africa for all the seasons, except JJA where warming signal is simulated over South Africa. There is general positive temperature anomalies (warming) over the western part of Southern Africa. By comparing the spatial distribution of AOD_{550} and surface temperature anomalies, it is quite apparent that temperature anomalies do not necessarily follow the AOD loading. High AOD_{550} results in cooling in some areas and warming in other areas. There is no relation between AOD and surface temperature anomalies, which indicates that AOD is not the only driver of surface temperature. Aerosols' composition also impacts surface temperature, for example aerosol species such as sulphates will result in cooling while BC will result in warming of surface temperature.

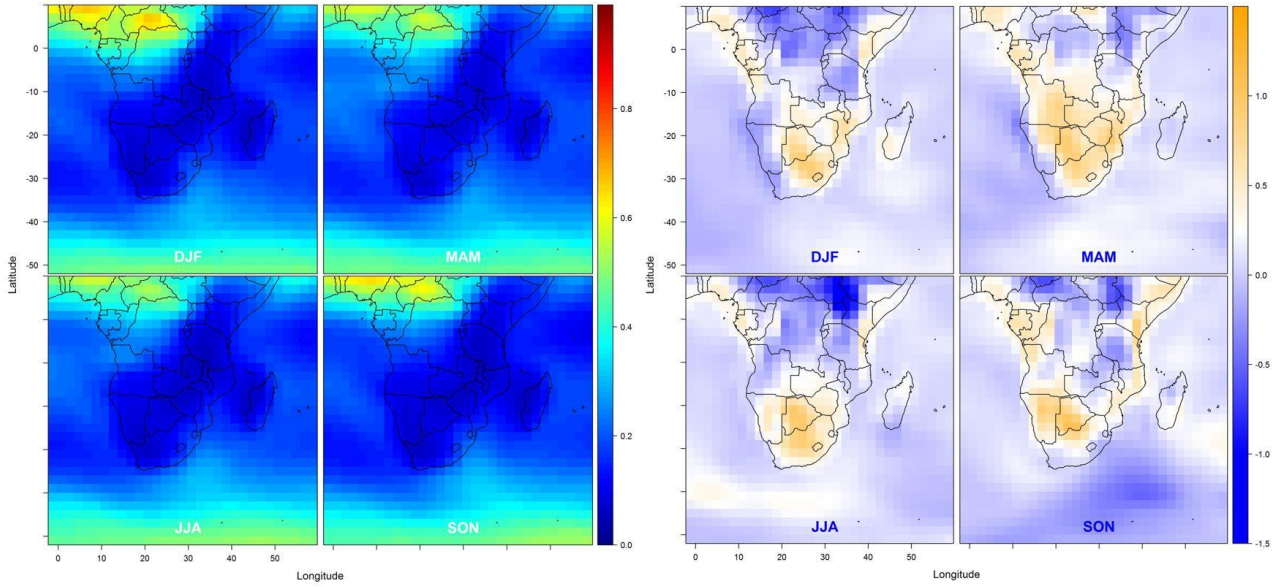

Figure 14: The relationship between the magnitude simulated AOD_{550} (on left) and warming/cooling (on right) according to MATRIX aerosol scheme. The figure on the left shows the simulated seasonal mean of AOD_{550} and figure on the right shows simulated seasonal mean aerosol induced changes in surface air temperature (°C), over Southern Africa, averaged over the period 2000 - 2014.

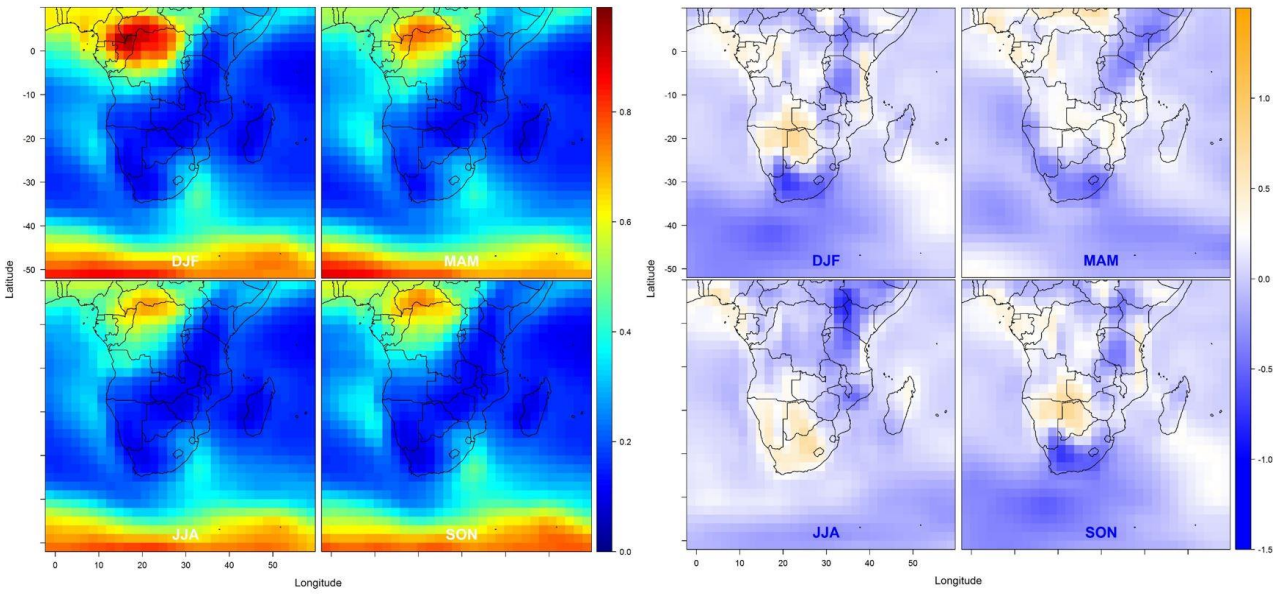

Figure 15: The relationship between the magnitude simulated AOD_{550} (on the left) and warming/cooling (on the right) according to OMA aerosol scheme. The figure on the left shows the simulated seasonal mean of AOD_{550} and the figure on the right shows the simulated seasonal mean aerosol induced changes in surface air temperature (°C), over Southern Africa, averaged over the period of 2000 - 2014.

4.3. Conclusion

The sensitivity of seasonal simulated temperatures to aerosols over Southern Africa was investigated using the GISS-modelE GCM with the effect of two aerosol schemes, namely MATRIX and OMA aerosol schemes. The climate model was able to reproduce the seasonal spatial distribution and historical climate. However, there was a bias over some regions of Southern Africa. For AOD_{550}, the model was able to reproduce the temporal distribution of AOD_{550} from the AERONET measurements in Southern Africa. The spatial distribution of simulated AOD_{550} closely matched MODIS satellite observations. However, the model tends to underestimate the magnitude of AOD_{550} over Southern Africa

The sensitivity of surface temperature to aerosols has been carried out through comparing simulated surface temperatures with the aerosol scheme and surface temperatures simulated without the aerosols scheme. The two simulations have been compared, using the quantitative statistics and these results show that there is a difference in magnitude between the two simulations. This implies that aerosols induce a change in surface temperature. Given that aerosols' distribution varies in both magnitude and characteristics from one season to another, seasonal spatial temperature anomalies of the two simulations were computed. These results show that aerosols induce a seasonal change in surface temperature that is varying spatially over Southern Africa. The general results point towards cooling of surface temperature in

some areas and warming in other areas that change from one season to the other. Spatial distribution of temperature anomalies does not necessarily follow the spatial distribution of AOD_{550}, as some areas with high AOD_{550} result in cooling of surface temperature whilst other areas are warming with high AOD_{550}.

The two aerosol schemes used in simulation, produce different results in terms of AOD_{550} and surface temperature change; this shows that the model is sensitive to the aerosol modules used. It is important to use the correct input parameters in the model to be able to assess how they affect climate. This is a preliminary investigation towards the better understanding of the drivers of the Southern Africa climate.

Chapter 5: The sensitivity of simulated temperatures in CCAM to aerosols over Southern Africa

5.1. Introduction

In this chapter, the sensitivity of simulated temperatures to aerosols over Southern Africa is being investigated using the CCAM developed by the CSIRO (McGregor, 2005; McGregor and Dix 2001, 2008). The CCAM model has been widely used for regional climate modelling research (e.g. Katzfey *et al*., 2009; Corney *et al*., 2010; Thatcher and McGregor, 2011; Nguyen *et al*., 2014). In recent years, it has been used increasingly in climate research over Africa region (e.g. Engelbrecht *et al*., 2009; Engelbrecht *et al*., 2011; Landman *et al*., 2012; Engelbrecht *et al*., 2015; Dekekind *et al*., 2016).

An evaluation of CCAM model in reproducing seasonal and spatial variability of AOD_{550} over Africa has been previously conducted. The results from that study shows that the model can reproduce the seasonality of AOD_{550nm} over Africa (Horowitz *et al*., 2017). The analysis with AERONET was thus not repeated here, but rather only the comparison to MODIS AOD_{550}. Here, is investigated how the change in seasonality and spatial variability of aerosols affects surface temperatures. This is a key towards understanding improving CCAM regional projection of African climate.

5.2. Results and Discussion

5.2.1. Surface Temperature Evaluation

In this section, CCAM seasonal control simulations against CRU TS3.22 surface temperatures were evaluated. CCAM simulates Southern African seasonal surface temperature relatively well. As shown in figure 16, the temperature anomalies over a large part of Southern Africa are approximately zero (very light blue colour). However, there is a positive bias that reaches approximately 10°C over the central and west coast of SADC during MAM, JJA, and SON. A slight negative bias of 1.5 – 2.0°C is seen over the eastern and the northern part of Southern Africa during DJF. The general spatial pattern of seasonal temperature anomalies between model and observation agrees with the results obtained in section 4.2.1 when evaluating the GISS modelE. The tendency of the simulated temperatures being overestimated over the western part of the domain and underestimated temperatures over the eastern part of Southern Africa, also agrees with the findings of Tummon *et al*. (2010).

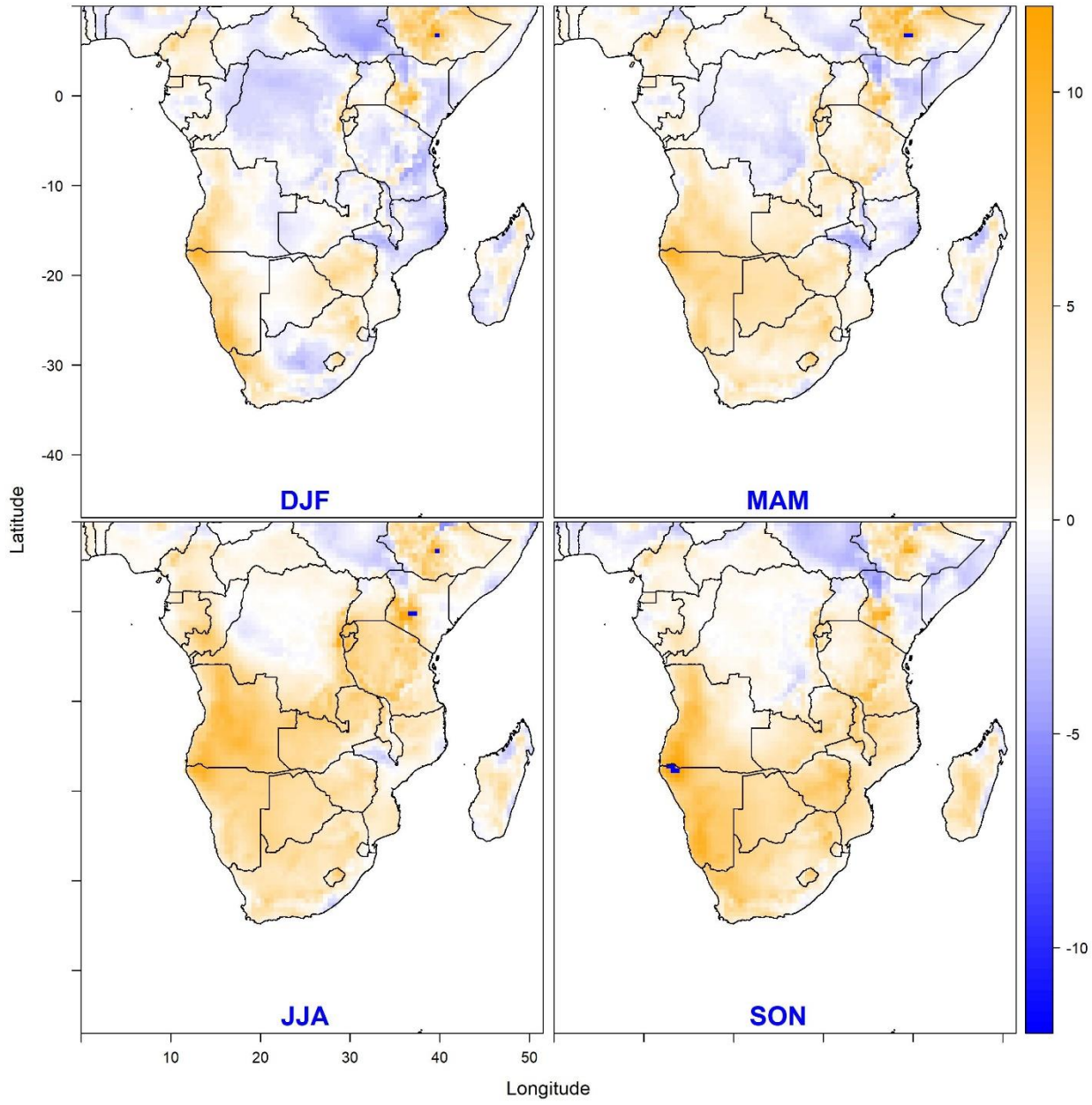

Figure 16: Southern Africa seasonal surface temperature bias (˚C) from CCAM simulated surface temperature compared to reference data (CRU TS3.22).

5.2.2. Aerosols' Optical Depth Evaluation

Figure 17 shows the seasonal distribution of CCAM simulated AOD_{550} averaged from 2000 - 2014 as compared to MODIS satellite data over Southern Africa. The top row shows MODIS AOD_{550}, while the bottom row shows CCAM simulations of AOD_{550}, and the seasons are depicted at the bottom of the bottom row maps. CCAM tends to perform well in simulating the spatial distribution of AOD_{550} in all the seasons. The general picture is that high AOD_{550} is seen to occur in the north-western part of Southern Africa between 10°S to 10°N of the equator. Although the spatial coverage is well simulated by the model, the CCAM tends to

underestimate the magnitude of AOD_{550} over the region. As seen from the MODIS peak of AOD_{550} that reached 0.8 during JJA, while in the CCAM AOD_{550} ranged between 0.3 – 0.6. The AOD_{550} simulated using CCAM follow a similar spatial pattern as that simulated using the GISS-modelE GCM. However, there is a clear peak in AOD_{550} that ranges between 0.2 to 0.4 over the region of KwaZulu Natal, Mpumalanga and Gauteng (latitude 30°S and longitude 30°E). There are many factors that could contribute to the simulated noticeable plume of AOD_{550} over that region. Firstly, this could be the result of anti-cyclonic circulation that transport dust from the west of Southern Africa to this region. Secondly, it could be the result of anthropogenic activities in Mpumalanga and Gauteng province, these include industrial emissions and regional biomass burning especially during SON season. (e.g. Scholes *et al*., 1996; Freim and Piketh, 2003).

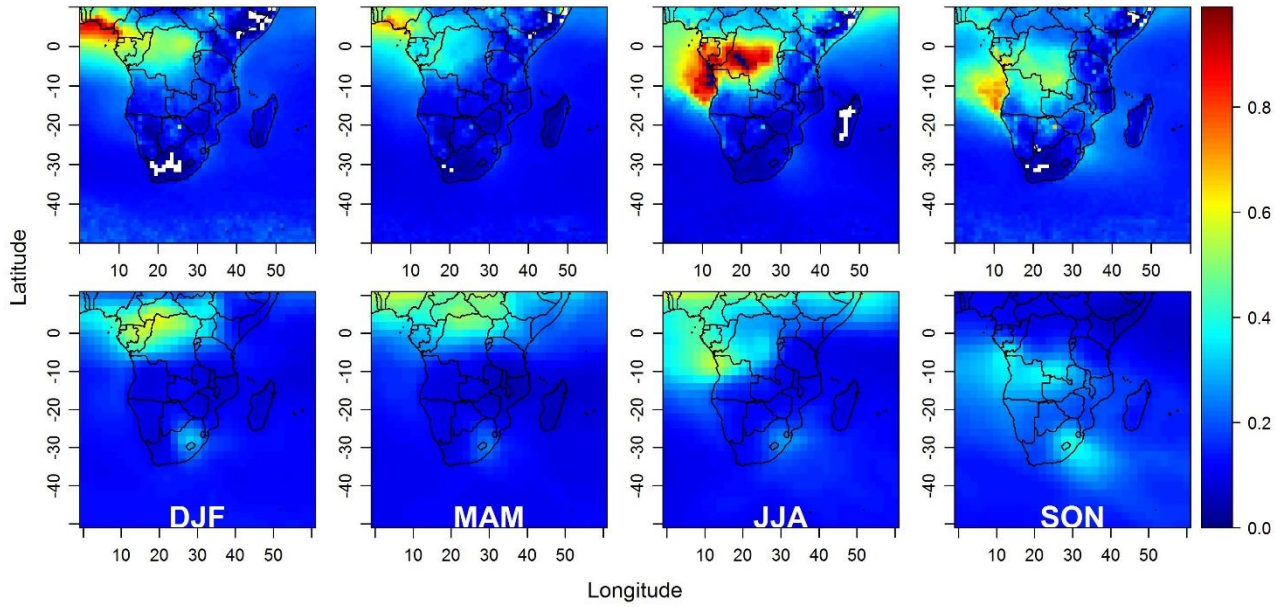

Figure 17: Seasonal mean of AOD_{550} over Southern Africa averaged over 2000 - 2014, top row show MODIS observations and bottom row show CCAM simulated AOD_{550} with the implementation of CCAM prognostic aerosol scheme. Seasons (i.e. DJF, MAM, JJA and SON) are labelled at the bottom.

5.2.3. Statistical Quantification of Aerosols' Impacts

Figure 18 shows the quantitative statistics of the difference in surface temperatures simulated with and without the implementation of aerosol schemes in the CCAM GCM, averaged over the years 2000 - 2014. The *SMAPE*, *MAE* and *RMSE* show relatively high error values that are greater than zero over the SADC region and the northeast of Southern Africa. MAE and RMSE get to a maximum error of 5.0. However, it is interesting to note that the error range in SMAPE is very small as compared to the other 3 tests, because in SMAPE the accuracy

measure is based on percentage (or relative errors). As far as *ME* is concerned, slight positive high values are simulated over the southern and western parts of Southern Africa. Over the east, negative values of *ME* that range between 1.5 to 2.0 have been estimated. These results show that there is a difference in surface temperature simulated with the effect of aerosols and surface temperature simulated without the effect of aerosols.

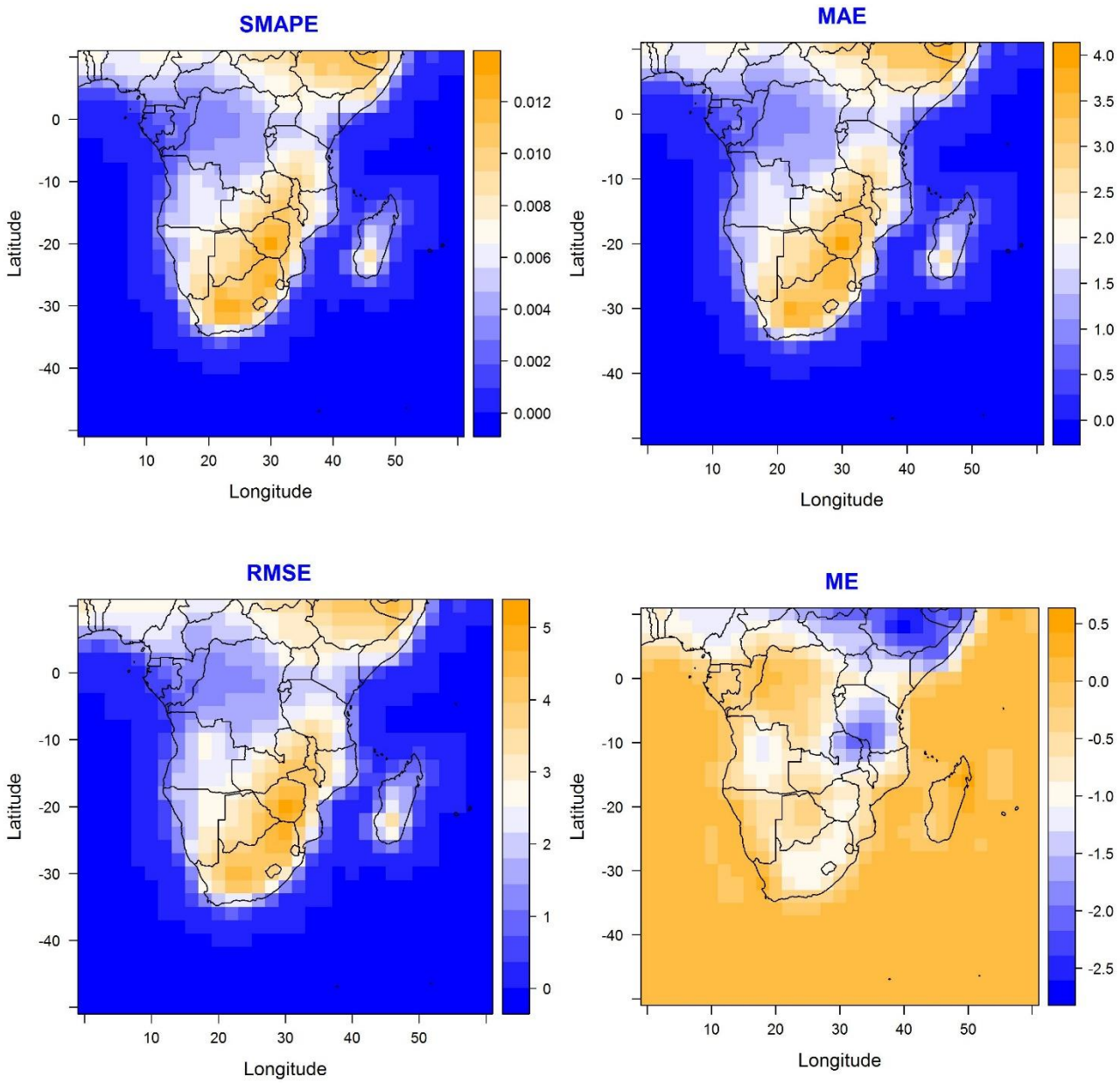

Figure 18: Statistical analysis of simulated mean aerosols induced changes in surface air temperature according to CCAM prognostic aerosols scheme, the statistics include SMAPE, MAE, RMSE and ME (This figure is comparable to GISS modelE analysis in figure 10 & 11).

5.2.4. Aerosols Induced Change in Surface Temperature

Figure 19 depicts the simulated seasonal mean aerosol-induced changes in surface air temperature (°C) according to the CCAM prognostic aerosols scheme, which has been averaged over the years 2000 – 2014. There is a general cooling that ranges between 1.0 – 3.5°C over Southern Africa during DJF and MAM season. Cooling of similar magnitude is simulated over Angola, South Africa, Zambia, Tanzania, Kenya, Somalia, Ethiopia, Uganda, Cameroon and Nigeria during JJA. During SON, such cooling was simulated over SADC and east of Ethiopia and Somalia. Slight warming of 0.5 – 1.0°C was simulated during JJA over Botswana, Zimbabwe, western Mozambique and over DRC and north-western part of Southern Africa during SON.

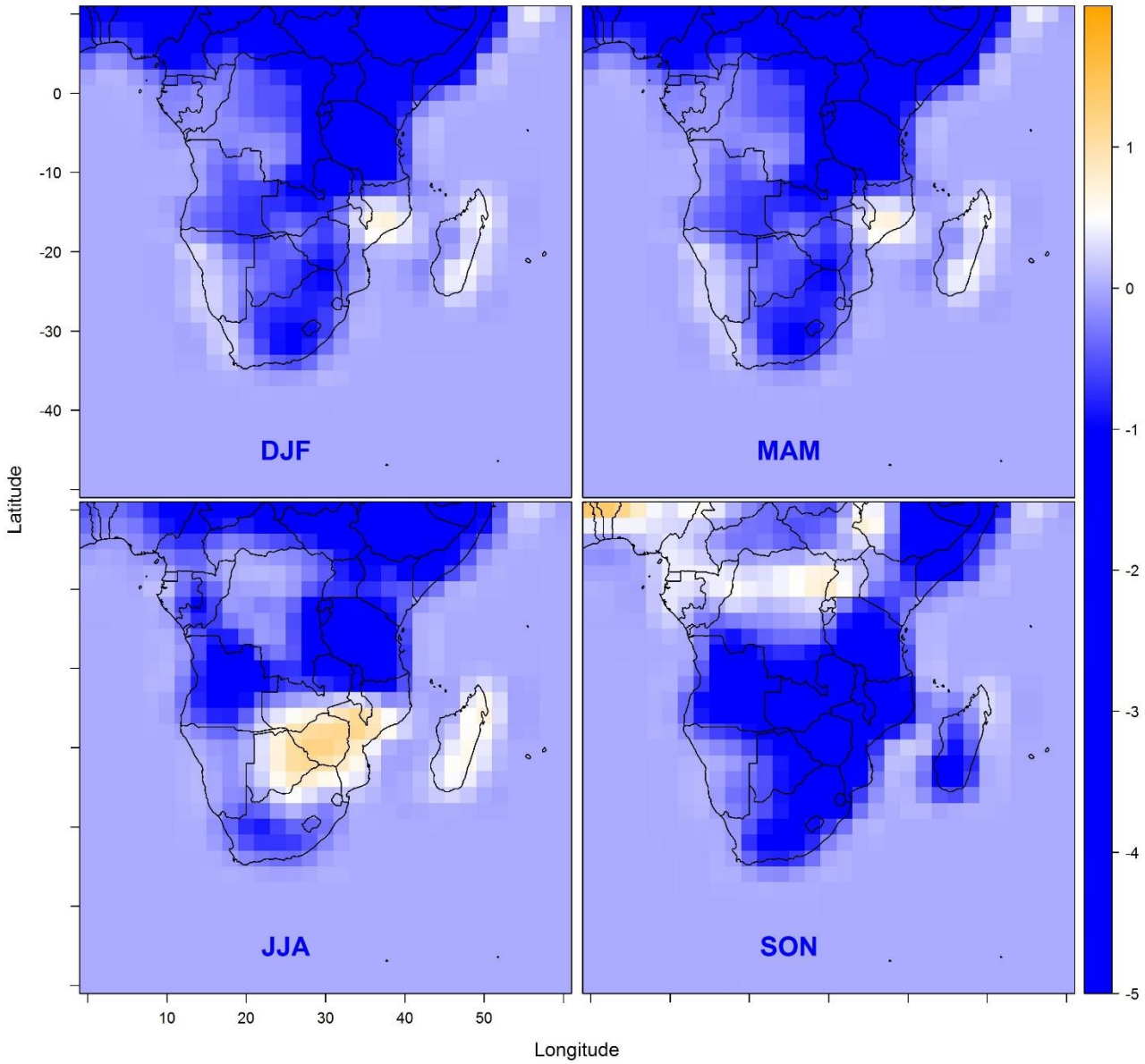

Figure 19: Simulated seasonal mean aerosol-induced changes in surface air temperature (°C) according to the CCAM prognostic aerosols scheme, which has been averaged over the years 2000 – 2014 (This figure is comparable to GISS modelE analysis in figure 12 & 13).

5.2.5 Relationship between warming/cooling and AOD

The same as 4.2.5, in figure 20, the spatial distribution of simulated AOD_{550} is compared with surface temperature anomalies. The four maps on the left show a simulated seasonal mean AOD_{550} according to CCAM aerosol scheme averaged from 2000 – 2014. High AOD_{550} was simulated over the northwestern part of Southern Africa between 10°N and 10°S, where the AOD_{550} reached a maximum of 0.6, and was relatively low (about 0.2) elsewhere, except at the southeast coast of Southern Africa where a plume of AOD_{550} of about 0.4 was simulated.

Regarding temperatures, negative temperature anomalies (cooling) of about 5°C is simulated over Southern Africa during all seasons except JJA where slight warming of 1.0°C was simulated over the regions of Zimbabwe, Botswana and south Mozambique and some central-west parts during JJA. By comparing the seasonal mean AOD_{550} and surface temperature anomalies (figure 20), it is obvious that the geographical distribution of surface temperature anomalies does not necessarily follow the distribution of AOD_{550}.

As in Chapter 4 Figures 14 and 15, there is no clear robust relationship between the spatial distribution of AOD and seasonal surface temperature. The sensitivity of seasonal surface temperature to aerosols differs for different seasons, this implies that there must be other sources of aerosol or factors that can be responsible for the seasonal temperature dependence on the spatial distribution of AOD. The vertical profile of aerosols is mostly dependent on large-scale synoptic conditions (e.g., Wang *et al*., 2018). Over Southern Africa, variation of aerosol concentration from one season to another is controlled by the development of synoptic weather. For example, the region is dominated by subtropical anticyclones, barotropic quasi-stationary easterly waves, baroclinic disturbance in the westerlies, and ridging anticyclones (e.g. Newell *et al*., 1972; Garstang *et al*., 1996c; Swap *et al*., 1996; Tyson *et al*., 1996a). Southern Africa is influenced by interaction of extratropical westerly and tropical easterly flows, and the anticyclonic gyres result in stagnant air mass over the region which causes re-circulation of aerosols and trace gases (Tyson, 1981; Swap *et al*., 1996).

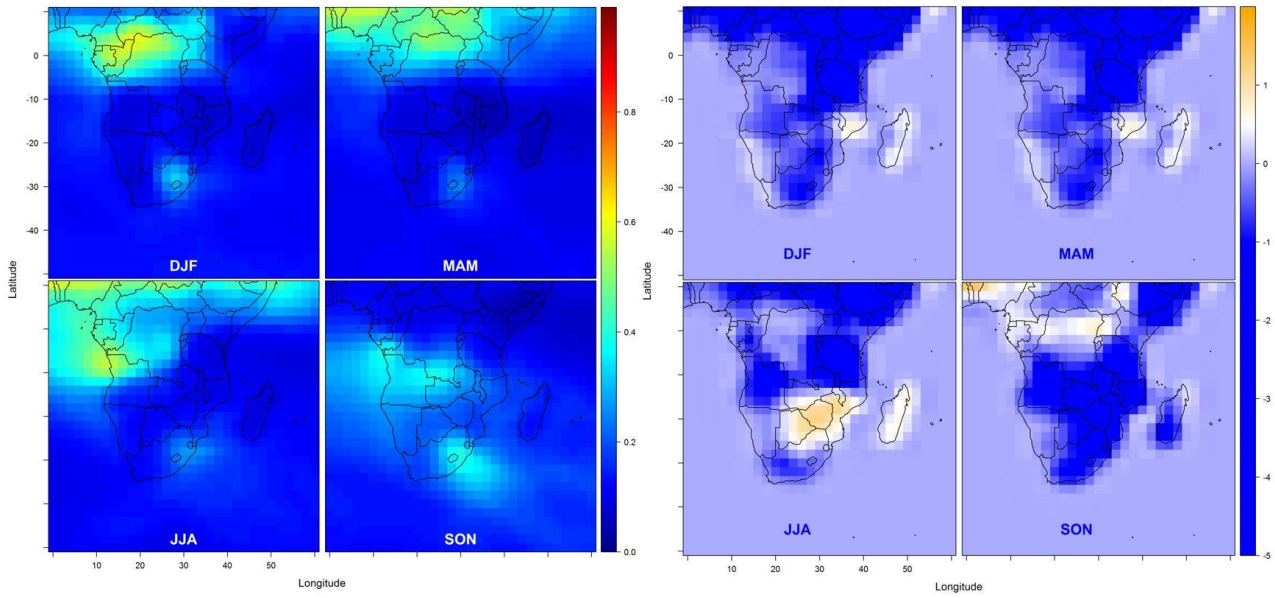

Figure 20: The relationship between the simulated AOD_{550} (on the left) and warming/cooling (on the right) according to CCAM aerosol scheme. The map on the left shows the simulated seasonal mean of AOD_{550} and the map on the right shows the simulated seasonal mean aerosol induced changes in surface air temperature (°C), over Southern Africa, averaged over the years 2000 - 2014.

5.3. Conclusion

The sensitivity of simulated temperatures in CCAM to aerosols over Southern Africa was investigated in this chapter. Firstly, the CCAM was evaluated against surface temperature observations and the results show that the model was able to reproduce Southern African surface temperature relatively well. Secondly, the spatial distribution of simulated AOD_{550} was compared against MODIS observations. The CCAM has shown an ability to simulate spatial distribution of AOD_{550} but underestimated the magnitude of AOD_{550} when compared to satellite retrievals. From the sensitivity experiment, the results have shown that aerosols affect Southern African surface temperatures. In general, aerosols induce cooling of surface temperatures that range between 1.0 – 3.5°C.

The overall results have shown that aerosols induce changes in temperature over Southern Africa (Chapter 4); the negative cooling that ranged between 0.25 – 1.5 °C was found in GISS modelE while warming was simulated in some areas. To a certain extent the results have been consistent with the Gettelman *et al*. (2015) sensitivity results for the Southern African region. The surface temperature sensitivity in CCAM (Chapter 5) models have been higher in magnitude as compared to previous studies carried out over Southern Africa (Tummon *et al*., 2010; Gettelman *et al*., 2015).

Chapter 6: Climate Models Inter-comparison

6.1. Introduction

The results from chapter 4 and 5 show that, to some degree, simulated surface temperature is sensitive to aerosols in both models. In this chapter, it is investigated whether there is a difference in simulated climate response across the two GCMs. The climate model simulations have been conducted with the implementation of different aerosol schemes. However, simulations from both models were AMIP-style runs, and use CMIP5 emissions. The first comparison is between simulations achieved using the same model (i.e. GISS-modelE) but driven by different aerosol schemes namely the MATRIX and OMA (simple) aerosol schemes. Lastly, simulations across the GCMs are compared; the following is the set of comparison experiments that are categorized as follows:

- **Comp-Exp1:** GISS-modelE (MATRIX) compared to GISS-model (OMA)
- **Comp-Exp2:** GISS-modelE (MATRIX) compared to CCAM
- **Comp-Exp3:** GISS-modelE (OMA) compared to CCAM

6.2. Results and Discussion

6.2.1. Statistical Quantification of Difference in Temperature Simulations

Figures 21, 22 and 23 show statistical analysis of simulated aerosol induced changes in simulated surface air temperature for comparison experiment, **Comp-Exp1**, **Comp- Exp2** and **Comp-Exp3,** respectively. For **Comp-Exp1** (figure 21), the *SMAPE* ranges between 0.1 – 0.2 over the SADC region and slightly below 0.1 over the higher latitude (from 10 °S and higher), the *MAE* & *RMSE* resemble a relatively similar spatial pattern with *MAE* & *RMSE* ranging between 1.2 – 2.0 over SADC region and 0.4 – 0.8 over the rest of Southern Africa. For *ME*, a magnitude of error of about 0.2 – 0.6 occurs over the eastern parts of the region and relatively low magnitude of is simulated over the north-central parts of Southern Africa.

The statistical analysis of **Comp-Exp2** is displayed in figure 22. The general spatial pattern of error is that a relatively higher magnitude of error is simulated over Botswana, Namibia, South Africa and Zimbabwe, especially for *SMAPE* (0.3 – 0.5), *MAE* (4.5 – 7) and *RMSE* (5 – 9). Everywhere else the magnitude of error is relatively low; ranges between 0.2 – 3.0 for aforementioned stats. Regarding *ME*, the spatial distribution of statistical error is similar to the **Comp-Exp1** (figure 21), however, the magnitude is higher than the error obtained in **Comp-Exp1** (figure 21).

Figure 23 shows the statistical analysis of **Comp-Exp3**. Surprisingly, all four quantitative statistics (*SMAPE*, *MAE*, *RMSE* & *ME*) show a similar pattern as the results of **Comp-Exp2** (figure 22). The spatial and magnitude of error resembles the results displayed in figure 22. The magnitude of error obtained while comparing the difference between CCAM and GISS-model is greater than the magnitude of difference between the two schemes within GISS-model (figure 21 Vs. figure 22 & 23).

A relatively higher magnitude of error that has been seen under **Comp-Exp1**, **Comp-Exp2** and **Comp-Exp3** implies that there are high discrepancies in surface temperatures simulated with the implementation of different aerosol schemes across the GCMs.

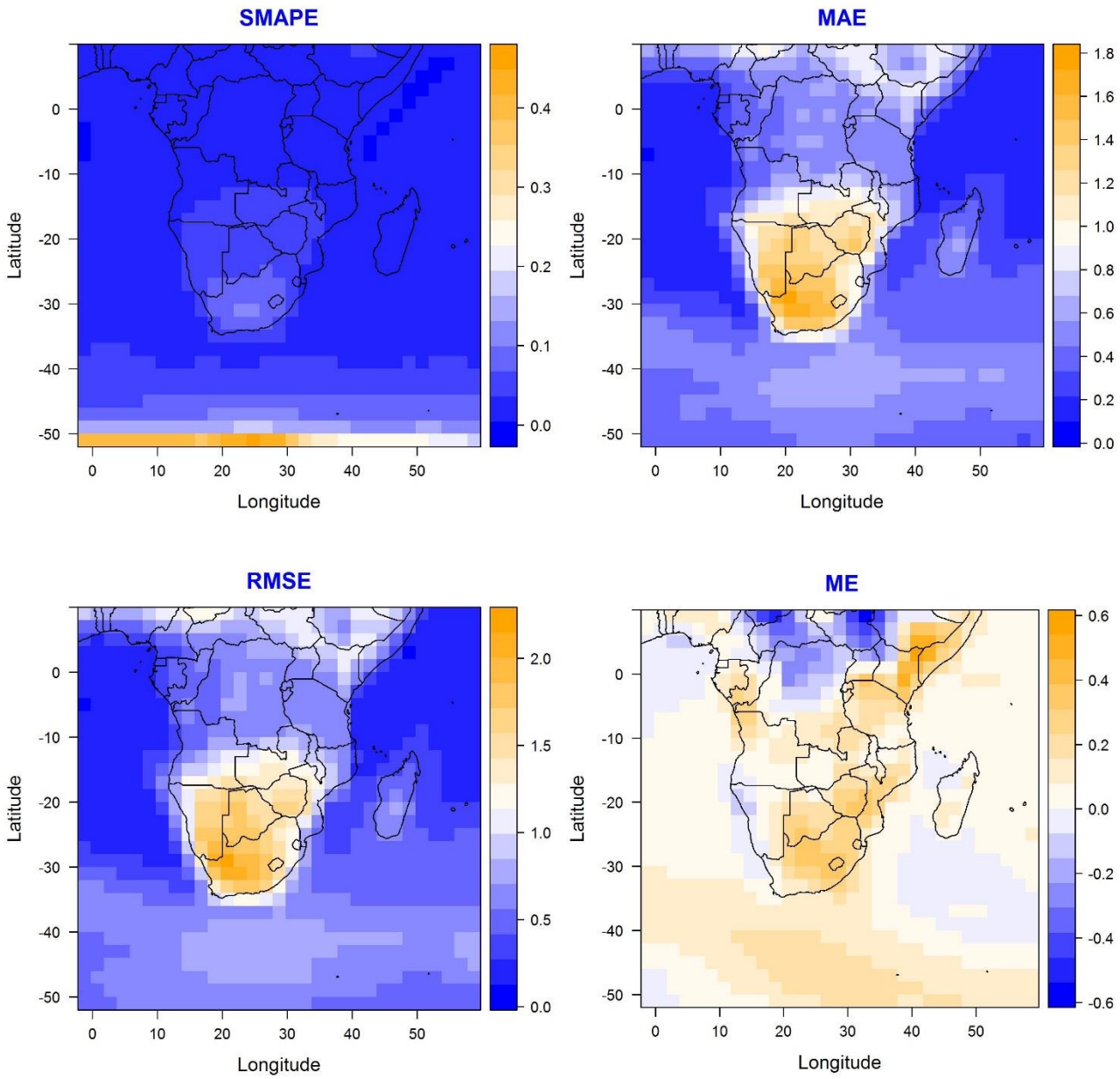

Figure 21: Statistical analysis of simulated mean aerosol induced changes in surface air temperature, the difference between GISS – modelE (OMA) and GISS – modelE (MATRIX), the statistics include SMAPE, MAE, RMSE and ME.

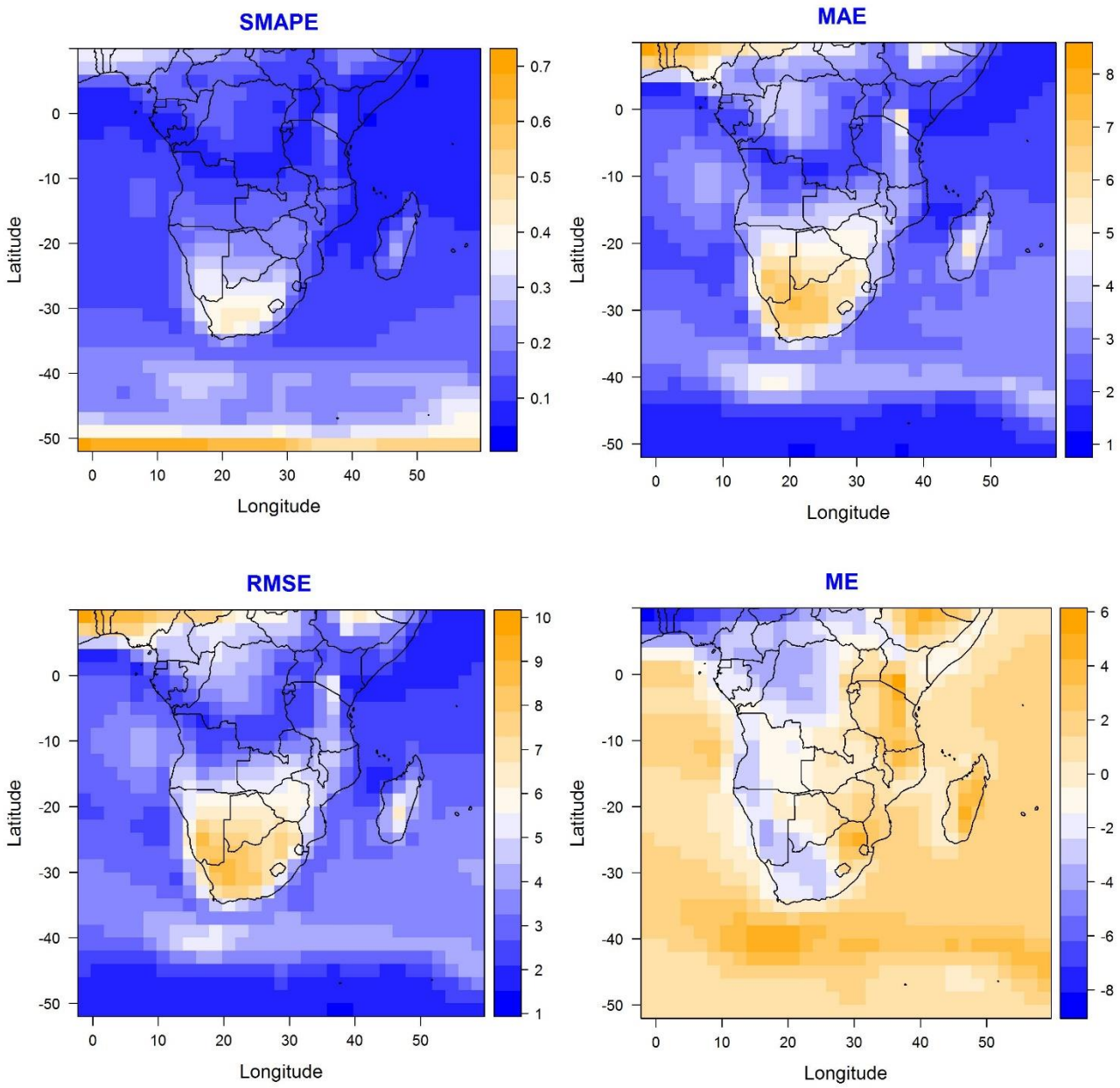

Figure 22: Statistical analysis of simulated mean aerosol induced changes in surface air temperature, the difference between GISS – modelE (MATRIX) and CCAM, the statistics include SMAPE, MAE, RMSE and ME.

.

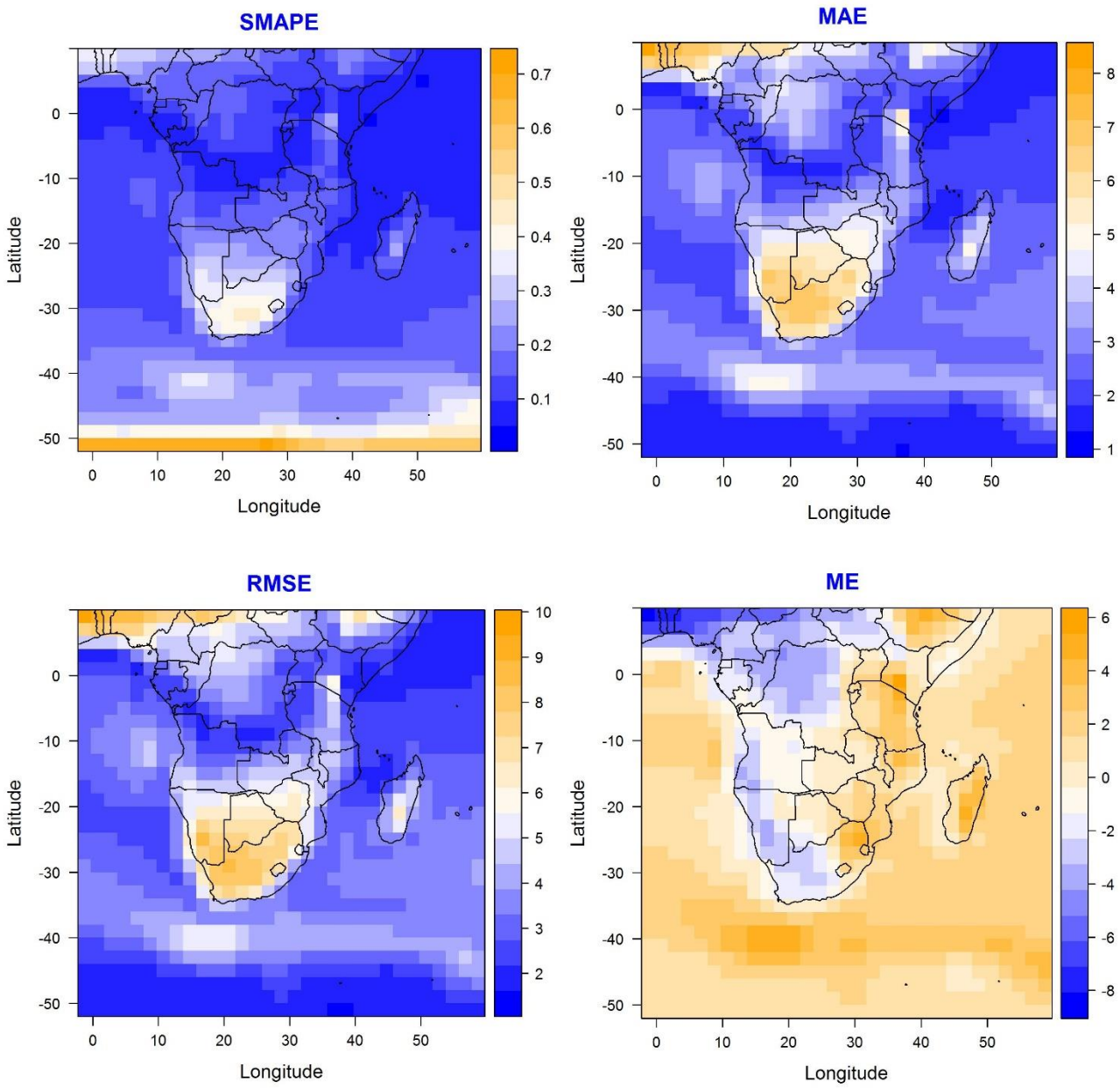

Figure 23: Statistical analysis of simulated mean aerosol induced changes in surface air temperature, the difference between GISS – modelE (OMA) and CCAM, the statistics include SMAPE, MAE, RMSE and ME.

6.2.2. Anomalies in Temperature Simulations

Figure 24 shows the seasonal spatial difference between the surface temperature simulated with GISS-modelE with the implementation of OMA and MATRIX aerosols scheme. Surface temperature anomalies were obtained by subtracting simulated surface temperature with aerosols on, in MATRIX, from simulated surface temperature with aerosols on, in OMA. It is clear from figure 24 that there is a difference of some degree on simulated surface temperature with the implementation of these in aerosol schemes. On average the seasonal temperature

anomalies range between +0.5 and -0.5 °C. Some regions exhibit localized positive temperature anomalies, while other regions show negative anomalies. This implies that there is no coherent surface temperature response across the two aerosol schemes.

The MATRIX and OMA simulation that is compared to one another in figure 24, are now compared to the CCAM simulation in figures 25 and 26, respectively. The difference between surface temperature simulation achieved with GISS-modelE and CCAM are quite different. The temperature anomalies range between +5.0 and -15.0°C for both MATRIX (figure 25) and OMA (figure 26) against the CCAM. Apart from relatively small positive anomalies over the eastern part of Southern Africa, there are significantly negative anomalies of about 15.0°C in all the seasons. Given that anomalies were computed by subtracting GISS-modelE simulation from CCAM simulation, a negative value indicates that CCAM simulations are cooler (lower in magnitude) as compared to GISS-modelE simulations.

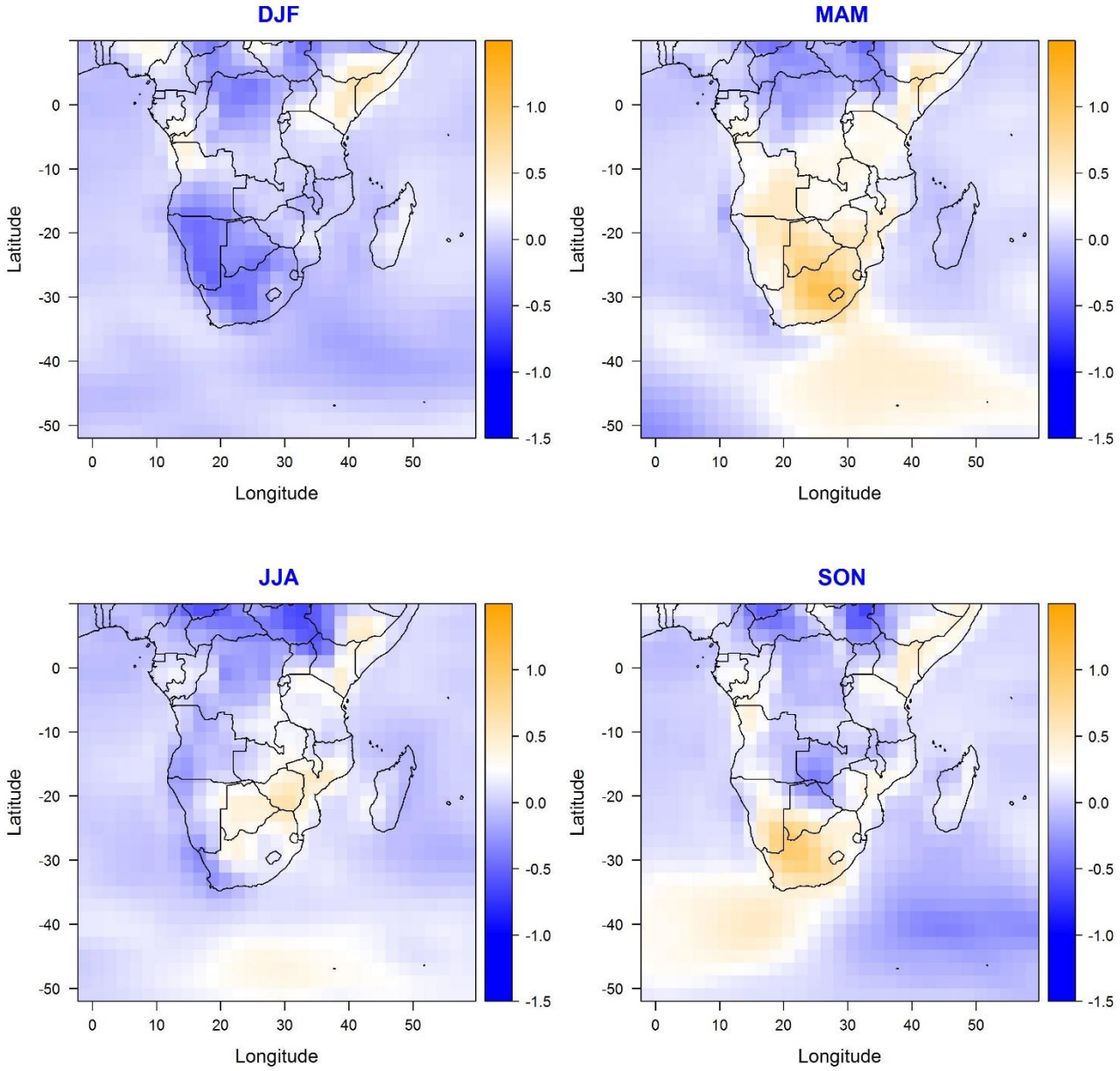

Figure 24: Simulated seasonal mean aerosol–induced changes in surface air temperature (°C), difference between GISS – modelE (OMA) and GISS – modelE (MATRIX), which has been averaged over the years 2000 – 2014.

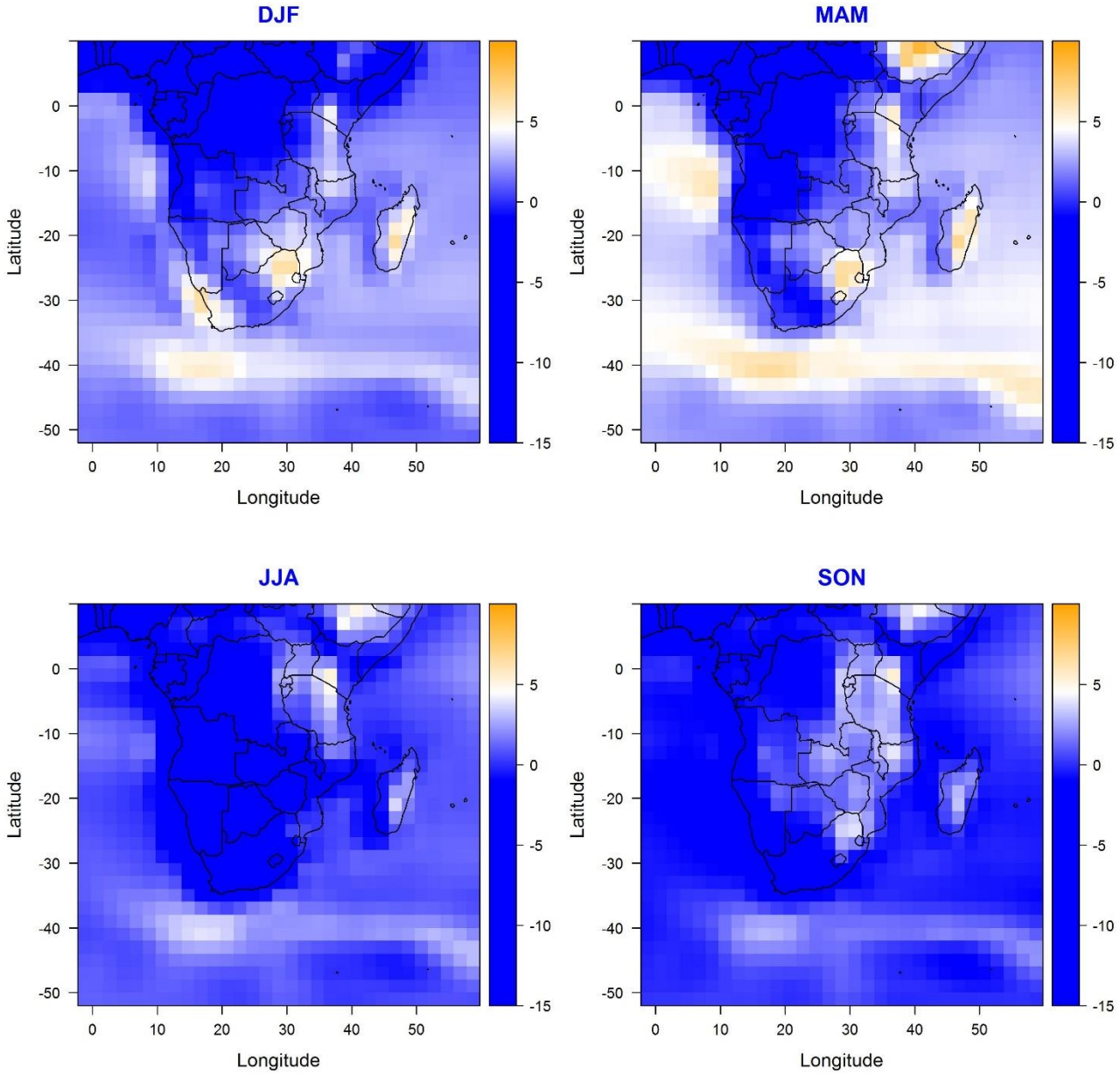

Figure 25: Simulated seasonal mean aerosol induced changes in surface air temperature (°C), difference between GISS – modelE (MATRIX) and CCAM, which has been averaged over the years 2000 – 2014.

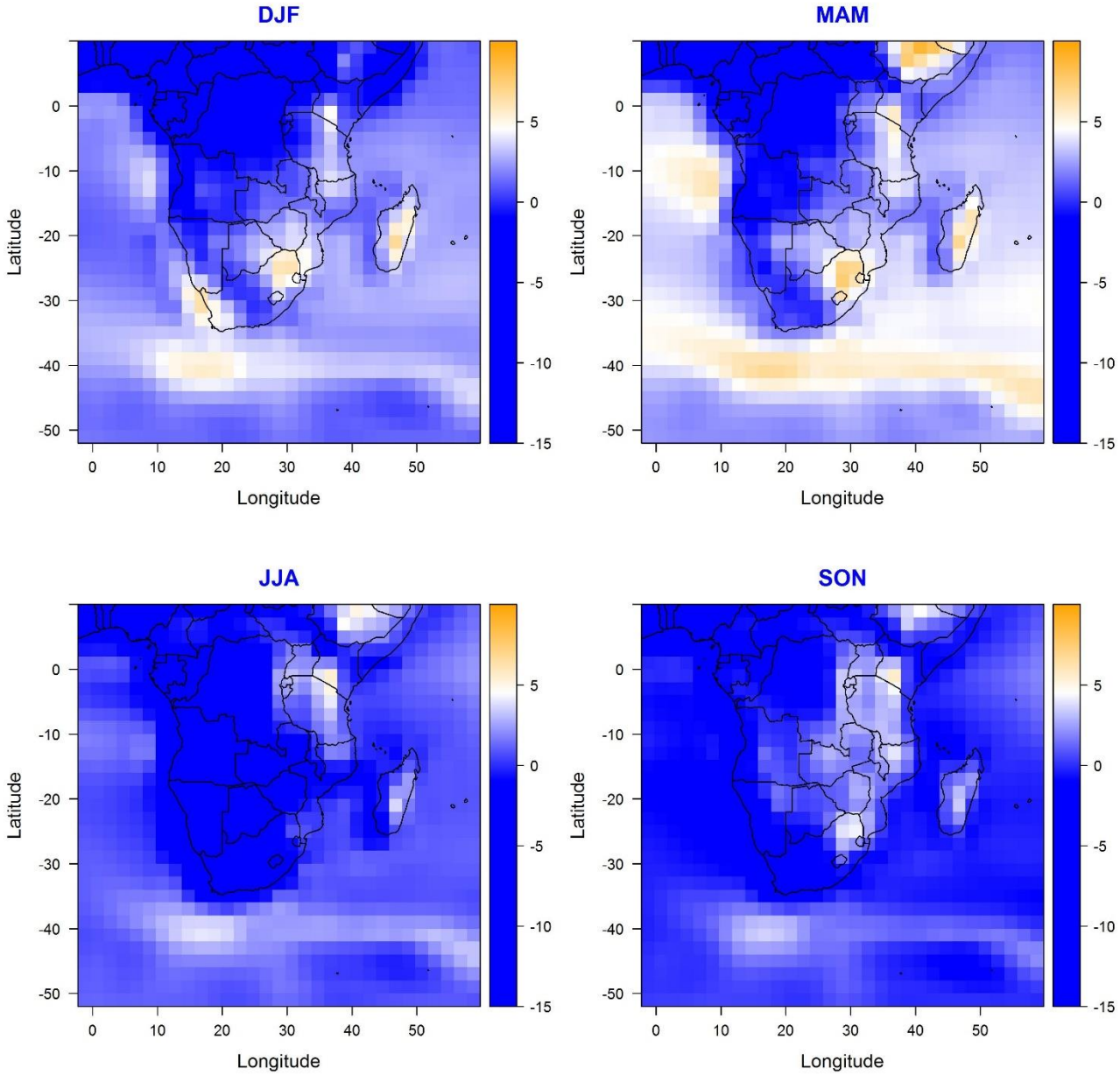

Figure 26: Simulated seasonal mean aerosol–induced changes in surface air temperature (°C), the difference between GISS – modelE (OMA) and CCAM, which has been averaged over the years 2000 – 2014.

6.3. Conclusion

The differences between seasonal surface temperature response between different models have been investigated. The results show that the models vary in both spatial distribution and magnitude of surface temperature response. The difference between GISS-modelE and CCAM simulation is somewhat higher as compared to the difference between GISS-modelE (MATRIX) and GISS-model (OMA). The seasonal surface temperature response is more pronounced in the CCAM model as compared to the GISS-modelE.

Chapter 7: Summary

A fourteen-year (2000 – 2014) study of simulations of surface temperatures and AOD_{550} was performed using two GCMs, namely the CCAM and the GISS-modelE GCMs, at coarse resolution (~200 km) with and without the effect of their respective aerosol schemes. Two distinct aerosol schemes, namely MATRIX and OMA, were utilized in GISS model simulation, while CCAM simulations used an interactive aerosol scheme from the Mk3 CSIRO. This study has aimed to investigate the sensitivity of simulated surface temperatures to aerosols over Southern Africa (10°N - 35°S and 0°W - 60°E) using the GCMs. Here is a summary of the significant research highlights and main conclusions in response to the study objectives posed in Chapter 1:

Objective 1: Evaluate the skill of GISS-modelE in simulating Southern African surface temperature.

The GISS-modelE was able to reproduce mean seasonal surface temperatures over Southern Africa relatively well. However, the model tends to overestimate (positive bias) surface temperatures over the western part by approximately 1.0 – 2.5°C and underestimate (negative bias) temperatures in the eastern part 1.0 – 2.0°C across all seasons.

Objective 2: Evaluate the skill of GISS-modelE in simulating Southern Africa AOD.

For the model to be suitable for a sensitivity study, it must be able to simulate the spatio-temporal patterns of AOD in the region. To assess that, simulated AOD was compared with corresponding measured AOD obtained from AERONET sites (namely Ascension Island, Etosha Pan, Mongu, Reunion Island and Skukuza). Comparison was done for both aerosol schemes (i.e. MATRIX and OMA) and it was found that the model with both schemes was able to produce the temporal distribution of AOD, but underestimated the magnitude. It must be noted that there were relatively few measurements of AOD at Ascension and Reunion Island sites. Simulations obtained with the effect of the MATRIX aerosol scheme have slightly overestimated the magnitude of AOD at Etosha Pan, Mongu and Skukuza, whilst the OMA aerosol scheme has underestimated AOD at all sites except Mongu site. The Mongu site is situated in the biomass burning region over central Zambia. The AOD_{550} reaches the highest during the peak of biomass burning activity. Spatial distribution comparison has also shown that the model can reproduce the spatial pattern of AOD_{550} over Southern Africa. However, the magnitude has significantly been underestimated during all seasons. These biases in spatio-temporal patterns of AOD could be the results of poor representation of aerosol properties and processes in climate models; moreover, aerosol emissions in CMIP5 are highly parameterized and have uncertainties themselves. Simulated time-resolved AODs were

compared against poor quality station observed data (i.e. some stations have a lot of data missing), which leads to uncertainty in comparison of temporal distribution between observed and simulated AOD. MODIS instrument samples once a day and the model simulated all day long, are another sources of biases in comparison to simulated and satellite observed AOD.

Objective 3: Investigate the sensitivity of simulated temperature in GISS-modelE climate model to aerosols over Southern Africa.

To assess the sensitivity of simulated surface temperature to aerosols, four simulations have been achieved. Seasonal surface temperature simulations *with* and *without* the aerosol schemes have been achieved using GISS-modelE for both MATRIX and OMA aerosol schemes. The sensitivity of surface temperature was investigated through calculating surface temperature anomalies between simulations achieved with the aerosol scheme and simulations achieved without the aerosol scheme. Quantitative statistics, namely the symmetric mean absolute percentage error (*SMAPE*), mean absolute error (*MAE*), root mean square error (*RMSE*) and mean error (*ME*) (see equations 3.4, 3.5, 3.6 and 3.7 respectively) have been used to investigate the difference in magnitude between simulation achieved with and without the aerosol scheme. Generally, all the quantitative statistics show the error value that is greater than zero, which indicates that the simulated surface temperatures are sensitive to aerosols.

To investigate the sensitivity of the simulated temperatures, the seasonal anomalies have been calculated. In general, it was found that aerosols induce a change in seasonal surface temperatures over Southern Africa. The change varies spatially. According to MATRIX, the region had a cooling that ranges between 0.25 – 1.5°C during DJF, JJA and SON except for the Botswana, Namibia, South Africa, Zimbabwe, Mozambique and Zambia regions that had a warming of approximately 0.5˚C. During MAM, warming of 0.25 – 0.75˚C was pronounced over the region. On the other hand, OMA aerosol scheme shows a relative cooling of 0.25 – 1.0°C during DJF, MAM, and SON season over South Africa and warming of 0.5°C during JJA. The eastern part shows a slight warming of 0.25°C throughout the seasons. The MATRIX and OMA aerosol schemes resulted in different surface temperature sensitivity that varies with space and time. However, comparing surface temperature anomalies with AOD_{550} distribution, reveal some interesting results. Surface temperature anomalies do not necessarily follow the distribution of AOD_{550}. Some areas experienced cooling with high AOD_{550} while others experienced warming and the reverse is true for both MATRIX and OMA aerosol schemes.

Objective 4: Evaluate the skill of CCAM in simulating Southern Africa surface temperature.

Evaluation of CCAM model against CRU dataset shows that the model overestimates surface temperature by about 10°C over the central and west coast of SADC during MAM, JJA, and SON, but underestimated it by about 2°C over the eastern and northern parts of Southern Africa during DJF.

Objective 5: Investigate the sensitivity of simulated temperature in CCAM climate model to aerosols over Southern Africa.

While comparing simulated AOD to satellite AOD was not an objective for CCAM, CCAM tends to perform well in simulating the spatial distribution of AOD_{550} in all seasons, though it also underestimates AOD_{550} when compared to MODIS.

Similar simulation as in objective 3 has been achieved, but in this case, with the use of the CCAM climate model, surface temperature anomalies simulated with and without the aerosol scheme have also been calculated and quantitative statistics was used to investigate the difference in magnitude of the simulations. All the metrics show relatively high error values that are greater than zero over the SADC region and northeast of Southern Africa. This implies that aerosols affect simulated surface temperatures over Southern Africa.

CCAM model sensitivity shows the general cooling of surface temperature that ranges between 1.0 – 3.5°C over Southern Africa during DJF and MAM while similar cooling is simulated over Angola, South Africa, Zambia, Tanzania, Kenya, Somalia, Ethiopia, Uganda, Cameroon, and Nigeria during JJA. Warming of 0.5 – 1.0°C was simulated during JJA over Botswana, Zimbabwe, western Mozambique, and over the DRC. This seasonal surface temperature cooling does not follow the seasonal distribution of AOD_{550}.

Objective 6: Investigate the difference between GCMs simulations of surface temperature with the implementation of different aerosol schemes.

Here it was investigated whether there are any differences in seasonal surface temperature anomalies simulated by the different GCMs. Firstly, the results from GISS modelE but driven by two different aerosol schemes (i.e. MATRIX and OMA) have been compared and these were later compared against CCAM. Generally, the error between MATRIX and OMA simulation ranges between -0.6 to +2.0 (SMAPE, MAE, RMSE and ME) over Southern Africa. For comparison of the GISS model with CCAM model, it was found that both GISS model aerosol schemes (MATRIX and OMA) simulations result in the error value of -.4.0 to +9.0 (SMAPE, MAE, RMSE and ME). The results have shown that all the simulations are different from one another, this implies that the aerosols simulated from these three aerosol schemes, have different effects on the simulated surface temperatures.

Regarding surface temperature sensitivity, the comparison between seasonal surface temperature anomalies simulated with the effect of MATRIX, OMA, and CCAM aerosol schemes, show that anomalies from the three aerosol schemes are different in magnitude during all seasons. Surface temperature anomalies simulated with GISS model forced with MATRIX and OMA range between -5.0°C and +5.0°C. Concerning surface temperature anomalies simulated with the GISS model and CCAM model, a difference ranging between -15.0°C and +5.0°C was found. This was relatively large as compared to the difference obtained from the GISS model forced with two different aerosol schemes. The difference in seasonal surface temperature anomalies from one aerosol scheme to another is the indication that each aerosol scheme impacts surface temperature differently, aerosols are quantified differently in the three-aerosol schemes; that is why seasonal surface temperature sensitivity is different for MATRIX, OMA and CCAM aerosol schemes.

Study limitations and suggestions for future research

This research study has been carried out with some methodological limitations; however, the results provide a foundation through which future research could be built on.

- The study has analysed relatively coarse resolution GCMs simulations. These models resolve aerosol mean properties and climate on a large scale. Given that aerosol concentrations are heterogeneous in space and time, the coarse resolution could mask out important effects of aerosols, especially at a regional scale like Southern Africa. Therefore, the use of higher resolution models for regional aerosol – climate studies is suggested.
- Observation data of AOD was insufficient and also had missing values and as a result, it was difficult to evaluate model simulated AOD_{550} which could lead to uncertainty in the interpretation of results. Therefore, to better understand the model‘s capability to simulate aerosol distribution good long term continuous observation data are needed.
- This study has investigated the effect of total aerosol loading on surface temperatures through use of AOD. Different aerosol species have different radiative properties. For example, some species, like sulphate aerosols, scatter results in negative radiative forcing, while black carbon results in positive radiative forcing. Given that, it is therefore advisable to investigate individual forcing mechanisms of each aerosol species on surface temperature within these models. Future research can also look at the effect of aerosols on direct and indirect radiative forcing.
- The comparison of modelled AOD and surface temperature anomalies averaged from 2000 – 2014, did not show any clear dependence, it is therefore recommended that such comparison be studied by separation of years especially years when there was a high burden of AOD.

- It was shown that the results from all three sensitivity experiments from three different aerosol schemes are different. This is an indication that aerosol characteristics and related processes are treated differently in the simulations. Aerosols are known to have a significant impact on radiative forcing and associated climatic impact. However, their properties are poorly quantified and characterized especially for a region like Southern Africa. Accurate representation of aerosols' properties and processes in climate models will be essential,particularly for the investigation of their impact on climate.
- The scope of this study was to investigate the response of mean surface temperature to aerosol. However, for future research, the maximum and minimum temperatures should also be investigated as there may be differences in their sensitivity to aerosols.
- This study only analyzed one ensemble member and the results could be considered as a poor presentation of GCM's capabilities because the models are not allowed to express some of their uncertainties through multiple realizations. The use of multiple ensemble members should be considered in future research.

References

Abel, S.J., Haywood, J. M, Highwood, E. J., Li J. and Buseck, P. R. (2003). Evolution of Biomass Burning Aerosol Properties from an Agricultural Fire in Southern Africa. *Geophys. Res. Lett*. 30, doi: 10.1029/2003GL017342 (2003).

Adachi, K., Chung, S. H., and Buseck, P. R. (2010). Shapes of soot aerosol particles and implications for their effects on climate, *J. Geophys. Res*., 115, D15206, https://doi.org/10.1029/2009jd012868.

Adesina, A. J., Kumar, K. R., Sivakumar, V., and Piketh, S. J. (2016). Inter-comparison and assessment of long-term (2004–2013) multiple satellite aerosol products over two contrasting sites in South Africa, *Journal of Atmospheric and Solar-Terrestrial Physics*, 148, 82 – 95.

Adesina, J. A., Piketh, S. J., Formenti, P., Maggs-Kölling, G., Holben, B. N. and Sorokin, M. G. (2019). Aerosol optical properties and direct radiative effect over Gobabeb, Namibia. *CLEAN AIR JOURNAL*, 19(2), https://doi.org/10.17159/caj/2019/29/2.751.

Ahn, H. J., Park, S. U., and Chang, L. S. (2007). Effect of Direct Radiative Forcing of Asian Dust on the Meteorological Fields in East Asia during an Asian Dust Event *Period, J. Appl. Met. Clim*., 46, 1655-1681.

Alexanrov, M. D., Carlson, B. E., Lacis, A. A., and Cairns, B. (2005). Separation of fine and coarse aerosol modes in MFRSR data sets. *J. Geophys. Res*., 110, D13204, doi: 10.1029/2004JD005226.

Anderson, T. R., Hawkins, E. and Jones, P. D. (2016). CO2, the greenhouse effect and global warming: from the pioneering work of Arrhenius and Calendar to today's Earth System Models, Endeavour, https://doi.org/10.1016/j.endeavour.2016.07.002.

Andreae, M. O., Jones, C. D., and Cox, P. M. (2005). Strong present-day aerosol cooling implies a hot future, *Nature*, 435, 1187–1190.

Andreas, E.L., Pattison, M. J. and S. E. Belcher, S. E. (2001). "Production rates of seas-spray droplets" by M.J. Pattisoin and S.E. Belcher: Clarification and elaboration, *J. Geophys. Res*., 106, 7157–7161.

Ayash, T., Gong, S. L. and Jia, C. Q., (2008). Direct and Indirect shortwave radiative effects of sea salt aerosols. *Journal of climate*, 21, 3207-3220.

Bauer, S. E., and Koch, D. (2005). Impact of heterogeneous sulphate formation at mineral dust surfaces on aerosol loads and radiative forcing in the Goddard Institute for Space Studies general circulation model. *Journal of Geophysical Research-Atmospheres*,110(D17), D17202.https://doi.org/10.1029/2005JD005870.

Bauer, S. E., Mishchenko, M. I., Lacis, A. A., Zhang, S., Perlwitz, J., and Metzger, S. M. (2007). Do sulphate and nitrate coatings on mineral dust have important effects on radiative properties and climate modeling?*Journal of Geophysical Research-Atmospheres,*112(D6), D06307.https://doi.org/10.1029/2005JD006977.

Bauer, S. E., Tsigaridis, K., and Miller, R. (2016). Significant atmospheric aerosol pollution caused by world food cultivation, *Geophys. Res. Lett*., 43, 5394–5400, doi: 10.1002/2016GL068354.

Bauer, S. E., Wright, D. L., Koch, D., Lewis, E. R., McGraw, R., Chang, L. S., Schwartz, S. E., and Ruedy, R. (2008). Matrix (Multi-configuration Aerosol Tracker of mIXing state): an aerosol microphysical module for global atmospheric models. *Atmos. Chem. Phys*, 8, 6003-6035.

Behera, S. K. and Yamagata, T., (2001). Subtropical SST dipole events in the southern Indian Ocean, *Geophysical Research Letters*, 28,2, 327-330. https://doi.org/10.1029/2000GL011451.

Bèque, N., Vignelles, D., Berthet, G., Portafaix, T., Payen, G., Jégou, F., Benchérif, H., Jumelet, J., Vernier, J., Lurton, T., Renard, J. Clarisse, L., Duverger, V., Posny, F., Metzger, J., and Godin-Beekmann, S. (2017). Long-range transport of stratospheric aerosols in the Southern Hemisphere following the 2015 Calbuco eruption, *Atmos. Chem. Phys*., 17, 15019 – 15036.

Beuer, S. E., Ault, A., and Prather, K. A., (2013). Evaluation of aerosol mixing state classes in the GISS-modelE-MATRIX climate model using single particle mass spectrometry measurements. *J. Geophys. Res*., 118, 9834-9844, doi:10.1002/jgrd.50700.

Bhattachan, A., D' Odorico, P., Baddock, M. C., Zobeck, T. M., Okin, G. S., and Cassar, N. (2012). The Southern Kalahari: A potential new dust source in the Southern Hemisphere? *Environ. Res. Lett*., 7(2), 024001.doi:10.1088/1748-9326/7/2/024001.

Black, E., Slingo, J. and Sperber, K. R., (2003). An observational study of the relationship between excessively strong short rains in coastal East Africa and Indian Ocean SST, *Monthly Weather Review*, 131, 1, 74-94. http://dx.doi.org/10.1175/1520-0493(2003)131<0074: AOSOTR>2.0.CO;2.

Blanchard, D. C. and Woodcock, A. H. (1980). THE PRODUCTION, CONCENTRATION, AND VERTICAL DISTRIBUTION OF THE SEA-SALT AEROSOL*. Annals of the New York *Academy of Sciences*, 338(1), 330-347.

Bohren, C. and Huffman, D. (2004). Absorption and Scattering of Light by Small Particles, Wiley-VCH, Weinheim, *Germany*, 82–129.

Bond, T. C., D. G. Streets, K. F. Yarber, S. M. Nelson, J. Woo, and Z. Klimont, (2004). A technology-based global inventory of black and organic carbon emissions from combustion, *J. Geophys. Res*., 109, D14203, doi:10.1029/2003JD003697.

Bond, T. C., Doherty, S. J., Fahey, D. W., Forster, P. M., Bernsten, T., DeAngelo, B. J., Flanner, M. G., Ghan, S., Karcher, B., Koch, D., Kinne, S., Kondo, Y., Quinn, P. K., Sarofim, M. C., Schultz, M. G., Schulz, M., Venkataraman, C., Zhang, H., Bellouin, N., Guttikunda, S. K., Hopke, P. K., Jacobson, M. Z., Kaiser, J. W., Klimont, U., Lohman, U., Schwarz, J. P., Shindell, D., Storelvmo, T., Warren, S. G., and Zender, C. S. (2013). Bounding the role of black carbon in the climate system: A scientific assessment. *Journal of Geophysical Research*. 118, 5380-5552.

Bondy, A. L., Bonanno, D., Moffet, R. C., Wang, B., Laskin, A. and Ault, A. P. (2018). The diverse chemical mixing state of aerosol particles in the southern United States. *Atmos. Chem. Phys*, 18, 12595-12612, 2018https://doi.org/10.5194/acp-18-12595-2018.

Boucher, O., Randall, D., Artaxo, P., Bretherton, C., Feingold, G., Forster, P., Kerminen, V.-M., Kondo, Y., Liao, H., Lohmann, U., Rasch, P., Satheesh, S. K., Sherwood, S., Stevens, B., and Zhang, X. Y. (2013). Clouds and Aerosols, in: Climate Change 2013: The Physical Science Basis. Contribution of Working Group I to the Fifth Assessment Report of the Intergovernmental Panel on Climate Change, edited by: Stocker, T. F., Qin, D., Plattner, G.-K., Tignor, M., Allen, S. K., Boschung, J., Nauels, A., Xia, Y., Bex, V., and Midgley, P. M., Cambridge University Press, Cambridge, United Kingdom and New York, NY, USA.

Budhavant, K., Bikkina, S., Andersson, A., Asmi, E., Backman J *et al*. (2018) Anthropogenic fine aerosols dominate the wintertime regime over the northern Indian Ocean. *Tellus B Chem Phys Meteorol* 70(1):1464871. https ://doi.org/10.1080/16000889.2018.14648 71.

Castillo S., Alastuey A., Cuevas E., Querol X., Avila A. (2017). Quantifying dry and wet deposition fluxes in two regions of contrasting African influence: The NE Iberian Peninsula and the Canary Islands. *Atmosphere*. 2017; 8:86. doi: 10.3390/atmos8050086.

Chand, D., Wood, R., Anderson, T., Satheesh, S., and Charlson, R. (2009). Satellite-derived direct radiative effect of aerosols dependent on cloud cover, *Nat. Geosci*., 2, 181–184.

Cherian, R., Quaas, J., Salzmann, M., and Tomassini, L. (2017). Black carbon indirect radiative effects in a climate model, *Tellus B: Chemical and Physical Meteorology*, 69(1), 1369342, DOI: 10.1080/16000889.2017.1369342.

Chou, M. D. and Lee, K. T., (2005). A parameterization of the effective layer emission for infrared radiation calculations. *Journal of the Atmospheric Sciences*, 62, 531- 541.

Christensen, J. H., Hewitson, B., Busuioc, A., Chen, A., Gao, X., Held, I., Jones, R., Koli, R. K., Kwon, W, T., Laprise, R., Rueda, V. M., Mearns, L., Menéndez, C. G., Räisänen, J., Rinke, A., Sarr, A. and Whetton, P. (2007). Regional climate projections. Climate Change 2007: The Physical Science Basis. Contribution of Working Group I to the Fourth Assessment Report of the Intergovernmental Panel on Climate Change, S. Solomon, D. Qin, M. Manning, Z. Chen, M. Marquis, K.B. Averyt, M. Tignor and H.L. Miller, Eds., *Cambridge University Press*, Cambridge,

Chung, S. H. and Seinfeld, J. H. (2005). Climate response of direct radiative forcing of anthropogenic black carbon. *J Geophys Res*, 110, (D11): D11102, doi:10.1029/2004JD005441.

Clark, C., Webster, P. and Cole, J., (2003). Interdecadal variability of the relationship between the Indian Ocean zonal mode and East African coastal rainfall anomalies, *Journal of Climate*, 16, 3, 548-554. http://dx.doi.org/10.1175/1520-0442(2003)016<0548: IVOTRB>2.0.CO;2.

Collins, J.M. (2011). Temperature variability over Africa. *Journal of Climate*, 24 (14), 3649-3666

Cook, K. H., (2000). The South Indian Convergence Zone and Interannual rainfall variability over southern Africa, *Journal of Climate*, 13, 21, 3789-3804. http://dx.doi.org/10.1175/1520-0442(2000)013<3789:TSICZA>2.0.CO;2.

Cooke, W. F., Wilson, J. J. N., (1996). A global black carbon aerosol model. *J. Geophys. Res*., 101, 19395-19409.

Corney, S. P., Katzfey, J. J., Mcgregor, J. L., Grose, M. R., Bennett, J. C., White, C. J., Holz, G. K., Gaynor, S. M., and Bindhoff, N. L. (2010). Climate Futures for Tasmania: Climate Modelling. Antarctic Climate and Ecosystems Technical Report.81 pp. ISBN: 978-1-921197-06-2.

Crétat, J., Pohl, B., Richard, Y., and Drobinski, P. (2012). Uncertainties in simulating regional climate of Southern Africa: Sensitivity to physical parameterizations using WRF*. Clim Dyn*, 38, 613 – 634.

Curci, G., Hogrefe, C., Bianconi, R., Im, U., Balzarini, A., Baró, R., Brunner, D., Forkel, R., Giordano, L., Hirtl, M., Honzak, L., Jiménez-Guerrero, P., Knote, C., Langer, M., Makar, P. A., Pirovano, G., Pérez, J. L., San José, R., Syrakov, D., Tuccella, P., Werhahn, J., Wolke, R., Žabkar, Zhang, R. J., and Galmarini, S. (2015). Uncertainties of simulated aerosol optical properties induced by assumptions on aerosol physical and chemical properties: An AQMEII-2 perspective, *Atmos. Environ*., 115, 541–552.

d'Almeida, G. A. (1987). On the variability of desert aerosol radiative characteristics, *J. Geophys. Res*., 92, 3017–3026.

Dalirian, M., Ylisirniö, A., Buchholz, A., Schlesinger, D., Ström, J., Virtanen, A. and Riipinen, I. (2018). Cloud droplet activation of black carbon particles coated with organic compounds of varying solubility, *Atmos. Chem. Phys*., 18(16), 12477–12489, doi:10.5194/acp-18-12477.

Das, L., Annan, J. D., Hargreaves, J.C. and Emori, S. (2012). Improvements over three generations of climate model simulations for eastern India. *Climate Research*, 51(3), 201–216. https://doi.org/10.3354/cr01064.

Dedekind, Z., Engelbrecht, F. A., and van der Merwe, J. (2016). Model simulations of rainfall over Southern Africa and its eastern escarpment, *Water SA*, 42 (1), 129 – 143.

Dubovik, O., A. Smirnov, B. N. Holben, M. D. King, Y. J. Kaufman, T. F. Eck, and I. Slutsker (2000). Accuracy assessments of aerosol optical properties retrieved from AERONET Sun and sky-radiance measurements, *J. Geophys. Res*.,105(D8), 9791–9806, doi:10.1029/2000JD900040.

Dubovik, O., Holben, B. N., Lapyonok, T., Sinyuk, A., Mishchenko, M. I., Yang, P., and Slutsker, I. (2002). Non-spherical aerosol retrieval method employing light scattering by spheroids. *Geophys. Res. Lett*., 29, no. 10, 1415, doi: 10.1029/2001GL014506.

Duce, R. A., LaRoche, J., Altieri, K., Arrigo, K., Baker, A., Capone, D., Cornell, S., Dentener, F., Galloway, J., Ganeshram, R., Geider, R., Jickells, T., Kuypers, M., Langlois, R., Liss, P., Liu, S. M., Middelburg, J., Moore, C., Nickovic, S., Oschlies, A., Pedersen, T., Prospero, J., Schlitzer, R., Seitzinger, S., Sorensen, L., Uematsu, M., Ulloa, O., Voss, M., Ward, B. and Zamora, L., (2008) Impacts of atmospheric anthropogenic nitrogen on the open ocean. *Science*, 320, 893–897, doi: https://doi.org/10.1126/science.1150369.

Dusek, U., Reischl, G., and Hitzenberger, R. (2006). CCN activation of pure and coated black carbon particles, *Environ. Sci. Technol*., 40(4), 1223–1230, doi:10.1021/es0503478.

Easterling, D. R., Meehl, G. A., Parmesan, C., Changnon, S. A., Karl, T. R., and Mearns, L. O. (2000). Climate extremes: observations, modelling, and impacts. *Science*, 289: 2068-2074.

Eck, T. F., Holben, B. N., Ward, D. E., Mukelabai, M. M., Dubovik, O., Smirnov, A., Schafer, J. S., Hsu, N. C., Piketh, S. J., Queface, A., Le Roux, J., Swap, R. J. and Slutsker, I., (2003). Variability of biomass burning aerosol optical characteristics in Southern Africa during the SAFARI 2000 dry season campaign and a comparison of single scattering albedo estimates from radiometric measurements. *Journal of Geophysical Research,* 108, NO. D13, 8477, doi: 10.1029/2002JD002321.

Emetere, M. E. and Akinyemi, M. L. (2017). A short review on the effects of aerosols on visibility impairment, *Journal of Physics Conference Series* 852(1) 012006, doi: 10.1088/1742-6596/852/1/012006.

Engelbrecht, F. A., Landman, W. A., Engelbrecht, C. J., Landman, S., Bopape, M. M., Roux, B., McGregor, J. L., and Thatcher, M. (2011). Multi-scale climate modelling over Southern Africa using a variable-resolution global model, *Water SA,* 37, 647-658.

Engelbrecht, F., Adegoke, J., Bopape, M. J., Naidoo, M., Garland, R. M., Thatcher, M., McGregor, J., Katsfey, J., Werner, M., Ichuku, C. and Gatebe, C. (2015). Projections of rapidly rising surface temperatures over Africa under low mitigation. *Environmental Research Letters*, 10.

Engelbrecht, F.A., McGregor, J. L. and Engelbrecht, C. J. (2009). Dynamics of the Conformal-Cubic Atmospheric Model projected climate-change signal over Southern Africa. *Roy. Meteor. Soc*., 29, 1013-1033.

Fauchereau, N., Trzaska, S., Richard, Y., Roucou, P. and Camberlin, P. (2003). Sea surface temperature co-variability in the southern Atlantic and Indian Oceans and its connections with the atmospheric circulation in the southern hemisphere. *Int. J. Climatol*., 23, 663-677

Feichter, J., Kjellstrom, E., Rodhe, H., Dentener, F., Lelieveld, J. and Roelofs, G. J., (1996). Simulation of the tropospheric sulphur cycle in a global climate model, *Atmos. Environ*., 30, 1693-1707.

Flato, G., Marotzke, J., Abiodun, B., Braconnot, P., Chou, S.C., Collins, W., Cox, P., Drioech, F., Emori, S., Eyring, V., Forest, C., Gleckler, P., Guilyard, E., Jakob, C., Kattsov, V., Reason,

C., and Rummukainen, M. (2013). Evaluation of Climate Models. In: Climate Change (2013), the Physical Science Basis. Contribution of Working Group I to the Fifth Assessment Report of the Intergovernmental Panel on Climate Change [Stocker, T.F., D. Qin, G.-K. Plattner, M. Tignor, S.K. Allen, J. Boschung, A. Nauels, Y. Xia, V. Bex and P.M. Midgley (eds.)]. Cambridge University Press, Cambridge, United Kingdom and New York, NY, USA.

Formenti, P., Elbert, W., Maenhaunt, W., Haywood, J. M., and Andreae, M. O. (2003). Chemical composition of mineral dust aerosol during the Saharan Dust Experiment (SHADE) airborne campaign in the Cape Verde region, September 2000, *J. Geophys. Res*., 108 (D18), doi: 10.1029/2002JD002648, in press.

Forster, P., Ramaswamy, V., Artaxo, P., Berntsen, T., Betts, R., Fahey, D. W., Haywood, J., Lean, J., Lowe, D. C., Myhre, G., Nganga, J., Prinn, R., Raga, G., Schulz, M. and Van Dorland, R. (2007). Changes in Atmospheric Constituents and in Radiative Forcing. In: Climate Change 2007: The Physical Science Basis. Contribution of Working Group I to the Fourth Assessment Report of the Intergovernmental Panel on Climate Change [Solomon, S., D. Qin, M. Manning, Z. Chen, M. Marquis, K.B. Averyt, M. Tignor and H.L. Miller (eds.)]. Cambridge University Press, Cambridge, United Kingdom and New York, NY, USA.

Freiman, M.T. and S.J. Piketh. (2003). Air transport into and out of the industrial Highveld region of South Africa. *J. Appl. Meteo*. 42. 994-1002.

Fu, D., Kulawik, S. S., Miyazaki, K., Bowman, K. W., Worden, J. R., Eldering, A., Livesey, N. J., Teixeira, J., Irion F. W., Herman, R. L., Osterman, G. B., Liu, X., Levelt, P., Thompson, A. M., Strow, L. L., and Luo, M. (2018). Retrievals of Tropospheric Ozone Profiles from the Synergic Observation of AIRS and OMI: Methodology and Validation, Atmos. Meas. Tech. Discuss., submitted.

Funk, C., Michaelsen, J., and Marshall, M. (2012). Mapping recent decadal climate variations in precipitation and temperature across Eastern Africa and the Sahel. In: Remote Sensing of Drought: Innovative Monitoring Approaches [Wardlow, B.D., M.C. Anderson, and J.P. Verdin (eds.)]. CRC Press, Boca Raton, FL, USA, pp.331358

Garstang, M., Tyson, P. D., Swap, R., Edwards, M., Kllberg, P., and Lindesay, J. A. (1996). Horizontal and vertical transport of air over Southern Africa. *J. Geophys. Res*., 101:23721–23736.

Gates, W. L., Boyle, J., Covey, C., Dease, C., Doutriaux, C., Drach, R., Fiorino, M., Gleckler, P., Hnilo, J., Marlais, S., Phillips, T., Potter, G., Santer, B., Sperber, K., Taylor, K. and Williams,

D. (1998). An Overview of the Results of the Atmospheric Model Inter-comparison Project (AMIP I). *Bull. Amer. Meteor. Soc*., 73, 1962-1970.

Gentner, D.R.; Isaacman, G.; Worton, D.R.; Chan, A.W.H.; Dallmann, T.R.; Davis, L.; Liu, S.; Day, D.A.; Russell, L.M. and Wilson, K.R. (2012). Elucidating secondary organic aerosol from diesel and gasoline vehicles through detailed characterization of organic carbon emissions. *Proc. Natl. Acad. Sci*. USA, 109,18318–18323.

Gershenzon, M., Davidovits, P., Jayne, J. T., Kolb, C. E., and Worsnop, D. R. (2001). Simultaneous uptake of DMS and ozone on water, *J. Physical Chemistry A*, 105, 7031–7036.

Gettelman, A., Shindell, D. T. and Lamarque, J. F. (2015). Impact of aerosol radiative effects on 2000-2010 surface temperatures. *Climate Dynamics*, 45, 2165-2179.

Giannini, A., Saravanan, R. and Chang, P. (2003). Oceanic forcing of Sahel rainfall on inter-annual to inter-decadal time scales. *Science*, 302, 1027-1030.

Giles, D. M., Sinyuk, A., Sorokin, M. S., Schafer, J. S., Smirnov, A., Slutsker, I., Eck, T. F., Holben, B. N., Lewis, J. R., Campbell, J. R., Welton, E. J., Korkin, S. and Lyapustin, A. (2019). Advancements in the Aerosol Robotic Network (AERONET) Version 3 database - automated near real-time quality control algorithm with improved cloud screening for Sun photometer aerosol optical depth measurements. *Atmospheric Measurement Techniques*, 12 (2019), pp. 169-209

Gordon, H. B., Rotstayn, L. D., McGregor, J. L., Dix, M. R., Kowalczyk, E. A., O'Farrel, S. P., Waterman, L. J., Hirst, A. C., Wilson, S. G., Collier, M. A., Watterson, I. G. and Elliott, T. I., (2002). *The CSIRO MK3 Climate System Model*. CSIRO Atmospheric Research Technical Paper No. 60.

Gregory, D. and Rowntree, P. R., (1990). A mass flux convection scheme with representation of cloud ensemble characteristics and stability dependent closure. *Monthly Weather Review*, 118, 1483- 1506.

Guo, L., Gu, W., Peng, C., Wang, W., Li, Y. J., Zong, T., Tang, Y., Wu, Z., Lin, Q., Ge, M., Zhang, G., Hu, M., Bi, X., Wang, X., and Tang, M. (2019). A comprehensive study of hygroscopic properties of calcium- and magnesium-containing salts: implication for hygroscopicity of mineral dust and sea salt aerosols, *Atmos. Chem. Phys*., 19, 2115–2133, https://doi.org/10.5194/acp-19-2115-2019.

Hansen, J., Ruedy, R., Glascoe, J., and Sato, M. (1999). GISS analysis of surface temperature change, *J. Geophys. Res.,* 104, 30997-31022, doi: 10.1029/1999JD900835.

Hansen, J., Ruedy, R., Sato, M., and Lo, K. (2010). Global surface temperature change. *Reviews of Geophysics*, 48 (RG4004).

Hansen, J., Russel, G., Rind, D., Stone, P., Lacis, A., Lebedeff, S., Ruedy, R., and Travis, L. (1983). Efficient three-dimensional global models for climate studies: Models I and II. *Monthly Weather Review*, 111, 609-662.

Hansen, J., Sato, M. and Ruedy, R. (1997). Radiative forcing and climate response. *J. Geophys. Res*. 102, 6831-6864

Hansen, J., Sato, M., Glascoe, J., and Ruedy, R. (1998). A common sense climate index: Is climate changing noticeably? *Proc. Natl. Acad. Sci*., 95, 4113-4120.

Hansen, J., Sato, M., Ruedy, R., Kharecha, P., Lacis, A., Miller, R., Nazarenko, L., Lo, K., Schmidt, G. A., Russell, G., Aleinov, I., Bauer, S., Baum, E., Cairns, B., Canuto, V., Chandler, M., Cheng, Y., Cohen, A., Del Genio, A., Faluvegi, G., Fleming, E., Friend, A., Hall, T., Jackman, C., Jonas, J., Kelley, M., Kiang, N. Y., Koch, D., Labow, G., Lerner, J., Menon, S., Novakov, T., Oinas, V., Perlwitz, Ja., Perlwitz, Ju., Rind, D., Ramanou, A., Schmunk, R., Shindell, D., Stone, P., Sun, S., Streets, D., Tausnev, N., Thresher, D., Unger, N., Yao, M., and Zhang, S. (2007). Climate simulations for 1880-2003 with GISS modelE. *Clim. Dyn*., 29, 661-696, DOI 10.1007/s00382-007-0255-8.

Hansen, J., Sato, M., Ruedy, R., Nazarenko, L., Lacis, A., Schmidt, G. A., Russel, G., Aleinov, I., Bauer, M., Bauer, S., Bell, N., Cairns, B., Canuto, V., Chandler, M., Cheng, Y., Del Genio, A., Faluvegi, G., Fleming, E., Friend, A., Hall, T., Jackman, C., Kelley, M., Kiang, N., Koch, D., Lean, J., Lerner, J., Lo, K., Menon, S., Miller, R., Minnis, P., Novakov, T., Oinas, V., Perlwitz, Ja., Perlwitz, Ju., Rind, D., Romanou, A., Shindell, D., Stone, P., Sun, S., Tausnev, N., Thresher, D., Wielicki, B., Wong, T., Yao, M., and Zhang, S. (2005). Efficacy of climate forcing. *Journal of Geophysical Research,* 110, D18104, doi: 10.1029/2005JD005776.

Harris, I., Jones, P. D., Osborn, T. J., and Lister, D. H., (2014). Updated high-resolution grids of monthly climatic observations – the CRU TS3.10 Dataset. *Int. J. Climatol*., 34, 623 – 642.

Hartmann, D.L., Klein Tank, A. M. G., Rusticucci, M., Alexander, L. V., Brnnimann, S., Charabi, Y., Dentener, F. J., Dlugokencky, E. J., Easterling, D. R., Kaplan, A., Soden, B. J., Thorne, P. W., Wild, M., and Zhai, P. M. (2013). Observations: Atmosphere and Surface. In: Climate Change 2013: The Physical Science Basis. Contribution of Working Group I to the Fifth

Assessment Report of the Intergovernmental Panel on Climate Change [Stocker, T.F., D. Qin, G.-K. Plattner, M. Tignor, S.K. Allen, J. Boschung, A. Nauels, Y. Xia, V. Bex and P.M. Midgley (eds.)]. Cambridge University Press, Cambridge, United Kingdom and New York, NY, USA.

Hatzianastassiou, N., Matsoukas, C., Drakakis, E., Stackhouse Jr, P. W., Koepke, P., Fotiadi, A., Pavlakis, K. G. and Vardavas, I., (2007): The direct effect of aerosols on solar radiation based on satellite observations, reanalysis datasets, and spectral aerosol optical properties from Global Aerosol Data Set (GADS). *Atmos. Chem. Phys*, 7, 2585-2599.

Haywood, J. M., Osborne, S. R., Francis, P. N., Keil, A., Formenti, P., Andreae, M. O. and Kaye, P. H., (2003). The mean physical and optical properties of regional haze dominated by biomass burning aerosol measured from the C-130 aircraft during SAFARI 2000. *Journal of Geophysical Research*, 108, NO. D13, 8473, doi: 10.1029/2002JD002226

Haywood, J., and Boucher, O. (2000). Estimates of the direct and indirect radiative forcing due to tropospheric aerosols: a review. *Rev. of Geophysics*, 38,513–543.

Heald, C. L., Ridley, D. A., Kroll, J. H., Barrett, S. R. H., Cady-Pereira, K. E., Alvarado, M. J. and Holmes, C. D., (2014). Contrasting the direct radiative effect and direct radiative forcing of aerosols. *Atmos. Chem. Phys*., 14, 5513-5527.

Helas, G. (1995). Emissions of atmospheric trace gases from vegetation fires. Phil. *Trans. Roy. Soc. Lond. A* 351, 297-312.

Hersey, S., Garland, R., Crosbie, E., Shingler, T., Sorooshian, A., Piketh, S. and Burger, R. (2015). An Overview of Regional and Local Characteristics of Aerosols in South Africa Using Satellite, Ground, and Modeling Data. *Atmos. Chem. Phys*. 15: 4259–4278.

Hess, M., Koepke, P., and Schult, I. (2010). Optical Properties of Aerosols and Clouds: The Software Package OPAC. *Bull. Amer. Meteor. Soc*., 79(5):831–844.

Hoell, A., Funk, C., Zinke, J. and Harrison, L., (2017). Modulation of the Southern Africa precipitation responseto the El Niño Southern Oscillation by the subtropical Indian Ocean Dipole, *Climate Dynamics*, 48, 7-8, 2529-2540. https://doi.org/10.1007/s00382-016-3220-6.

Holben, B. N., Eck, T. F., Slutsker, I., Tanre, D., Buis, J. P., Setzer, A., Vermote, E., Reagan, J. A., Kaufman, Y. J., Nakajima, T., Lavenu, F., Jankowiak, I., and Smirnov, A. (1998), AERONET—A federated instrument network and data archive for aerosol characterization. Rem. Sens. Env.66:1 – 16.

Horowitz, H., Garland, R. M., Thatcher, M., Landman, W. A., Dadekind, Z., van der Merwe, J., and Engelbrecht, F. A. (2017). Evaluation of climate model aerosol seasonal and spatial variability over Africa using AERONET, *Atmos. Chem. Phys*., 17, 13999–14023.

Huang Z. W., Huang, J., Hayasaka, T., Wang, S., Zhou, T., and Jin, H. (2015). Short-cut transport path for Asian dust directly to the arctic: a case study. *Environ Res Lett*. 10(11):114018.

Hubanks, P. A., King, M. D., Platnick, S. A. and Pincus, R. A. (2008). Modis atmosphere L3 gridded product algorithm theoretical basis, Tech. Rep. ATBD-MOD-30, National Aeronautics and Space Administration.

Hulme, M., Doherty, R., Ngara, T. and New, M. (2005). Global warming and African climate change. Climate Change and Africa, P.S Low, Ed., *Cambridge University Press*, Cambridge, 29-40.

Huneeus, N., Schulz, M., Balkanski, Y., Griesfeller, J., Kinne, S., Prospero, J., Bauer, S., Boucher, O., Chin, M., Dentener, F., Diehl, T., Easter, R., Fillmore, D., Ghan, S., Ginoux, P., Grini, A., Horowitz, L., Koch, D., Krol, M. C., Landing, W., Liu, X., Mahowald, N., Miller, R. L., Morcrette, J. –J., Myhre, G., Penner, J. E., Perlwitz, J. P., Stier, P., Takemura, T., and Zender, C. (2011). Global dust model inter-comparison in AeroCom phase I. *Atmos. Chem. Phys*., 11, 7781-7816, doi: 10.5194/acp-11-7781-2011.

Ichoku, C., Remer, L. A., Kaufman, Y. J., Levy, R., Chu, D. A., Tanre, D., and Holben, B. N. (2003). MODIS observation of aerosols and estimation of aerosol radiative forcing over Southern Africa during SAFARI 2000. *Journal of Geophysical Research-Atmospheres*, 108 (D13), 8499.

IPCC, 2013. Climate Change 2013: the physical science basis. In: Contribution of working Group I to the Fifth Assessment Report of the Intergovernmental Panel on Climate Change. Cambridge University Press, Cambridge, United Kingdom and New York.

Jacobson, M. Z., (2001). Strong radiative heating due to the mixing state of black carbon in atmospheric aerosols, *Nature*, 409, 695-697.

Jacobson, M. Z., (2002). Control of fossil-fuel particulate black carbon and organic matter, possibly the most effective method of slowing global warming, *J. Geophys. Res*., 107, D19, 4410, doi: 10.1029/2001JD001376.

Jickells, T. D., An, Z. S., Andersen, K. K., Baker, A. R., Bergametti, G., Brooks, N., Cao, J. J., Boyd, P. W., Duce, R. A., Hunter, K. A., Kawahata, H., Kubilay, N., LaRoche, J., Liss, P. S., Mahowald, N., Prospero, J. M., Rigwell, A. J., Tegen, I., and Torres, R. (2005): Global iron connections between desert dust, ocean biogeochemistry, and climate, Science, 308(5718), 67–71.

Jones, A., Haywood, J. M. and Boucher, O. (2007). Aerosol forcing, climate response and climate sensitivity in the Hadley Centre climate model, *J. Geophys. Res*., 112, D20211, doi:10.1029/2007JD008688.

Jones, P., Lister, D., Osborn, T., Harpham, C., Salmon, M., and Morice, C. (2012). Hemispheric and large-scale land-surface air temperature variations: An extensive revision and an update to 2010, *Journal of Geophysical Research: Atmospheres,* 117, D5.

Jurányi, Z., Burtscher, H., Loepfe, M., Nenkov, M., and Weingartner, E. (2015). Dual-wavelength light-scattering technique for selective detection of volcanic ash particles in the presence of water droplets, *Atmos. Meas. Tech*., 8, 12, 5213-5222, doi: 10.5194/amt-8 -5213-2015.

Jury, M. R., and Levey, K., (1993b). The Eastern Cape drought. *Water SA*, Vol. 19, No. 2, 133-137.

Kalnay, E. (2018). Atmospheric Modeling, Data Assimilation and Predictability, *Cambridge University Press, Second Edition*.

Kanakidou, M., Kanakidou, J.H., Seinfeld, S.N. Pandis, I., Barnes, F.J. Dentener, M.C., Facchini, R., Van Dingenen, B., Ervens, A., Nenes, C.J., Nielsen, E., Swietlicki, J.P., Putaud, Y., Balkanski, S., Fuzzi, J., Horth, G.K., Moortgat, R., Winterhalter, C.E.L., Myhre, K., Tsigaridis, E., Vignati, E.G., Stephanou, J. and Wilson (2005). Organic aerosol and global climate modelling: A review Atmospheric Chemistry and Physics, 5 (2005), pp. 1053-1123.

Kanika, K., Anil, K. G., and Rhythm, G. (2013). A Comparative Study of Supervised Image Classification Algorithms for Satellite Images, *International Journal of Electrical, Electronics and Data Communication*, 1(10), 10-16.

Katzfey, J. J., McGregor, J. L., Nguyen, K. C., and Thatcher, M. (2009). Dynamical downscaling techniques: Impacts on regional climate change signals. Proceedings, World IMACS/MODS IM Congress, Cairns.

Kaufman, Y.J., Tanré, D. and Boucher, O. (2002). A satellite view of aerosols in the climate system. *Nature*. 419. 215-223.

Keihl, J. T., and Rodhe, H. (1995). Modeling geographical and seasonal forcing due to aerosols, In: Aerosol Forcing of Climate [Charlson, R.J. and J. Heintzenberg, eds.], J. Wiley and Sons Ltd, pp 281-296.

Kim, D., Del Genio, A. and Yao, M. -S. (2011). Moist Convection scheme in ModelE2, Technical note (PDF).

Kinne, S., Lohmann, U., Feichter, J., Schulz, M., Timmreck, C., Ghan, S., Easter, R., Chin, M., Ginoux, P., Takemura, T., Tegen, I., Koch, D., Herzog, M., Penner, J., Pitari, G., Holben, B., Eck, T., Smirnov, A., Dubovik, O., Slutsker, I., Tanre, D., Torres, O., Mischenko, M., Geogdzhayev, I., Chu, D.A., and Kaufman, Y. (2003). Monthly averages of aerosol properties: A global comparison models, satellite data and AERONET ground data. *J. Geophys. Res.*108 (D20, 4634). Doi: 10.1029/2001JD001253

Kirchstetter, T. W., Novakov, T., Hobbs, P. V., and Magi, B. (2003). Airborne measurements of carbonaceous aerosols in Southern Africa during the biomass burning season, J. Geophys. Res., 108, doi: 10.1029/2002JD2171.

Knippertz P., and Todd M. C. (2012). Mineral dust aerosols over the Sahara: Meteorological controls on emission and transport and implications for modelling, *Rev. Geophys*., 50, RG1007, doi:10.1029/2011RG000362.

Knote, C., Hodzic, A., and Jimenez, J. L. (2015). The effect of dry and wet deposition of condensable vapours on secondary organic aerosols concentrations over the continental US, *Atmos. Chem. Phys*., 15, 1–18, https://doi.org/10.5194/acp-15-1-2015.

Knutti, R., Furrer, R., Tebaldi, C., and Cermark, J. (2010b). Challenges in combining projections from multiple climate models, *J. Clim.,* 23 (10), 2739-2758, doi:10.1175/2009JCLI3361.1.

Koch, D., Bauer, S. E., Del Genio, A. D., Faluvegi, G., McConnell, J. R., Menon, S., Miller, R. L., Rind, D., Ruedy, R., Schmidt, G. A., and Shindell, D. (2011). Coupled aerosol-chemistry-climate twentieth-century transient model investigation: Trends in short-lived species and climate responses. *J. Climate*., 24, 2693–2714.

Koch, D., Bauer, S. E., Del Genio, A., Faluvegi, G., McConnell, J.R., Menon, S., Miller, R. L., Rind, D., Ruedy, R., Schmidt, G. A., and Shindell, D. (2011): Coupled Aerosol-Chemistry-ClimateTwentieth-Century Transient Model Investigation: Trends in Short-Lived Species and Climate Responses, *J. Climate*, 24,2693–2714, doi:10.1175/2011jcli3582.1.

Koch, D., Bond, T. C., Streets, D., Unger, N., and van der Werf, G. R. (2007). Global impacts of aerosols from particular source regions and sectors, *J. Geophys. Res.-Atmos*., 112, D02205, doi:10.1029/2005jd007024.

Koch, D., Schmidt, G. A., and Field, C. V. (2006). Sulphur, sea salt, and radionuclide aerosols in GISS ModelE, *Journal of Geophysical Research-Atmospheres*,111(D6), D06206. https://doi.org/10.1029/2004JD005550.

Krishman, R. and Ramanathan, V., (2002). Evidence of surface cooling from absorbing aerosols. *Geophysical Research Letters*, 29, NO. 9, 1340, 10.1029/2002GL014687.

Kruger, A. C. and Shongwe, S. (2004). Temperature trends in South Africa: 1960–2003, *Int. J. Climatol.* 24, 1929–1945

Kruger, A.C. and Sekele, S. S. (2012). Trends in extreme temperature indices in South Africa: 1962-2009. *International Journal of Climatology*, 33(3), 661-676.

Kuik, F., Lauer, A., Beukes, J. P., Van Zyle, P. G., Josipovic, M., Vakkari, V., Laakso, L., and Feig, G. T. (2015). The anthropogenic contribution to atmospheric black carbon concentrations in Southern Africa: a WRF-Chem modelling study, *Atmos. Chem. Phys*., 15, 8809-8830. Doi: 10.5194/acp-15-8809-2015.

Kumar, K. R., Sivakumar, V., Yin, Y., Reddy, R. R., Kang, N., Diao, Y., Adesina, A. J., and Yu, X. (2014). Long-term (2003 – 2013) climatological trends and variations in aerosol optical parameters retrieved from MODIS over three stations in South Africa, *Atmospheric Environment*, 95, 400-408.

Laakso, L., Laakso, H., Aalto, P. P., Keronen, P., Petaja, T., Nieminen, T., Pohja, T., Siivola, E., Kulmala, M., Kgabi, N., Molefe, M., Mabaso, D., Phalatse, D., Pienaar, K. and Kerminen, V. M., (2008). Basic characteristics of atmospheric particles, trace gases and meteorology in a relatively clean Southern African Savannah environment. *Atmos. Chem. Phys*., 8, 4823-4839.

Laakso, L., Vakkari, V., Virkkula, A., Laakso, H., Backman, J., Kulmala, M., Beukes, J. P., van Zyl, P. G., Tiitta, P., Josipovic, M., Pienaar, J. J., Chiloane, K., Gilardoni, S., Vignati, E., Wiedensohler, A., Tuch, T., Birmili, W., Piketh, S., Collett, K., Fourie, G. D., Komppula, M., Lihavainen, H., de Leeuw, G., and Kerminen, V.-M. (2012). South African EUCAARI measurements: Seasonal variation of trace gases and aerosol optical properties, *Atmos. Chem. Phys*., 12 (4), 1847–1864.

Lacis, A. A. and Hansen, J. E. (1974). A parameterization for the absorption of solar radiation in the Earth's atmosphere. *Journal of the Atmospheric Sciences*, 31, 118-133.

Langner, J. and Rodhe, H. (1991). A global three-dimensional model of the tropospheric sulphur cycle. *J. Atmos. Chem*. 13, 225-263.

Lau, K. M. and Kim, K. M. (2007). Cooling of the Atlantic by Saharan dust, *Geophysical Research Letters*, VOL. 34, L23811, doi: 10. 1029/2007GL031538.

Leahy, L. V., Anderson, T. L., Eck, T. F. and Bergstrom, R. W. (2007), A synthesis of single scattering albedo of biomass burning aerosol over Southern Africa during SAFARI 2000, *Geophys. Res. Lett*., 34, L12814, doi:10.1029/2007GL029697.

Lee, J., Kim, J., Song, C. H., Ryu, J. H., Ahn, Y. H., and Song, C. K. (2010). Algorithm for retrieval of aerosol optical properties over the ocean from the Geostationary Ocean Colour Imager, *Remote Sens Environ*, 114, 1077-1088.

Lee, L. A., Reddington, C. L., and Carslaw, K. S. (2016). On the relationship between aerosol model uncertainty and radiative forcing uncertainty, *PNAS*, 113 (21), 5820-5827

Lee, Y. H. and Adams, P. J. (2010). Evaluation of aerosol distributions in the GISS-TOMAS global aerosol microphysics model with remote sensing observations, *Atmos. Chem. Phys*., 10, 2129–2144, doi:10.5194/acp-10-2129-2010.

Leibensperger, E. M., Mickley, L. J., Jacob, D. J., Chen, W. T., Seinfeld, J. H., Nenes, A., Adams, P. J., Rind, D., Streets, D. G., Kumar, N., and Rind, D. (2012). Climatic effects of 1950–2050 changes in US anthropogenic aerosols – Part 2: Climate response, *Atmos. Chem. Phys*., 12, 3349–3362, doi: 10.5194/acp-12-33492012.

Levy II, H., Horowitz, L. W., Schwarzkopf, M. D., Ming, Y., Golaz, J. C., Naik, V. and Ramaswamy, V. (2013). The roles of aerosol direct and indirect effects in past and future climate change: *Journal of Geophysical Research: Atmospheres*, 118, 1-12, doi:10.1002/jgrd.50192.

Levy, R. C., Remer, L. A., Mattoo, S., Vermote, E. and Kaufman, Y. J. (2007). The second-generation operational algorithm for retrieving aerosol properties over land from MODIS spectral reflectance, *J Geophys. Res*., 112, D13211, doi: 1029/2006/JD007811.

Lindesay, J. A., Andreae, M. O., Goldammer, J. G., Harris, G., Annegarn, H. J., Garstang, M., Scholes, R. J., and van Wilgen, B. W. (1996). International Geosphere-Biosphere

Programme/International Global Atmospheric Chemistry SAFARI-92 field experiment: Background and overview. *J. Geophys. Res*., 101:23521–23530.

Liu, C., Shen, X., Gao, W., Liu, P., and Sun, Z. (2014). Evaluation of CALIPSO aerosol optical depth using AERONET and MODIS data over China, In SPIE Optical Engineering Applications 2014 Oct 2 (92210F-92210F), *International Society for Optics and Photonics*, doi:10.1117/12.2058929.

Liu, J., Lin, P., Laskin, A., Laskin, J., Kathmann, S. M., Wise, M., Caylor, R., Imholt, F., Selimovic, V., and Shilling, J. E. (2016). Optical properties and aging of light-absorbing secondary organic aerosol, *Atmos. Chem. Phys*., 16, 12815-12827, 10.5194/acp-16-12815-2016.

Liu, R and Liao, H. (2017). Assessment of aerosol effective radiative forcing and surface air temperature response over eastern China in CMIP5 models, *Atmospheric and Oceanic Science Letters*, 10 (3), 228-234, DOI: 10.1080/16742834.2017.1301188.

Liu, X. D., Van Espen, P., Adams, F., Cafmeyer, J., and Maenhaut, W. (2000). Biomass burning in Southern Africa: Individual particle characterization of atmospheric aerosols and savannah fire samples, *J. Atmos. Chem*., 36, 135-155.

Lohmann, U., and Feichter, J. (2005). Global indirect aerosol effects: a review. *Atmos. Chem. Phys.,* 5, 715-737

Louis, J. F., (1979). A parametric model of vertical eddy fluxes in the atmosphere. *Boundary Layer Meteorology*, 17, 187-202.

Lu, H, and Shao, Y. P. (1999). A new model for dust emission by saltation bombardment, J *Geophys Res-Atmos,* 104, 16827–16841, Doi 10.1029/1999jd900169.

Lu, Z., Liu, X., Zhang, Z., Zhao, C., Meyer, K., Rajapakshe, C., Wu, C., Yang, Z., and Penner, J. E. (2018). Biomass smoke from Southern Africa can significantly enhance the brightness of stratocumulus over the south eastern Atlantic Ocean, *PNAS,* 115, 2924-2929.

Mahowald, N. M., R. Scanza, J. Brahney, C. L. Goodale, P. G. Hess, J. K. Moore, and Neff, J. (2017). Aerosol deposition impacts on land and ocean carbon cycles. *Current Climate Change Reports* 3(1):16-31. http://dx.doi.org/10.1007/s40641-017-0056-z.

Martinez Avellaneda, N., Serra, N., Minnett, P. J. and Stammer, D. (2010). Response of the eastern subtropical Atlantic SST to Saharan dust: A modelling and observational study, *Journal of Geophysical Research*, VOL. 115, C08015, doi: 10.1029/2009JC005692.

Matichuk, R. I., Colarco, P. R., Smith, J. A., and Toon, O. B. (2007). Modeling the transport and optical properties of smoke aerosols from African savannah fires during the Southern African Regional Science Initiative campaign (SAFARI 2000), J. *Geophys.Res*., 112, D08203, doi: 10.1029/2006JD007528.

Matsui, T., and Pielke, R. A. (2006). Measurement-based estimation of the spatial gradient of aerosol radiative forcing, *Geophys. Res. Lett*., 33, L11813, doi: 10.1029/2006GL025974.

McGregor J. L. (2005). C-CAM: geometric aspects and dynamical formulation CSIRO, *Atmospheric Research Tech*, 70. pp 43.

McGregor J. L., and Dix, M. R. (2008). An updated description of the Conformal-Cubic Atmospheric Model. In: Hamilton K, Ohfuchi W (*eds*.) High resolution simulation of the atmosphere and ocean. *Springer, Berlin*, pp 51 – 76

McGregor J. L., and Dix, M.R. (2001). The CSIRO conformal-cubic atmospheric GCM. In: Hodnett PF (*ed*.) IUTAM Symposium on advances in mathematical modelling of atmosphere and ocean dynamics. *Kluwer, Dordrecht*, pp 197 – 202.

McGregor, J. L. (1996). Semi-Langrangian advection on conformal-cubic grids. *Mon. Wea. Rev*., 124, 1311-1322

McGregor, J. L. (2005a): C-CAM: Geometric aspects and dynamical formulation [electronic publication]. Technical Report 70, CSIRO Atmospheric Research, 43 pp.

McGregor, J. L., (2005b). Geostrophic adjustment for reversibly staggered grids. *Mon Wea. Rev*., 133, 1119-1128.

McGregor, J. L., Gordon, H. B., Watterson, I. G., Dix, M. R. and Rotstayn, L. D. (1993). The CSIRO 9-level atmospheric general circulation model. CSIRO Aust. Div. *Atmos. Res. Technical Paper*, 26, 1-89.

Meehl, G. A., Karl, T., Esterling, D. R., Changnon, S., Pielke Jr, R., Changnon D., Evans, J., Groisman, P. Y., Knutson, T. R., Kunkel, K. E., Mearns, L. O., Parmesan, C., Pulwarty, R., Root, T., Sylves, R. T., Whetton, P. and Zwiers, F. 2000. An Introduction to Trends in Extreme

Weather and Climate Events: Observations, Socioeconomic Impacts, Terrestrial Ecological Impacts, and Model Projections, *Bulletin of the American Meteorological Society*, 81, 3.

Mélin, F., Holben, B. N., and Courcoux, Y. (2013). Validation of aerosol products derived from ocean colour in East African coastal waters, *African Journal of Marine Science*, 35:3, 351-356, DOI: 10.2989/1814232X.2013.830577.

Miller, R. L., Cakmur, R. V., Perlwitz, J., Geogdzhayev, I. V., Ginoux, P., Koch, D., Kohfeld, K. E., Prigent, C., Ruedy, R., Schmidt, G. A., and Tegen, I. (2006). Mineral dust aerosols in the NASAgoddard institute for Space Sciences ModelE atmospheric general circulation model, *J. Geophys. Res.-Atmos.,* 111, D06208, doi:10.1029/2005jd005796.

Miller, R. L., Cakmur, R. V., Perlwitz, J., Geogdzhayev, I. V., Ginoux, P., Koch, D., Kohfeld, K. E., Prigent, C., Ruedy, R., Schmidt, G. A. and Tegen, I., (2006). Mineral dust aerosols in the NASA Goddard Institute for Space Sciences ModelE atmospheric general circulation model. *Journal of Geophysical Research*, 111, D06208.

Miller, R. L., Schmidt, G. A., Nazarenko, L. S., Tausney, N., Bauer, S. E., Del Genio, A. D., Kelley, M., Lo, K. K., Ruedy, R., Shindell, D. T., Aleinov, I., Bauer, M., Bleck, R., Canuto, V., Chen, Y. -H., Cheng, Y., Clune, T. L., Faluvegi, G., Hansen, J. E., Healy, R. J., Kiang, N. Y., Koch, D., Lacis, A. A., LeGrande, A. N., Lerner, J., Menon, S., Oinas, V., Pérez García-Pando, C., Perlwitz, J. P., Puma, M. J., Rind, D., Romanou, A., Russell, G. L., Sato, M., Sun, S., Tsigaridis, K., Unger, N., Voulgarakis, A., Yao, M. -S. and Zhang, J. (2014). CMIP5 historical simulations (1850-2012) with GISS ModelE2. *J. Adv. Model. Earth Syst*., 6, no. 2, 441-477, doi:10.1002/2013MS000266.

Mishra, A. K., Rudich, Y., and Koren, I. (2016). Spatial boundaries of Aerosol Robotic Network observations over the Mediterranean basin, *Geophys. Res. Lett*., 43, 2259–2266, doi: 10.1002/2015GL067630.

Mitchell, T. D., and Jones, P. D. (2005). An improvement method of constructing a database of monthly climate observations and associated high-resolution grids. *International Journal of Climatology*, 25: 693-712.

Montilla E, Mogo S, Cachorro V, López J. and de Frutos A. (2011). Absorption, scattering and single scattering albedo of aerosols obtained from in situ measurements in the subarctic coastal region of Norway. *Atmospheric Chemistry and Physics* 11:2161-2182. DOI: 10.5194/acpd-11-2161-2011.

Mùller, T., Schladitz, A., Massling, A., Kaaden, N., Kandler, K., and Wiedensohler, A. (2009). Spectral absorption coefficients and imaginary parts of refractive indices of Saharan dust during SAMUM1, *Tellus* B, 61, 79–95.

Murphy, D. M., Anderson, J. R., Quinn, P. K., Mclnnes, L. M., Brechtel, F. J., Kreidenweis, S. M., Middlebrook, A. M., Posfai, M. Thomason, D. S. and Buseck, P. R. (1998), Influence of sea salt on aerosol radiative properties in the Southern Ocean marine boundary layer, *Nature*, 392(6671), 62– 65.

Myhre, G., Berntsen, T. K., Haywood, J. M., Sundet, J. K., Holben, B. N., Johnsrud, M., and Stordal, T. K. (2003). Modeling the solar radiative impact of aerosols from biomass burning during the Southern African Regional Science Initiative (SAFARI-2000) experiment. *Journal of Geophysical Research*, 108, NO. D13, 8501, doi: 10.1029/2002JD002313.

Myhre, G., F. Stordal, M. Johnsrud, D.J. Diner, I.V. Geogdzhayev, J.M. Haywood, B.N. Holben, T. Holzer-Popp, A. Ignatov, R.A. Kahn, Y.J. Kaufman, N. Loeb, J.V. Martonchik, M.I. Mishchenko, N.R. Nalli, L.A. Remer, M. Schroedter-Homscheidt, D. Tanre, O. Torres, and M. Wang, (2005). Inter-comparison of satellite retrieved aerosol optical depth over ocean during the period September 1997 to December 2000. *Atmos. Chem. Phys*., 5, 1697-1719, doi:10.5194/acp-5-1697-2005.

Myhre, G., Samset, B. H., Schulz, M., Balkanski, Y., Bauer, S., Berntsen, T. K., Bian, H., Bellouin, N., Chin, M., Diehl, T., Easter, R. C., Feichter, J., Ghan, S. J., Hauglustaine, D., Iversen, T., Kinne, S., Kirkevag, A., Lamarque, J. F., Lin, G., Liu, X., Lund, M. T., Luo, G., Ma, X., van Noije, T., Penner, J. E., Rasch, P. J., Ruiz, A., Seland, O., Skeie, R. B., Stier, P., Takemura, T., Tsigaridis, K., Wang, P., Wang, Z., Xu, L., Yu, H., Yoon, J. H., Zhang, H. and Zhou, C. (2013). Radiative forcing of the direct aerosol effect from AeroCom Phase II simulations. *Atmos. Chem. Phys*., 13, 1853-1877.

Nakata, M., Sano, I. and Mukai, S. (2016). Investigation of air pollution and regional climate change due to anthropogenic aerosols, *Remote Sensing Technologies and Applications in Urban Environments*, 100080Z, doi: 10.1117/12.2240153.

New, M., Hewitson, B., Stephenson, D.B., Tsiga, A., Kruger, A., Manhique, A., Gomez, B., Coelho, C.A., Masisi, D.N. & Kululanga, E. (2006). Evidence of trends in daily climate extremes over southern and West Africa, *Journal of Geophysical Research*, 111(7), pp. D14102.

New, M., Hulme, M. and Jones, P., (2000). Representing twentieth –century space-time climate variability. Part II: Development of 1901-96 Monthly grids of terrestrial surface climate. *Journal of Climate*, 13, 2217-2238.

New, M., Hulme, M., and Jones, P., (1999). Representing twentieth –century space- time climate variability. Part I: Development of a 1961-90 mean monthly terrestrial climatology. *Journal of Climate*, 12, 829-856.

Newell, R. E., Kidson, J. W., Vincent, D. G. and Boer, G. J. (1972). The general circulation of the tropical atmosphere and inter-actions with extratropical latitudes. Vol. 1. *MIT Press*, 258 pp.

Nguyen, K. C., Katzfey, J. J., and McGregor, J. L. (2014). Downscaling over Vietnam using the stretched-grid CCAM: verification of the mean and inter-annual variability of rainfall, *Climate Dynamics*, 43(3), 861 – 879.

Niang, I., Ruppel, O. C., Abdrabo, M. A., Essel, A., Lennard, C., Padgham, J. (2014). Africa. In V. R. Barros *et al*. (Eds.), Impacts, adaptation, and vulnerability. Part B: Regional aspects. Contribution of Working Group II to the Fifth Assessment Report of the Intergovernmental Panel on Climate Change (pp. 1199–1265). Cambridge, U.K. *Cambridge University Press*.

Nicholson, S. E. and Grist, J. P. (2003). The seasonal evolution of the atmospheric circulation over West Africa and Equatorial Africa. *J. Climate*, 16, 1013-1030.

Nicholson, S. E. and Selato, J. C. (2000). The influence of La Niña on African rainfall. *Int. J. Climatol*., 20, 1761-1776.

Nicholson, S. E., Nash, D. J., Chase, B. M., Grab, S. W., Shanahan, T. M., Verschuren, D., Asrat, A., Lézine. A. –M., and Umer, M. (2013). Temperature variability over Africa during the last 2000 years. Holocene, 23(8), 1085-1094.Watterson, I.G., 2009: Components of precipitation and temperature anomalies and change associated with modes of the Southern Hemisphere. *International Journal of Climatology*, 29(6), 809-826.

Northrop P. J. and Chandler, R. E. (2014). Quantifying Sources of Uncertainty in Projections of Future Climate. *American Meteorological Society*. 27. 8793-8808. DOI: 10.1175/JCLI-D-14-00265.1.

O'Dowd, C. D., Smith, M. H., Consterdine, I. E. and Lowe, J. A. (1997). Marine aerosol, sea-salt, and the marine sulphur cycle: A short review. *Atmospheric Environment*, 31, 73-80.

Palmer, T. N. (2016). A personal perspective on modelling the climate system, *Proc. R. Soc. A* 472: 20150772.

Penner, J. E., Andreae, M., Annegarn, H., Barrie, L., Feichter, J., Hegg, D., Jayaraman, A., Leaitch, R., Murphy, D., Nganga, J., and Pitari, G. (2001) Aerosols, their direct and indirect effects, in *Climate Change 2001: The Scientific Basis. Contribution of Working Group I to the Third Assessment Report of the Intergovernmental Panel on Climate Change,* edited by J. T. Houghton, Y. Ding, D. J. Griggs, M. Noguer, P. J. van der Linden, X. Dai, K. Maskell, and C. A. Johnson, chap. 5, 291–336, Cambridge Univ. Press, Cambridge, UK, and New York, NY, USA, 2001.

Perlwitz, J. P., Pérez García-Pando, C. and Miller, R. L. (2015). Predicting the mineral composition of dust aerosols — Part 1: Representing key processes. *Atmos. Chem. Phys*., 15, 11593-11627, doi: 10.5194/acp-15-11593-2015.

Persad, G. G. and Caldeira, K. (2018).), Divergent global-scale temperature effects from identical aerosols emitted in different regions, *Nature Communications*| (2018) 9:3289 | DOI: 10.1038/s41467-018-05838-6.

Petroff, A., Mailliat, A., Amielh, M., Anselmet, F. (2008). Aerosol dry deposition on vegetative canopies. Part II: A new modelling approach and applications, *Atmos. Environ*., 42, 3654–3683.

Piketh, S. J., Annegam, H. J., and Tyson, P. D. (1999a). Lower-tropospheric loadings over South Africa: The relative contribution of Aeolian dust, industrial emissions and biomass burning, *J. Geophys. Res*., 104, 1597-1607.

Platnick, S., King, M. D., Meyer, K. G., Wind, G., Amarasinghe, N., Marchant, B., Arnold, G. T., Zhang, Z., Hubanks, P. A., Ridgway, B., and Riedi, J. (2015). MODIS cloud optical properties: User Guide for the Collection 6 Level-2 MOD06/MYD06 product and associated Level-3 datasets.

Podgorny, I. A. and Ramanathan, V. (2001). A modelling study of the direct effect of aerosols over the tropical Indian Ocean. *Journal of Geophysical Research*, 106, 24097-24105.

Pomposi, C., Funk, C., Shukla, S., Harrison, L. and Magadzire, T., (2018). Distinguishing southern Africa precipitation response by strength of El Nĩno events and implications for decisionmaking, *Environmental Research Letters*, 13, 074015. https://doi.org/10.1088/1748-9326/aacc4c.

Posfai, M., Simonics, R., Li, J., Hobbs, P. V. and Buseck, P. R. (2003). Individual aerosol particles from biomass burning in Southern Africa: 1. Composition and size distributions of carbonaceous particles. *Journal of Geophysical Research*, 108, NO. D13, 8483, doi: 10.1029/2002JD002291.

Preston-Whyte, R. A. and Tyson, P. D. (1988). The Atmosphere and Weather of Southern Africa, Oxford University Press, Cape Town 374 pp.

Pretorius, I. (2016). Impacts and control of coal-fired power station emissions in South Africa. North West University.

Pretorius, I., Piketh, S. J., Burger, R. P., and Neomagus, H. W. J. P. (2015). A perspective of South African coal fired power station emissions. *Journal of Energy in Southern Africa*, 26(3), 27 – 40.

Prospero, J. M. (1999). Long-term measurements of the transport of African mineral dust to the southern United States: implications for regional air quality, *J. Geophys. Res*, 104, 15 917-15 927.

Prospero, J. M. and Mayol-Bracero, O. L. (2013). Understanding the transport and impact of African dust on the Caribbean Basin. *Bull Amer Meteor Soc* 94:1329-1337.

Putaud, J.P., Raes, F., Van Dingenen, R., Brüggemann, E., Facchini, M. C., Decesari, S., Fuzzi, S., Gehrig, R., Hüglin, C., Laj, P., Lorbeer, G., Maenhaut, W., Mihalopoulos, N., Muller, K., Querol, X., Rodriguez, S., Schneider, J., Spindler, G., Ten Brink, H., Torseth, K., Wiedensohler, A. (2010). A European aerosol phenomenology 2: chemical characteristics of particulate matter at kerbside, urban, rural and background sites. *Atmos Environ*. 2004; 38:2579–2595. doi: 10.1016/j.atmosenv.2004.01.041.

Qi, L. and Wang, S. (2019). Fossil fuel combustion and biomass burning sources of global black carbon from GEOS-Chem simulation and carbon isotope measurements, *Atmos. Chem. Phys*., 19, 11545–11557, https://doi.org/10.5194/acp-19-11545-2019.

Queface, A. J., Piketh, S. J., Eck, T. F., Tsay, S.-C. and Mavume, A. F. (2011). Climatology of aerosol optical properties in Southern Africa. *Atmospheric Environment*, 45(17), 2910-2921. https://doi.org/10.1016/j.atmosenv.2011.01.0.

Ramanathan, V. and Carmichael, G. (2008). Global and regional climate changes due to black carbon. *Nature*, doi: 10.1038/ngeo156.

Ramanathan, V., Crutzen, P. J., Kiehl, J. T. and Rosenfeld, D. (2001). Aerosols, Climate and the Hydrological Cycle, *Science*, 294 (5549), 2119-21.

Rap, A., Scott, C. E., Spracklen, D. V., Bellouin, N., Forster, P. M., Carslaw, K. S., Schmidt, A. and Mann, G. (2013). Natural aerosol direct and indirect radiative effects. *Geophysical Research Letters*, 40, 3297-3301.

Rayner, N. A., Parker, D. E., Horton, E. B., Folland, C. K., Alexander, L. V., Rowell, D. P., Kent, E. C., and Kaplan, A. (2003). Global analysis of sea surface temperatures, sea ice, and night marine air temperatures since the late nineteenth century. *Journal of Geophysical Research*, 108, NO. D14, 4407, doi: 10.1029/2002JD002670.

Reason, C. J. C. and Jagadheesha, D. (2005). A model investigation of recent ENSO impacts over southern Africa. *Meteorol. Atmos. Phys*. 89 181–205.

Reason, C. J. C., Allan, R. J., Lindesay, J. A. and Ansell, T. J., (2000). ENSO and climatic signals across the Indian Ocean basin in the global context: Part I, Interannual composite patterns. , *International Journal of Climatology*, 20, 11, 1285-1327. https://doi.org/10.1002/1097-0088(200009)20:11<1285:AIDJOC536>3.0.CO;2-R.

Regayre, L. A., Pringle, K. J., Lee, L. A., Booth, B. B. B., Rap, A., Browse, J., Mann, G. W., Woodhouse, M. T., Reddington, C. L. S., and Carslaw, K. S. (2015). The climatic importance of uncertainties in regional aerosol-cloud radiative forcing over recent decades, *J. Climate*. 28, 6589–6607, https://doi.org/10.1175/JCLI-D-15-0127.1.

Reid, J. S., and Hobbs, P. V. (1998). Physical and optical properties of young smoke from individual biomass fires in Brazil, *J. Geophys. Res*., 103, 32,013– 32,030.

Richard, Y., Fauchereau, N., Poccard, I., Rouault, M. and Trzaska, S. (2001). 20th century droughts in Southern Africa: spatial and temporal variability, teleconnections with oceanic and atmospheric conditions. *Int. J. Climatol*., 21, 873-885.

Robinson, A.L.; Donahue, N.M.; Shrivastava, M.K.; Weitkamp, E.A.; Sage, A.M.; Grieshop, A.P.; Lane, T.E.; Pierce, J.R. and Pandis, S.N. (2007). Rethinking organic aerosols: Semivolatile emissions and photochemical aging. *Science*, 315, 1259–1262.

Roden, C. A., T. C. Bond, S. Conway and A. B. O. Pinel, (2005). Emission Factors and Realtime Optical Properties of Particles Emitted from Traditional Wood Burning Cook stoves, submitted to Env. Sci. Tech.

Roeckner, E., Brokopf, R., Esch, M., Giorgetta, M., Hagemann, S., Kornblueh, L., Manzini, E., Schlese, U., and Schulzweida, U. (2006a). Sensitivity of Simulated Climate to Horizontal and Vertical Resolution in the ECHAM5 *Atmosphere Model. J. Climate*, 19(16):3771–3791.

Rotstayn, L. D. (1997). A physical based scheme for the treatment of strati form clouds and precipitation in large-scale models. I: Description and evaluation of the microphysical processes. *Quart. J. Roy. Meteor. Soc*., 123, 1227-1282.

Rotstayn, L. D. and Liu, Y. (2005). A smaller global estimate of the second indirect aerosol effect. *Geophysical Research Letters*, 32, L05708.

Rotstayn, L. D. and Liu, Y. (2009). Cloud droplet spectral dispersion and the indirect aerosol effect: Comparison of two treatments in a GCM. *Geophysical Research Letters*, 36, L10801.

Rotstayn, L. D. and Lohmann, U. (2002). Simulation of the tropospheric sulphur cycle in a global model with a physically based cloud scheme. *Journal of Geophysical Research*, 107, D21.

Rotstayn, L. D., Chai, W., Dix, M. R., Farquhar, G. D., Feng, Y., Ginoux, P., Herzog, M., Ito, A., Penner, J. E., Roderick, M. L. and Wang, M. (2007). Have Australian rainfall and cloudiness increased to the remote effects of Asian anthropogenic aerosols? *Journal of Geophysical Research*, 112, D09202.

Rotstayn, L. D., Collier, M. A., Chrastansky, A., Jeffrey, S. J. and Luo, J. J. (2013). Projected effects of declining aerosols in RCP4.5: unmasking global warming? *Atmos. Chem. Phys*., 13, 10883-10905.

Rotstayn, L. D., Jeffrey, S. J., Collier, M. A., Dravitzki, S. M., Hirst, A. C., Syktus, J. I. and Wong, K. K. (2012). Aerosol- and greenhouse gas-induced changes in summer rainfall and circulation in the Australasian region: a study using single-forcing climate simulations. *Atmos. Chem. Phys*., 12, 6377-6404.

Rouault, M. and Richard, Y. (2005). Intensity and spatial extent of droughts in southern Africa. *Geophys. Res. Lett*. 32 L15702.

Russell, G. L., Miller, J. R. and Rind, D. (1995). A coupled atmosphere-ocean model for transient climate change, *Atmos*. *Ocean*, 33,683–730.

Saji, N. H., Goswami, B. N., Vinayachandran, P. N. and Yamagata, T., (1999). A dipole mode in the tropical Indian Ocean", *Nature*, n401, 360-363. https://doi.org/10.1038/43854.

Schmidt, G. A., Hoffmann, G., Shindell, D. T., and Hu, Y. (2005). Modeling atmospheric stable water isotopes and the potential for constraining cloud processes and stratosphere-troposphere water exchange. *Journal of Geophysical Research*, 110. D21314, doi: 10.1029/2005JD005790.

Schmidt, G. A., Kelley, M., Nazarenko, L., Ruedy, R., Russel, G. L., Aleinov, I., Bauer, M., Bauer, S. E., Bhat, M. K., Bleck, R., Canuto, V., Chen, Y. -H., Cheng, Y., Clune, T. L., Del Genio, A., de Fainchtein, R., Faluvegi, G., Hansen, J. E., Healy, R. J., Kiang, N. Y., Koch, D., Lacis, A. A., LeGrande, A. N., Lerner, J., Lo, K. K., Matthews, E. E., Menon, S., Miller, R. L., Oinas, V., Oloso, A. O., Perlwitz, J. P., Puma, M. J., Putman, W. M., Rind, D., Romanou, A., Sato, M., Shindell, D. T., Sun, S., Syed, R. A., Tausnev, N., Tsigaridis, K., Unger, N., Voulgarakis, A., Yao, M. -S. and Zhang, J. (2014). Configuration and assessment of the GISS ModelE2 contributions to the CMIP5 archive. J. Adv. Model. Earth Syst., 6, no. 1, 141-184, doi:10.1002/2013MS000265

Schmidt, G. A., Ruedy, R., Hansen, J. E., Aleinov, I., Bell, N., Bauer, M., Bauer, S., Cairns, B., Canuto, V., Cheng, Y., Genio, A. D., Faluvegi, G., Friend, A. D., Hall, T. M., Hu, Y., Kelley, M., Kiang, N. Y., Koch, D., Lacis, A. A., Lerner, J., Lo, K. K., Miller, R. L., Nazarenko, L., Oinas, V., Perlwitz, J., Perlwitz, J., Rind., D., Romanou, A., Russell, G. L., Sato, M., Shindell, D. T., Stone, P. H., Sun, S., Tausnev, N., Thresher, D., and Yao, M. S. (2006). Present-day atmospheric simulations using GISS ModelE: Comparison to in situ, satellite, and reanalysis data. *Journal of Climate*, 19, 153-192.

Scholes, R.J., J. Kendall and C.O. Justice. (1996). The quantity of biomass burned in Southern Africa. *J. Geophys. Res*. 101. 23,667-23,676.

Seidel, F. C. and Popp, C. (2012). Critical surface albedo and its implications to aerosol remote sensing. *Atmospheric Measurement Techniques*, 5(7):1653–1665.

Seiki, T., C. Kodama, A. T. Noda, and Satoh, M. (2015). Improvement in global cloud-system resolving simulations by using a double-moment bulk cloud microphysics scheme*, J. Clim*., 28, 2405–2419, doi:10.1175/JCLI-D-14-00241.1.

Seinfeld, J. H., and Pandis, S. N. (2006). *Atmospheric Chemistry and Physics*: From Air Pollution to Climate Change, 2nd ed., John Wiley and Sons, New Jersey, USA, 908–911.

Seinfeld, J.H. and Pandis, S.N. (1998) Atmospheric chemistry and physics: From air pollution to climate change, John Wiley & Sons, Inc., New York, USA.

Seneviratne, S. I., Nicholls, N., Easterling, D., Goodess, C. M., Kanae, S., Kossin, J., Luo, Y., Marengo, J., Mclnnes, K., Rahimi, M., Reichstein, M., Sorteberg, A., Vera, C. and Zhang, X. (2012). Changes in climate extremes and their impacts on the natural physical environment. In: *Managing the Risks of Extreme Events and Disasters to Advance Climate Change Adaptation*. [Field, C.B., V. Barros, T.F. Stocker, D. Qin, D.J. Dokken, K.L. Ebi, M.D. Mastrandrea, K.J. Mach, G.-K. Plattner, S.K. Allen, M. Tignor, and P.M. Midgley (eds.)]. A Special Report of Working Groups I and II of the Intergovernmental Panel on Climate Change (IPCC). Cambridge University Press, Cambridge, UK, and New York, NY, USA, pp. 109-230.

Shikwambana, L., and Sivakumar, V. (2018). Long-range transport of volcanic aerosols over South Africa a case study of the Calbuco volcanic eruption in Chile during April 2015, *South African Geographical Journal*, 100:3, 349-363, DOI:10.1080/03736245.2018.1498383.

Shindell, D. T., Pechony, O., Voulgarakis, A., Faluvegi, G., Nazarenko, L., Lamarque, J. -F., Bowman, K., Milly, G., Kovari, B., Ruedy, R. and Schmidt, G. (2013). Interactive ozone and methane chemistry in GISS-E2 historical and future climate simulations. *Atmos. Chem. Phys*., 13, 2653-2689, doi:10.5194/acp-13-2653-2013.

Singleton, A. T. and Reason, C. J. C., (2007b). Variability in the characteristics of Cut-off low pressure systems over subtropical Southern Africa. *International Journal of Climatology*, 27, 295-310.

Sinha, P., Hobbs, P. V., Yokelson, R. J., Bertschi, I. T., Black, D. R., Simpson, I. J., Gao, S., Kirchstetter, T. W., and Novakov, T. (2003). Emissions of trace gases and particles from savannah fires in Southern Africa, *J. Geophys. Res*., 108 (D13), 8487, doi: 10.1029/2002JD002325.

Smirnov, A., Holben, B. N., Eck, T. F., Dubovik, O., and Slutsker, I. (2000). Cloud screening and quality control algorithms for the AERONET database, *Remote Sens. Environ*., 73, 337–349, https://doi.org/10.1016/S0034-4257(00)00109-7.

Solomon, S., Daniel, J. S., Sanford, T. J., Murphy, D. M., Plattner, G. K., Knutti, R. and Friedlingstein, P. (2010). Persistence of climate changes due to a range of greenhouse gases, *PNAS,* 10.1073. https://doi.org/10.1073/pnas.1006282107

Solomon, S., Qin, D., Manning, M., Chen, Z., Marquis, M., Averyt, K. B., Tignor, M., and Miller, H. L., (eds), (2007). *Contribution of Working Group I to the Fourth Assessment Report of the Intergovernmental Panel on Climate Change*. Cambridge University Press. Cambridge, United Kingdom and New York, NY, USA.

Stanley, S. (2017). New supercomputers allow climate models to capture convection, Eos, 98, doi.org/10.1029/2017EO074615.

Stevens, B. and Feingold, G. (2009). Untangling aerosol effects on clouds and precipitation in a buffered system. *Nature* 461, doi: 10.1038/nature08281.

Stocker, T., Qin, D., Plattner, G., Tignor, M., Allen, S., Boschung, J., Nauels, A., Xia, Y., Bex, B., and Midgley, B. (2013b). Climate Change 2013: The physical science basis. Contribution of Working Group I to the Fifth Assessment Report of the Intergovernmental Panel on Climate Change, *Cambridge Univ. Press*, Cambridge, UK.

Stone, R.S., Sharma, S., Herber, A., Eleftheriadis, K. and Nelson, D.W., (2014). A characterization of Arctic aerosols on the basis of aerosol optical depth and black carbon measurements. *Elem Sci Anth*, 2, p.000027. DOI: http://doi.org/10.12952/journal.elementa.000027.

Strawa, A. W., Castaneda, R., Owano, T., Baer, D. S., and Paldus, B. A. (2003). The measurement of aerosol optical properties using continuous wave cavity ring-down techniques, *J. Atmos. Oceanic Teck*.,20, 454-465.

Sun, S. and Bleck, R. (2006). Multi-century simulations with the coupled GISS-HYCOM climate model: Control experiments, *Clim. Dy-nam*., 26, 407–428.

Swap, R. J., Annegam, H. J., Suttles, J. T., King, M. D., Platnick, S., Privette, J. L., and Scholes, R. J. (2003). African burning: A thematic analysis of the Southern African Regional Science Initiative (SAFARI 2000), *J. Geophys. Res*., 108 (D13), 8465, doi: 10.1029/2003JD003747.

Swap, R., Garstang, M., Macko, S. A., Tyson, P. D., Maenhaut, W., Artaxo, P., Kllberg, P., and Talbot, R. (1996). The long-range transport of Southern Africanaerosols to the tropical South Atlantic. *J. Geophys. Res*., 101:23777–23792. doi:10.1029/95JD01049.

Sylla, M.B., Coppola, E., Moriotti, L., Giorgi F., Rutti, P.M., Dell' Aquila, A., and Bi X. (2009). Multiyear simulation of the African climate using a regional climate model (RegCM3) with the high-resolution ERA-interim reanalysis. *Clim. Dyn*. 35. 231-247.

Tadross, M. A., Gutowski Jr, W. J., Hewitson, B.C., Jack C., and New, M. (2006). MM5 simulations of inter-annual change and the diurnal cycle of Southern African regional climate. *Theor*. Appl. *Climatol*. 86. 63-80.

Taljaard, J. J., (1996). Atmospheric circulation systems, synoptic climatology and weather phenomena of South Africa. Part 6: Rainfall in South Africa. *South African Weather Bureau,mTechnical paper* 32

Tanaka, T. Y., and Chiba, M. (2006). A numerical study of the contributions of dust source regions to the global dust budget. *Global and Planetary Change,* 52, 88–104.

Tang, I. N., and Munkelwitz, H. R. (1994). Aerosol phase transformation and growth in the atmosphere, *Journal of Applied Meteorology*,33(7),791–796. https://doi.org/10.1175/1520-0450(1994)033<0791: APTAGI>2.0.CO;2

Tegen, I., and Lacis, A. A. (1996). Modeling of particle size distribution and its influence on the radiative properties of mineral dust aerosol. *J. Geophys. Res*., 101, 19237-19244, doi: 10.1029/95JD03610.

Tegen, I., Harrison, S. P., Kohfeld, K., Prentice, I. C., Coe, M., and Heimann, M. (2002). Impact of vegetation and preferential source areas on global dust aerosol: results from a model study, *J. Geophys. Res*., 107, 4576, doi: 10.1029/2001JD000963.

Tegen, I., Werner, M., Harrison, S.P., Kohfeld, K.E., (2004). Relative importance of climate and land use in determining present and future global soil dust emission. *Geophys. Res. Lett*. 31, L05105. http://dx.doi.org/10.1029/2003GL019216.

Tesfaye, M., Mengistu Tsidu, G., Botai, J., Sivakumar, V. and Rautenbah, C. J. deW. (2015). Mineral dust aerosol distributions, its direct and semi-direct effects over South Africa based on regional climate model simulation, *Journal of Arid Environments*, 114. 22-40.

Tesfaye, M., Sivakumar, V., Botai, J., and Mengistu Tsidu G. (2011). Aerosol climatology over South Africa based on 10 years of Multiangle Imaging Spectro-radiometer (MISR) data, *J. Geophys. Res*., 116, D20216, doi: 10.1029/2011JD016023.

Thatcher, M., McGregor, J. L. (2011). A technique for dynamically downscaling daily-averaged GCM datasets using the conformal cubic atmospheric model. *Mon Weather Rev*. https://doi.org/10.1175/2010MWR3351.1

Tighe T. (2015). A case study of high sea salt aerosol (SSA) concentrations as a hazard to aviation. *Meteorol. Appl*. 22: 806–810, DOI: 10.1002/met.1529.

Tiitta, P., Vakkari, V., Josipovic, M., Croteau, P., Beukes, J. P., van Zyl, P. G., Venter, A. D., Jaars, K., Pienaar, J. J., Ng, N. L., Canagaratna, M. R., Jayne, J. T., Kerminen, V. M., Kulmala, M., Laaksonen, A., Worsnop, D. R. and Laakso, L. (2013). Chemical composition, main source and temporal variability of PM1 aerosols in Southern Africa grassland. *Atmos. Chem. Phys*. Discuss., 13, 15517-15566.

Tinker, J., Lowe, J., Pardaens, A., Holt, J. and Barciela, R. (2016). Uncertainty in climate projections for the 21st century northwest European shelf seas. *Progress in Oceanography*, 148. 56-73.

Trenberth, K. E., Jones, P. D., Ambenje, P., Bojariu, R., Easterling, D., Klein Tank, A., Parker, D., Rahimzadeh, F., Renwick, J. A., Rusticucci, M., Soden, B., and Zhai, P. (2007). Observations: Surface and Atmospheric Climate Change. In: Climate Change 2007. *The Physical Science Basis*. Contribution of WG 1 to the Fourth Assessment Report of the Intergovernmental Panel on Climate Change. [S. Solomon, D. Qin, M. Manning, Z. Chen, M. C. Marquis, K. B. Averyt, M. Tignor and H. L. Miller (eds)]. Cambridge University Press. Cambridge, U. K., and New York, NY, USA, 235−336, plus annex online.

Tsigaridis, K. and Kanakidou, M. (2007). Secondary organic aerosol importance in the future atmosphere, *Atmos. Environ*., 41, 4682–4692, doi: 10.1016/j.atmosenv.2007.03.045.

Tsigaridis, K., Koch, D., and Menon, S. (2013). Uncertainties and importance of sea spray composition on aerosol direct and indirect effects, *Journal of Geophysical Research-Atmospheres*,118(1), 220–235. https://doi.org/10.1029/2012JD018165.

Tummon, F., Solmon, F., Liousse, C., and Tadross, M. (2010). Simulation of the direct and semi direct aerosol effects on the Southern Africa regional climate during the biomass burning season, *J. Geophys. Res*., 115, d19206, doi: 10.1029/2009JD013738.

Tyson, P. D., Cooper, G. R. J., and McCarthy, T. S. (2002). Millennial to multi-decadal variability in the climate of Southern Africa, *Int. J. Climatol*., 22:1105-1117. doi: 10.1002/joc.787.

Tyson, P. D., Garstang, M., and Swap, R. (1996a). Large-Scale Recirculation of Air over Southern Africa. *Journal of Applied Meteorology*, 35:2218–2236. doi:10.1175/1520-0450(1996)035.

United Nations Environment Programme (UNEP) and Word Agroforestry Centre (ICRAF). (2006). Climate Change and Variability in the Sahel Region: Impacts and Adaptation Strategies in the Agricultural Sector. Serigne Tacko Kandji, Louis Verchot, Jens Mackensen, *eds*.

Vakkari, V., Beukes, J. P., Laakso, H., Mabaso, D., Pienaar, J. J., Kulmala, M. and Laakso, L. (2013). Long-term observations of aerosol size distributions in semi-clean and polluted savannah in South Africa. *Atmos. Chem. Phys*., 13, 1751-1770.

Van der Werf, G. R., Randerson, J. T., Giglio, L., Collatz, G. J., Mu, M., Kasibhatla, P. S., Morton, D. C., DeFries, R. S., Jin, Y. and Leeuwen, T. T. (2010). Global fire emissions and the contribution of deforestation, savannah, forest, agricultural, and peat fires (1997–2009), *Atmos. Chem. Phys*., 10(23), 11707– 11735, doi:10.5194/acp-10-11707-2010.

Van Leer, B., (1977). Towards the ultimate conservation difference scheme. V. A new approach to numerical convection. *J. Comp. Phys*., 23, 276-299.

Wallace, J. M. and Hobbs, P. V. (2006). Atmospheric Science: An Introductory Survey (2nd edition). International Geophysics Series 92, Associated press, 484pp.

Wang, M. X., Zhang, R. J., and Pu, Y. F. (2001). Recent research on aerosol in China, *Adv. Atmos. Sci*., 18(4), 576 – 586

Wang, Z., Huang, X., and Ding, A. (2018). Dome effect of black carbon and its key influencing factors: a one-dimensional modelling study, *Atmos. Chem. Phys*., 18, 2821–2834, https://doi.org/10.5194/acp-18-2821-2018.

Washington, R., Todd, M. C., Goudie, A. S. and Middleton, N. (2003). Global dust storm sources areas determined by the total ozone monitoring spectrometer and ground observations. *Ann. Assoc. Am. Geogr*., 93, 297–313.

Weldon, D. and Reason, C. J. C., (2014). Variability of rainfall characteristics over the South Coast region of South Africa. *Theoretical and Applied Climatology* 115: 177-185. DOI:10.1007/s00704-013-0882-4.

Whitby, K.T., and Cantrell BK. (1976) Atmospheric aerosols: characteristics and measurement. In: Proceedings of the International Conference on Environmental Sensing and Assessment (ICESA), Institute of Electrical and Electronic Engineers (IEEE). IEEE #75-CH 1004-1, ICESA 29-1, Washington, DC: IEEE. p. 6.

Wolf, M. E. and Hidy G. M. (1997). Aerosols and climate: anthropogenic emissions and trends for 50 years, *Journal of Geophysical Research*,102(D10): 11 113–11 121.

Wu, Y., Liu, J., Zhai, J., Cong, L., Wang, Y., Ma, W., Zhang, Z., and Li, C. (2018) Comparison of dry and wet deposition of particulate matter in near-surface waters during summer. PLoS ONE 13(6): e0199241.https://doi.org/10.1371/journal. pone.0199241.

Xue, Y., Xu, H., Mei, L., Guang, J., Guo, J., and Li, Y., (2012). Merging aerosol optical depth data from multiple satellite missions to view agricultural biomass burning in Central and East China. *Atmos. Chem. Phys*. Discuss. 12,10461–10492.doi:10.5194/acpd-12-10461-2012.

Yu, H., Chin, M., Yuan, T., Bian, H., Remer, L. A., Prospero, J. M., Omar, A., Winker, D., Yang, Y., Zhang, Y., Zhang, Z. and Zhao, C. (2015). The fertilizing role of African dust in the Amazon rainforest: A first multiyear assessment based on data from Cloud-Aerosol Lidar and Infrared Pathfinder Satellite Observations, *Geophys. Res. Lett*.,42, doi:10.1002/2015GL063040.

Zhang, H. and Wang, Z., (2011). Advances in the study of black carbon effects on climate. *Advances in Climate Change Research*, 2, 23-30.

Zhang, R., Ho, K., and Shen, Z. (2012). The Role of Aerosol in Climate Change, the Environment, and Human Health, *Atmospheric and Oceanic Science Letters*, 5:2, 156-161, DOI: 10.1080/16742834.2012.11446983.

Zhang, X., Lin, Y.-H., Surratt, J. D., and Weber, R. J (2013). Sources, Composition and Absorption Ångström Exponent of Light-absorbing Organic Components in Aerosol Extracts from the Los Angeles Basin, *Environmental Science & Technology*, 47, 3685-3693, 10.1021/es305047b.